The Source Apportionment of Volatile Organic Compounds on Sable Island, Nova Scotia, Canada

by

Haya Qadoumi

Submitted in partial fulfillment of the requirements
for the degree of Master of Applied Science

at

Dalhousie University
Halifax, Nova Scotia
March 2016

TABLE OF CONTENTS

LIST OF TABLES

LIST OF FIGURES

ABSTRACT

Volatile organic compounds (VOCs) emitted by phytoplankton play an important role in the formation of fog and clouds that mediate climate. However, they are not well quantified due to a lack of long-term sampling platforms in the marine environment. In this study on Sable Island, 31 contiguous days of VOC species were actively sampled onto thermal desorption tubes followed by gas chromatography-mass spectrometry. Source apportionment of the VOCs was achieved using USEPA Positive Matrix Factorization v5.0. The source identification of VOCs was augmented by the use of the National Oceanic Atmospheric Association, Hybrid Single-Particle Lagrangian Integrated Trajectory model, visible satellite images and remotely sensed chlorophyll-a data from the Scotian Shelf. It was found that 27% of the total VOCs observed was associated with continental outflow, 40% of the VOCs were associated with marine phytoplankton emissions and 33% of the VOCs were associated with the combustion of carbonaceous material on the North American mainland.

LIST OF ABBREVIATIONS USED

1,2-$C_2H_4Br_2$	1,2-Dibromoethane
APCS	Absolute Principal Component Scores
AS	Air Server
AFRG	Atmospheric Forensics Research Group
CCl_4	Tetrachloromethane
$CHBr_3$	Bromoform
$CHBrCl_2$	Bromodichloromethane
$CHCl_3$	Chloroform
CH_2BrCl	Bromochloromethane
CH_4	Methane
CI	Chemical ionization
CMB	Chemical Mass Balance
CO	Carbon monoxide
CO_2	Carbon dioxide
CSLR	Calibration Solution Loading Rig
DMS	Dimethylsulphide
DMSP	Dimethylsulphoniopropionate
ECD	Electron capture detector
ESRF	Environmental Studies Research Funds
FID	Flame Ionization Detector
FPD	Flame Photometric Detector
FT-IR	Fourier transform-infrared
GC	Gas Chromatograph
H_2O_2	Hydrogen peroxide
H_2S	Hydrogen sulphide
H_2SO_4	Sulphuric acid
HYSPLIT	Hybrid Single-Particle Lagrangian Integrated Trajectory
i.d.	Internal diameter
LRT	Long-Range Transport

MIM	Multiple Ion Monitoring
MODIS	Moderate Resolution Imaging Spectroradiometer
MS	Mass Spectrometer
MSA	Methane sulphonic acid
NASA	National Aeronautics and Space Administration
NMHC	Non-methane hydrocarbon
NOAA	National Oceanic and Atmospheric Administration
NSE	Nova Scotia Environment
NO	Nitric oxide
NO_2	Nitrogen dioxide
NO_3	Nitrates
NO_x	Nitrogen oxides
O	Atomic oxygen
O_3	Ozone
OA	Organic aerosol
OH	Hydroxide
PCA	Principal Component Analysis
PID	Photo Ionization Detector
PM	Particulate matter
$PM_{1/2.5/4/10/TSP}$	Atmospheric particles with a median aerodynamic diameter less than, or equal to, 1.0 μm , 2.5 μm, 4.0 μm (also known as respirable particles), 10 μm and total suspended particles below 60 μm
PMF	Positive Matrix Factorization
PTR	Proton transfer reaction
RH	Denotes a NMHC radical
$RONO_2$	Organic nitrates
RO_2	Peroxy radical
RRF	Relative response factor
SIM,	Selective ion monitoring
SOA	Secondary organic aerosol

SO_2	Sulphur dioxide
SO_x	Sulphur oxides
SVI	Soil Vapor Intrusion
TCD	Thermal conductivity detector
TD	Thermal Desorber
TDT	Thermal desorption tube
TRG	Trace reactive gas
TSP	Total suspended particles
USEPA	US Environmental Protection Agency
UV	Ultraviolet
VIIRS	Visible Infrared Imaging Radiometer Suite
VOC	Volatile organic compound
WAS	Whole air sample
WHO	World Health Organization

ACKNOWLEDGEMENTS

I am grateful to my wonderful supervisor Dr. Mark Gibson for his continuous support and guidance and for giving me the opportunity to carry out my research on Sable Island. I would also like to thank Codey Barnett and the rest of the Atmospheric Forensics Research Group, my supervisory committee members Dr. Susanne Craig and Dr. Jan Haelssig, and Graduate Program Administrator Paula Colicchio for their assistance and encouragement. Special thanks goes to the Faculty of Graduate Studies for granting me the Nova Scotia Graduate Scholarship, Thermo Fisher Scientific for providing the ISQ single quadruple mass spectrometer that was used for the analysis of the VOC species studied in this thesis, Environmental Studies Research Funds and Natural Resources Canada for funding the project, and Maritime Air Charter for arranging travel to Sable Island. Finally, I would like to acknowledge everyone in Environment Canada and Parks Canada, as well as Dave Taylor and Eric Theriault for their advice and guidance.

CHAPTER 1 INTRODUCTION

The release of anthropogenic and natural trace reactive gases (TRG), and particulate matter (PM) to the lower troposphere can have tremendous impacts on climate forcing, ecosystems, health and the perturbation of tropospheric and stratospheric ozone formation and loss (Monks et al., 2009). The IPCC highlight that the biggest uncertainty in climate models is with the formation of aerosols and clouds, with much of the aerosol precursors TRG being emitted by marine phytoplankton emissions (IPCC, 2007).

Understanding the primary sources of these TRGs and PM and their impacts is necessary for raising awareness and developing policies for air pollution control and mitigation. An important source of TRGs is natural biogenic marine emissions from oceanic phytoplankton (Monks et al., 2009). Examples of the TRGs produced by marine phytoplankton include dimethylsulphide (DMS), non-methane hydrocarbons (NMHC), and halocarbons (e.g. bromomethane) (Moore, Geen, & Tait, 1995; Moore, Oram, & Penkett, 1994; O'Dowd, Aalto, Hmeri, Kulmala, & Hoffmann, 2002; O'Dowd & de Leeuw, 2007; O'Dowd et al., 2004). These compounds undergo photochemical reactions when ventilated into the atmosphere and result in the formation of the secondary pollutants, PM, tropospheric ozone (O_3) and formaldehyde that can influence the atmospheric reactivity and composition and result in positive or negative climate forcing (Monks et al., 2009). Moreover, TRGs including the halocarbon methyl iodide emit radicals that can destroy tropospheric ozone and result in negative climate forcing (Guenther et al., 2006; Monks et al., 2009; Palmer et al., 2013; Palmer & Shaw, 2005). However, the oceanic contribution of biogenic volatile organic compounds (VOCs) emission to the troposphere is not well quantified and only a few short-term ship and

aircraft studies have been performed (e.g. Butler et al., 2007). Also, most studies have been performed in the lab (i.e. algal cultures) and/or in seawater samples, but there have been a few long-term monitoring studies of oceanic VOCs due to limited accessibility to sampling platforms such as ships, aircraft, and islands. Moreover, global satellite observations are improving by providing more valuable tools for monitoring natural emissions (Monks et al., 2009). In order to better estimate the environmental and health effects of marine biogenic TRGs, their source apportionment must be quantified. The source apportionment of TRGs can be accomplished using receptor modelling techniques such as Positive Matrix Factorization (PMF), Absolute Principal Component Scores (APCS) or Chemical Mass Balance (CMB) receptor modelling (Brown, Frankel, & Hafner, 2007; Gibson et al., 2015; Hopke, 1991; Paatero & Hopke, 2003).

Due to mitigating circumstances, e.g. research contract delays, the primary objective of conducting 12-months of VOC sampling to capture seasonality was not achievable. In addition, the Nova Scotia Provincial Government ceased their management of air monitoring on Sable Island, removing their $PM_{2.5}$, NO_x, SO_2, H_2S and O_3 instruments in the process, which would have improved VOC data interpretation in this thesis. However, despite these issues, for the first time, an extremely valuable data set comprising 31 days of contiguous VOC species data has been collected from Sable Island.

CHAPTER 2 LITERATURE REVIEW

2.1 Air Pollution

Air pollution is a global problem that affects human health, ecosystems, air quality, and climate forcing. According to The World Health Organization (WHO), 2.4 million die every year from causes that are directly linked to air pollution (WHO, 2002). Large quantities of pollutants are emitted to the atmosphere are produced by anthropogenic sources such as fuel production, transportation, energy production and consumption, and industrial activities (Monks et al., 2009). Some of the air pollutants are naturally occurring and come from forest fires, soil erosion, dust storms, and sea spray (Environment Canada, 2012; Gibson et al., 2009b; Gibson et al., 2013b; Gibson et al., 2015). The most climate-influential pollutants produced are sulphur oxides (SO_x), nitrogen oxides (NO_x NO and NO_2), O_3, PM, carbon monoxide (CO), carbon dioxide (CO_2), and volatile organic compounds (VOC) (Environment Canada, 2013; Gibson et al., 2013a).

2.2 Marine Biogenic Emissions

The surface layer of the ocean and the boundary layer troposphere are largely linked by the chemical exchanges that occur between them. To understand the drivers of the temporal variation in marine VOC emissions, the biogenic contribution must be understood and quantified. One method of accomplishing this is source apportionment (Hayes, 2014; Paatero & Hopke, 2003; Gibson et al., 2015). Since phytoplankton contribute to most of the biogenic emissions from the ocean (Guenther et al., 2006;

Palmer & Shaw, 2005; Thomas et al., 2012; Craig et al., 2006), it is necessary to establish an understanding what TRGs these species produce.

Phytoplankton are microscopic plant like organisms that play a key role in the oceanic food web (Lindsey & Scott, 2010; Craig et al., 2012; Craig et al., 2006). Oceanic phytoplankton are the source of approximately half the biospheric net primary production of the globe and they contribute to most of the biogenic marine emissions (Guenther et al., 2006; Palmer & Shaw, 2005; Thomas et al., 2012). When sufficient nutrients are available, these organisms may grow rapidly to form algal blooms which then emit trace reactive climate relevant gases (Monks et al., 2009). Phytoplankton emit methane and non-methane VOCs including DMS, halocarbons, and NMHCs, all of which can influence atmospheric chemistry, cloud and fog formation and ultimately mediate climate (Behrenfeld et al., 2001; Monks et al., 2009; Teather et al., 2013).

2.3 Volatile Organic Compounds

Volatile organic compounds (VOCs) are carbon-containing organic compounds that have high vapour pressure and evaporate readily (Liu et al., 2008; USEPA, 2009). Since the majority of biogenic VOC emissions are emitted from photosynthetic phytoplankton, identifying and quantifying algal emissions is critical for understanding their contribution to the tropospheric and stratospheric chemistries (Buckley & Mudge, 2002; Colomb et al., 2008; Liss, 2007; O'Dowd & de Leeuw, 2007; Shaw, Gantt, & Meskhidze, 2010).

2.3.1 Halogenated Hydrocarbons

Halogenated hydrocarbons or halocarbons are, as the name implies, hydrocarbons with one or more halogen atoms, i.e. fluorine, chlorine, bromine or iodine (Liu et al., 2008). These are produced by phytoplankton as a form of oxidative stress relief, chemical

defense mechanism, or other cell metabolic applications (Moore et al., 1994; Moore & Tokarczyk, 1993; O'Dowd et al., 2004). Phytoplankton form poly- and mono-halocarbons in their stationary growth phase by peroxidases and s-adenosyl methionine transfer mechanism respectively.

2.3.1.1 Halomethanes

Marine algae are known to produce halomethanes or methyl halides (Moore & Tokarczyk, 1993; Shaw, 2001; Shaw et al., 2010). The long-lived hydrocarbons such as methyl chloride and methyl bromide are transported to the stratosphere where they are broken down by photolysis to produce highly reactive halide radicals and molecular oxygen (Moore & Tokarczyk, 1993; Shaw, 2001). Free radicals then react with the unstable ozone (ozone layer) converting it to the more stable oxygen molecule. The ozone layer in the stratosphere filters out the harmful ultraviolet (UV) radiation from the sun; therefore, the destruction of this layer results in more radiation reaching the Earth's surface. UV radiation may have adverse effects on human and animal health (i.e. cause skin cancer and sunburns), growth of crops, marine life (particularly plankton), and other non-living objects (Shaw et al., 2010).

Moreover, shorter-lived methyl iodides release reactive iodine radicals in the marine-air boundary and participate in catalytic reactions that destroy tropospheric ozone (Colomb et al., 2008; Muir, 2000). Although the contribution of natural sources to the total ground-level O_3 is not significant compared to anthropogenic sources, it is still necessary to consider their role in the accumulation of ozone in the troposphere.

Ozone is a highly reactive molecule that can damage forests and crops, and materials including nylon and rubber. It also has harmful impacts on human health by promoting

scar tissue formation and cell damage by oxidation, and by causing asthma, inflammation of lungs, chest pain, and eye irritation (Environment Canada, 2014). Aside from being an irritating pollutant, O_3 is an important source of OH-radicals which clean the atmosphere from the harmful VOCs and NO_x (Gibson et al., 2009a). Hence, its destruction would result in a reduction of the concentration of these radicals and, in turn, reduction of the atmosphere's "self-cleaning" capacity (Smythe-Wright et al., 2006).

2.3.2 Non-Methane Hydrocarbons

Non-methane hydrocarbons (NMHCs) are also typically produced by phytoplankton (Paul & Pohnert, 2011; Moore et al., 1995; Moore, Oram, & Penkett, 1994; O'Dowd et al., 2002; O'Dowd & de Leeuw, 2007; O'Dowd et al., 2004). A brief summary of some of the studies that reported production of halogenated hydrocarbons from marine phytoplankton are listed in Table 1. NMHCs are short-lived VOCs that can readily become oxidized by OH and O_3. The oxidation process of NMHCs in the troposphere produces CO and CO_2 along with other important intermediates such as peroxy radicals (RO_2), which can oxidize nitric oxide (NO) to nitrogen dioxide (NO_2). Nitrogen dioxide can then photo-dissociate into NO and atomic oxygen (O) to form ground-level ozone impacting the environment on a local or regional scale (Gibson et al 2009a).

Peroxy radicals also produce organic nitrates ($RONO_2$) by reacting with NO. The nitrates can act as NO_X reservoirs but with longer lifetimes and thus can be transported over long distances (Gibson et al 2009a). According to Poisson et al. (2000), this process alters concentrations of NO_X, O_3, and OH that affect the concentrations of the photo-chemically active trace gases such as methane (CH_4), CO, and O_3. NMHC radical (RH) can account for removal of OH (Guenther et al., 2006; Palmer & Shaw, 2005).

Isoprene is one of the most abundant phytoplankton-derived hydrocarbons and plays a key role in the production of O_3 and peroxy radicals (Kleindienst, Lewandowski, Offenberg, Jaoui, & Edney, 2007; Liakakou et al., 2007). It can affect air quality by the formation of SOA during oxidation (Palmer & Shaw, 2005). High yields of SOA are formed at night when isoprene reacts with nitrate (NO_3) (Guenther et al., 2006). In the United States, it is estimated that 50% of SOA present is contributed by isoprene photo-oxidation. Oxidation of isoprene is considered a significant source of formaldehyde that impacts human and animal health by causing irritation of the eye and upper respiratory tract as well as compromised lung function (Guigard et al., 2006).

Table 1. VOC emissions from marine algae reported by previous studies

	Colomb et al. (2008)	Scarratt & Moore (1999)	Sabolis (2010)	Tokarczyk & Moore (1994)	Moore & Tokarczyk (2008)
Chloroform	*Calcidiscus leptoporus; Emiliania huxleyi; Chaetoceros neogracilis; Dunaliella tertiolecta; Phaeodactylum tricornutum*		*Pleurochrysis carterae; Rhodomonas salina; Karenia brevis; Prorocentrum minimum; Thalassiosira pseudonana; Thalassiosira weissflogii*		
Bromoform		*Nitzschia sp. (CCMP 580)*	*Pleurochrysis carterae; Rhodomonas salina; Karenia brevis;*	*Nitzschia seriata; Porosira glacialis*	*Ascophyllun nodosum; Elachista fuciculoa*
1,1-Dichloroethane	*Calcidiscus leptoporus; Emiliania huxleyi; Chaetoceros neogracilis; Dunaliella tertiolecta; Phaeodactylum tricornutum*				
Trichloroethene	*Calcidiscus leptoporus; Emiliania huxleyi; Chaetoceros neogracilis; Dunaliella tertiolecta; Phaeodactylum tricornutum*				
Bromodichloromethane			*Pleurochrysis carterae; Rhodomonas salina; Karenia brevis;*		
Chlorobenzene	*Calcidiscus leptoporus; Dunaliella tertiolecta; Phaeodactylum tricornutum*				
1,2-Dichloroethane	*Calcidiscus leptoporus; Emiliania huxleyi; Chaetoceros neogracilis; Dunaliella tertiolecta; Phaeodactylum tricornutum*				
Tetrachloroethene	*Calcidiscus leptoporus; Emiliania huxleyi; Chaetoceros neogracilis; Dunaliella tertiolecta; Phaeodactylum tricornutum*		*Pleurochrysis carterae; Rhodomonas salina; Karenia brevis; Prorocentrum minimum; Thalassiosira pseudonana; Thalassiosira weissflogii*		
Dibromochloromethane			*Pleurochrysis carterae*	*Nitzschia sp.* (CCMP 580); *Porosira glacialis*	
Dibromomethane				*Nitzschia sp.* (CCMP 580); *Porosira glacialis*	

Table 2 below shows the halogenated hydrocarbons produced by red alga. These organisms produce various halogen-containing secondary metabolites, i.e. fatty acids, which could produce volatile hydrocarbons when degraded (Nightingale et al., 1995; Sundstrom et al., 1996; Kladi, Vagias, & Roussis, 2004).

Table 2. Halogenated VOCs emitted from marine red alga

Metabolite	Algae
CH_3Br	*Corallina officinalis*[1], *Phycodrys quercifolia*[2], *Gymnogongrus antarcticus*[2], *Georgiella confluens*[2], *Iridaea cordata*[3]
CH_3Cl	*Corallina officinalis*[1], *Endocladia muricata*[1], *Phycodrys quercifolia*[2], *Gymnogongrus antarcticus*[2], *Georgiella confluens*[2]
CH_3I	*Corallina officinalis*[1,4,5], *Phycodrys quercifolia*[2], *Gymnogongrus antarcticus*[2], *Georgiella confluens*[2], *Eucheuma denticulatum*[6], *Meristiella gelidium*[7], *Pterocladia capillacea*[4], *Rhodymenia californica*[4], *Gigartina stellata*[5], *Polysiphonia lanosa*[5], *Hypnea spinella*[8], *Gracilaria cornea*[8]
CH_2Br_2	*Phycodrys quercifolia*[2], *Gymnogongrus antarcticus*[2,9], *Georgiella confluens*[2,9], *Meristiella gelidium*[7], *Rhodomela lycopodioides*[10], *Palmaria palmata*[10], *P. decipiens*[9,3], *Devalaerea ramentacaea*[10], *Polysiphonia arctica*[10], *Porphyra endiviifolium*[9], *Kallymenia antarctica*[9], *Curdiea racovitzae*[9], *Plocamium coccineum*[9], *Gigartina papillosa*[9], *G. stellata*[5], *Iridaea cordata*[9,3], *Delesseria lancifolia*[9], *Myriogramme mangini*[9], *Pantoneura plocamioides*[9], *Picconiella plumosa*[9], *Hymenocladiopsis crustigena*[9], *Phyllophora ahnfeltioides*[9], *Corallina officinalis*[5,4], *C. pilulifera*[11], *Pterocladia capillacea*[4], *Rhodymenia californica*[4], *Lithophyllum yessoense*[11], *Gracilaria cornea*[8]
CH_2Cl_2	*Corallina officinalis*[1]
CH_2I_2	*Phycodrys quercifolia*[2], *Gymnogongrus antarcticus*[2,9], *Georgiella confluens*[2,9], *Meristiella gelidium*[7], *Rhodomela lycopodioides*[10], *Palmaria palmata*[10], *Porphyra endiviifolium*[9], *Kallymenia antarctica*[9], *Curdiea racovitzae*[9], *Gigartina papillosa*[9], *G. stellata*[12], *Iridaea cordata*[3], *Palmaria decipiens*[9], *Myriogramme mangini*[9], *Pantoneura plocamioides*[9], *Picconiella plumosa*[9], *Hymenocladiopsis crustigena*[9], *Phyllophora ahnfeltioides*[9], *Hypnea spinella*[8], *Gracilaria cornea*[8]
$CHBr_3$	*Phycodrys quercifolia*[2], *Gymnogongrus antarcticus*[2,9], *Georgiella confluens*[2,9], *Eucheuma denticulatum*[6], *Meristiella gelidium*[7], *Rhodomela lycopodioides*[10], *Palmaria palmata*[10], *P. decipiens*[9,3], *Devalaerea ramentacaea*[10], *Polysiphonia arctica*[10], *P. lanosa*[5], *Porphyra endiviifolium*[9], *Kallymenia antarctica*[9], *Curdiea racovitzae*[9], *Plocamium coccineum*[9], *Gigartina papillosa*[9],*G. stellata*[5,12], *Iridaea cordata*[9,3], *Delesseria lancifolia*[9], *Myriogramme mangini*[9], *Pantoneura plocamioides*[9], *Picconiella plumosa*[9], *Hymenocladiopsis crustigena*[9], *Phyllophora ahnfeltioides*[9], *Corallina officinalis*[5,4], *C. pilulifera*[11], *Pterocladia capillacea*[4], *Rhodymenia californica*[4], *Lithophyllum yessoense*[11], *Hypnea spinella*[8], *Gracilaria cornea*[8]
$CHCl_3$	*Corallina officinalis*[5,1], *Eucheuma denticulatum*[6,1], *Meristiella gelidium* [7], *Gigartina stellata*[5], *Polysiphonia lanosa*[5], *Hypnea spinella*[8], *Gracilaria cornea*[8]
CH_2ClI	*Corallina officinalis*[1], *Phycodrys quercifolia*[2], *Gymnogongrus antarcticus*[2,9], *Georgiella confluens*[2,9], *Meristiella gelidium*[7], *Rhodomela lycopodioides*[10], *Palmaria palmata*[10], *P. decipiens*[9,3], *Devalaerea ramentacaea*[10], *Polysiphonia arctica*[10], *Porphyra endiviifolium*[9], *Kallymenia antarctica*[9], *Curdiea racovitzae*[9], *Gigartina papillosa*[9], *Iridaea cordata*[9,3], *Delesseria lancifolia*[9], *Myriogramme mangini*[9], *Pantoneura plocamioides*[9], *Picconiella plumosa*[9], *Hymenocladiopsis crustigena*[9], *Phyllophora ahnfeltioides*[9], *Eucheuma denticulatum*[1], *Hypnea spinella*[8], *Gracilaria cornea*[8]
CH_2BrCl	*Phycodrys quercifolia*[2], *Gymnogongrus antarcticus*[2], *Georgiella confluens*[2]
$CHBrCl_2$	*Phycodrys quercifolia*[2], *Gymnogongrus antarcticus*[2,9], *Georgiella confluens*[2,9], *Meristiella gelidium*[7], *Rhodomela lycopodioides*[10], *Palmaria palmata*[10], *P. decipiens*[9,3], *Devalaerea ramentacaea*[10], *Polysiphonia arctica*[10], *P. lanosa*[5], *Porphyra endiviifolium*[9], *Kallymenia antarctica*[9], *Curdiea racovitzae*[9], *Plocamium coccineum*[9], *Gigartina papillosa*[9], *G. stellata*[5,12], *Iridaea cordata*[9,3], *Delesseria lancifolia*[9], *Myriogramme mangini*[9], *Pantoneura plocamioides*[9], *Picconiella plumosa*[9], *Hymenocladiopsis crustigena*[9], *Phyllophora ahnfeltioides*[9], *Corallina officinalis*[5]
$CHBr_2Cl$	*Meristiella gelidium*[7], *Rhodomela lycopodioides*[10], *Palmaria palmata*[10], *P. decipiens*[9,3], *Devalaerea ramentacaea*[10], *Polysiphonia arctica*[10], *P. lanosa*[5], *Porphyra endiviifolium*[9], *Kallymenia antarctica*[9], *Curdiea racovitzae*[9], *Plocamium coccineum*[9], *Gymnogongrus antarcticus*[9], *Gigartina papillosa*[9], *G. stellata*[5,12], *Iridaea cordata*[9,3], *Georgiella confluens*[9], *Delesseria lancifolia*[9], *Myriogramme mangini*[9], *Pantoneura plocamioides*[9], *Picconiella plumosa*[9], *Hymenocladiopsis crustigena*[9], *Phyllophora ahnfeltioides*[9], *Corallina officinalis*[5], *C. pilulifera*[11], *Lithophyllum yessoense*[11], *Hypnea spinella*[8], *Gracilaria cornea*[8]
CH_3CH_2I	*Phycodrys quercifolia*[2], *Gymnogongrus antarcticus*[2], *Georgiella confluens*[2], *Palmaria decipiens*[3], *Gigartina stellata*[12]
CH_3CH_2Br	*Phycodrys quercifolia*[2], *Gymnogongrus antarcticus*[2], *Georgiella confluens*[2], *Iridaea cordata*[3], *Palmaria decipiens*[3]

Note: Adapted from "Volatile halogenated metabolites from marine red algae", by M. Kladi, C. Vagias and V. Roussis. Copyright 2005 by Springer

Table 2. *Continued*

1,2-$C_2H_4Br_2$	*Phycodrys quercifolia*[2], Gymnogongrus antarcticus[2], *Georgiella confluens*[2,9], *Rhodomela lycopodioides*[10], *Palmaria palmata*[10], *P. decipiens*[3,9], *Devalaerea ramentacaea*[10], *Polysiphonia arctica*[10], *Porphyra endiviifolium*[9], *Kallymenia antarctica*[9], *Curdiea racovitzae*[9], *Gymnogongrus antarcticus*[9], *Gigartina papillosa*[9], *Iridaea cordata*[9,3], *Delesseria lancifolia*[9], *Myriogramme mangini*[9], *Pantoneura plocamioides*[9], *Picconiella plumosa*[9], *Hymenocladiopsis crustigena*[9], *Phyllophora ahnfeltioides*[9]
$CHCl{=}CCl_2$	*Eucheuma denticulatum*[6], *Meristiella gelidium*[13], *Chondrus crispus*[13], *Phyllophora pseudoceranoides*[13], *Porphyra umbilicalis*[13], *Polysiphonia nigrescens*[13], *Furcellaria lumbricalis*[13], *Ceramium rubrum*[13], *Ahnfeltia plicata*[13], *Hypnea musciformis*[13], *H. spinella*[8], *Gelidium canariensis*[13], *Laurencia obtusa*[13], *Corallina officinalis*[13], *Gracilariopsis lemaneiformis*[13], *Gracilaria cornea*[13]
$Cl_2C{=}CCl_2$	*Chondrus crispus*[13], *Ahnfeltia plicata*[13], *Gelidium canariensis*[13], *Laurencia obtusa*[13]
C_3H_7Br	*Gigartina stellata*[12]
CH_3CHICH_3	*Hypnea spinella*[8]
C_4H_9I	*Meristiella gelidium*[7], *Gracilaria cornea*[8], *Hypnea spinella*[8], *Gigartina stellata*[12]
$CH_3CHIC_2H_5$	*Hypnea spinella*[8]

Note: Adapted from "Volatile halogenated metabolites from marine red algae", by M. Kladi, C. Vagias and V. Roussis. Copyright 2005 by Springer

Table 3 shows the halogenated volatile metabolites produced by *Asparagopsis taxiformis* and *Asparagopsis armata* algae that belong to family *Bonnemaisoniaceae*. These have shown to be a source of a wide range of halogenated metabolites which are composed of halomethanes (McCombs et al., 1988; Kladi et al., 2004).

Table 3. Halogenated volatile metabolites of the marine algae *Asparagopsis taxiformis* and *Asparagonis armata*

Asparagopsis taxiformis	
Haloforms[1,2]	$CHBr_3$, $CHBr_2I$, $CHBrI_2$, CHI_3, $CHBr_2Cl$, CHBrClI
Dihalomethanes[1]	CH_2Br_2, CH_2BrI, CH_2I_2
Carbon tetrahalides[1]	CBr_4
Carbonyl dihalides[1]	COI_2
2-Haloethanols[1]	ICH_2CH_2OH
1,2-Dihaloethanes[1]	$BrCH_2CH_2I$
Halogenated ethylenes[3,]	$Cl_2C=CCl_2$, $CHCl=CCl_2$
Halogenated acetaldehydes[1,2]	Br_2CHCHO, $BrCH_2CHO$
Halogenated acetones[1,2,4]	CH_3COCH_2Br, CH_3COCH_2I, $CH_3COCHBr_2$, $BrCH_2COCH_2Br$, $BrCH_2COCH_2I$, CH_3COCBr_3, CH_3COCBr_2Cl, $BrCH_2COCHBr_2$, $ICH_2COCHBr_2$, $Br_2CHCOCHBr_2$, $Cl_3CCOCCl_3$, $BrCH_2COCH_2Cl$, $ClCH_2COCHBr_2$, $ClBrCHCOCH_2Br$, $ClBrCHCOCHBr_2$, $ClCH_2COCH_2Cl$, $ClCH_2COCHCl_2$, $Cl_2CHCOCHCl_2$, $Cl_2CHCOCH_2Br$, $ClBrCHCOCH_2Cl$, $Cl_2CHCOCHBrCl$, $Cl_2CHCOCHBr_2$, $ClBrCHCOCHBrCl$, $ClCH_2COCH_2I$,
Dihaloisopropanols[5]	$Br_2CHCH(OH)CH_3$, $BrCH_2CH(OH)CH_2Br$, $ClCH_2CH(OH)CH_2I$, $BrCH_2CH(OH)CH_2I$, $ICH_2CH(OH)CH_2I$
Trihaloisopropanols[1,5]	$BrCH_2CH(OH)CHBr_2$, $BrClCHCH(OH)CH_2Cl$, $Cl_2CHCH(OH)CH_2Br$, $BrClCHCH(OH)CH_2Br$, $Br_2CHCH(OH)CH_2Cl$, $Br_2CHCH(OH)CH_2Br$, $BrClCHCH(OH)CH_2I$, $Br_2CHCH(OH)CH_2I$
Tetrahaloisopropanols[5]	$Cl_2CHCH(OH)CHCl_2$, $BrClCHCH(OH)CHCl_2$, $Br_2CHCH(OH)CHCl_2$, $Br_2CHCH(OH)CHBrCl$, $Br_3CCH(OH)CH_2Cl$, $Br_2CHCH(OH)CHBr_2$, $Br_2CHCH(OH)CHBrI$, $Br_2CHCH(OH)CHI_2$
1,1,4-Trihalobut-3-en-2-ols[5]	$Br_2C=CHCH(OH)CH_2Cl$, $Br_2C=CHCH(OH)CH_2Br$
1,1,4,4-Tetrahalobut-3-en-2-ols[5]	$Br_2C=CHCH(OH)CHCl_2$, $Cl_2C=CHCH(OH)CHBr_2$, $Br_2C=CHCH(OH)CHBrCl$, $BrClC=CHCH(OH)CHBr_2$, $Br_2C=CHCH(OH)CHBr_2$
1,1,1,4,4-Pentahalobut-3-en-2-ols[5]	$Br_2C=CHCH(OH)CBr_3$
Dihaloacetamides[5]	$BrClCHCONH_2$, $Br_2CHCONH_2$, $ClICHCONH_2$, $BrICHCONH_2$, $I_2CHCONH_2$
Halogenated 2-acetoxypropanes[1]	$BrCH_2CH(OAc)CHBr_2$, $Br_2CHCH(OAc)CHBr_2$
Halogenated 1,2-epoxypropanes[1]	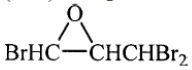
1,1,3,3-Tetrahalopropenes[1]	$Br_2C=CHCHBr_2$, $Br_2C=CHCHBrCl$, $Br_2C=CHCHCl_2$, $BrIC=CHCHBr_2$
3,3-Dihaloacroleins	$Br_2C=CHCHO$[1]
Halogenated but-3-en-2-ones[1,2,4,6]	$Br_2C=CHCOCH_3$, $Br_2C=CHCOCH_2Br$, $Br_2C=CHCOCH_2I$, $Br_2C=CHCOCHBr_2$, $Br_2C=CHCOCHBrCl$, $BrClC=CHCOCHBr_2$, $Cl_2C=CHCOCHBr_2$, $BrClC=CHCOCHBrCl$, $BrCH=CBrCOCHBr_2$, $BrCH=CBrCOCH_3$, $BrCH=CBrCOCH_2Br$, $BrCH=CBrCOCH_2I$, $Br_2C=CHCOCH_2Cl$[2]
Pentabromopropen-2-yl tribromoacetate[11]	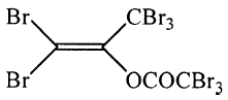
Pentabromopropen-2-yl dibromoacetate[11]	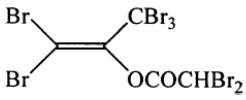
Haloacetic acids[7]	$ClCH_2CO_2H$, $BrCH_2CO_2H$, ICH_2CO_2H
Dihaloacetic acids[2,7]	Cl_2CHCO_2H, $BrClCHCO_2H$, $ClICHCO_2H$, Br_2CHCO_2H, $BrICHCO_2H$, I_2CHCO_2H
Trihaloacetic acids[2]	CBr_3CO_2H
Haloacrylic acids[2,7]	$ClCH=CHCO_2H$ or $CH_2=CClCO_2H$, $BrCH=CHCO_2H$, $ICH=CHCO_2H$ or $CH_2=ClCO_2H$
Dihaloacrylic acids[2,7]	$Cl_2C=CHCO_2H$ or $CHCl=CClCO_2H$, $Br_2C=CHCO_2H$, $BrIC=CHCO_2H$ or $CHBr=ClCO_2H$ or $CHI=CBrCO_2H$, $I_2C=CHCO_2H$ or $CHI=ClCO_2H$, $CHBr=CBrCO_2H$
Trihaloacrylic acids[7]	$Br_2C=CBrCO_2H$, $BrIC=CBrCO_2H$ or $Br_2C=ClCO_2H$
Asparagopsis armata	
Haloforms[2,8,9,10]	$CHBrCl_2$, $CHCl_3$, $CHBr_3$, CH_3I, CH_2ClI, CCl_4, $CHBr_2Cl$, CBr_4, $CHBr_2I$, CH_2BrCl, CH_2Br_2

Note: Adapted from "Volatile halogenated metabolites from marine red algae", by M. Kladi, C. Vagias and V. Roussis. Copyright 2005 by Springer

Table 3. *Continued*

Halogenated hydrocarbons[10]	$Cl_2C=CCl_2$, $CH_2BrCHBrCH_3$, $CH_2=CHBrCH_2Br$, 2,3-dibromo-2-methylbutane, 1,3-dibromo-3-methylbutane, iodohexane, 1-bromo-6-chlorohexane, bromooctane, iodooctane, bromodecane, bromoundecane, bromododecane, bromotetradecane, bromocyclohexane, iodocyclohexane
Halogenated isopropanols[10]	$BrCH_2CH(OH)CH_2Br$, $Br_2CHCH(OH)CHBr_2$
Haloacetones[9,2,10]	$Br_2CHCOCH_2I$, $BrCH_2COCHBr_2$, $Br_2CHCOCHBr_2$, $BrCH_2COCH_2Cl$, $ClCH_2COCHBr_2$, $ClBrCHCOCH_2Br$, $ClBrCHCOCHBr_2$ $ClCH_2COCH_2Cl$, $ClCH_2COCHCl_2$, $Cl_2CHCOCHCl_2$, $Cl_2CHCOCH_2Br$, $ClBrCHCOCH_2Cl$, $Cl_2CHCOCHBrCl$, $Cl_2CHCOCHBr_2$, $ClBrCHCOCHBrCl$, $BrCH_2COCH_2Br$,
Halogenated but-3-en-2-ones[2,10]	$Br_2C=CHCOCHBr_2$, $Cl_2C=CHCOCH_3$ or $ClCH=CClCOCH_3$
Halogenated acetaldehydes[2]	Br_2CHCHO, $BrCH_2CHO$
Halogenated acetic acids[7,2,10]	Br_2CHCO_2H, $BrICHCO_2H$, CBr_3CO_2H, $BrCH_2CO_2H$, Cl_2CHCO_2H,
Halogenated acrylic acids[7,2,10]	$BrCH=CHCO_2H$ or $CH_2=CBrCO_2H$, $ICH=CHCO_2H$ or $CH_2=CICO_2H$, $CHBr=CClCO_2H$ or $CHCl=CBrCO_2H$ or $BrClC=CHCO_2H$, $BrIC=CHCO_2H$ or $CHBr=CICO_2H$ or $CHI=CBrCO_2H$, $I_2C=CHCO_2H$ or $CHI=CICO_2H$, $CHBr=CBrCO_2H$, $Br_2C=CHCO_2H$
Dihaloacetamides[10]	$BrClCHCONH_2$, $Br_2CHCONH_2$, $BrICHCONH_2$

Note: Adapted from "Volatile halogenated metabolites from marine red algae", by M. Kladi, C. Vagias and V. Roussis. Copyright 2005 by Springer

Table 4 shows the halogenated volatile metabolites of *Falkenbergia rufolanosa* and *Falkenbergia hillebrandii*, which are the sporophyte forms of *A. armata* and *A. taxiformis* respectively (Kladi et al., 2004).

Table 4. Halogenated volatile metabolites of *Falkenbergia sp*.

Falkenbergia rufolanosa	
Halomethanes	$CHBr_3$, $CHBr_2I$, CH_2BrCl, CH_2ClI
Halogenated hydrocarbons	$Cl_2C=CCl_2$, 1-bromo-2-methyl-butane
Halogenated acetaldehydes	$BrCH_2CHO$, Br_2CHCHO
Halogenated acetones	$BrCH_2COCH_3$, $Br_2CHCOCH_3$, $ClCH_2COCHCl_2$, $BrCH_2COCH_2Br$, $BrCH_2COCHCl_2$, $Cl_2CHCOCHBrCl$, $Br_2CHCOCHCl_2$, $Br_2CHCOCH_2Br$, $BrClCHCOCHBrCl$, $Br_2CHCOCHBrCl$, $Br_2CHCOCHBr_2$
Halogenated methyl and ethyl acetates	ICH_2COOCH_3, $Br_2CHCOOCH_3$, $Br_2CHCOOC_2H_5$, $BrICHCOOC_2H_5$
Falkenbergia hillebrandii	
Halomethanes	$CHCl_3$, CH_3I, CH_2ClI, CH_2Br_2, $CHBrCl_2$, $CHBr_2Cl$, $CHBr_3$, CH_2I_2
Halogenated ethylenes	$CHCl=CCl_2$, $Cl_2C=CCl_2$,
Halogenated hydrocarbons	CH_3CHICH_3, $CH_3CHICH_2CH_3$, $CH_3CH_2CH_2CH_2I$

Note: Adapted from "Volatile halogenated metabolites from marine red algae", by M. Kladi, C. Vagias and V. Roussis. Copyright 2005 by Springer

2.3.3 Dimethylsulphide

Dimethylsulphoniopropionate (DMSP) is an organosulphur compound abundantly found in phytoplankton for regulating their internal osmotic environment; it is the dominant volatile sulphur compound found in marine surface waters and its production depends on the availability of light, temperature, and salinity of the water (O'Dowd & de Leeuw, 2007). DMSP is suggested to have an antioxidant role which helps organisms destroy the harmful hydroxyl radicals (OH) that are produced when ultraviolet (UV) radiation dissociate hydrogen peroxide (H_2O_2) (Sunda, Kieber, Kiene, & Huntsman, 2002). When phytoplankton cells are degraded, intracellular DMSP is released into the water column. It then breaks down by marine microbial enzymes (DMSP lyase) to produce the trace sulphur-containing gas, DMS (Buckley & Mudge, 2002). DMS accounts for more than 50% of the total biogenic sulphur entering the atmosphere, therefore, by releasing DMS, phytoplankton play a key role in biogeochemical cycle of sulphur. When DMS crosses the sea-air interface and enters the atmosphere, it is oxidized by OH to form SO_2 and methane sulphonic acid (MSA) in the presence of high UV radiation (Sinha et al., 2007). SO_2 can then oxidize to sulphuric acid (H_2SO_4); both H_2SO_4 and MSA condense to form aerosols. Aerosols can directly influence the climate by scattering sunlight and resulting in reduced atmospheric visibility, and indirectly by acting as cloud condensation nuclei (CCN) (Yu et al., 2006). CCN are atmospheric particles that are soluble and sufficiently large to take up water vapour and form cloud droplets by serving as nuclei (Quinn & Bates, 2011). CCN abundance in the atmosphere affects the sensitivity of clouds to reflect solar radiation back to space and therefore alter planetary albedo which results in cooling of the Earth's surface (Shaw, 1983; Buckley & Mudge, 2002). The CLAW hypothesis,

proposed in 1987, suggested that production of DMS could have a role in regulating the climate since cloud albedo is sensitive to the CCN density. In other words, phytoplankton that are exposed to high irradiance or high sea surface temperatures may emit higher amounts of DMS which increase CCN formation and therefore decrease the amount of solar radiation reaching the Earth (Hatakeyama, Izumi, & Akimoto, 1985; Sinha et al., 2007). Reducing solar radiation results in changing the speciation and abundance of phytoplankton and in turn reduces irradiance and temperature; this is known as negative climate forcing. However, Quinn and Bates, 2011 reported that this process been recently shown to be more complex than what the claw hypothesis suggested 20 years ago. Figure 1 is the modified DMS climate regulatory negative feedback loop.

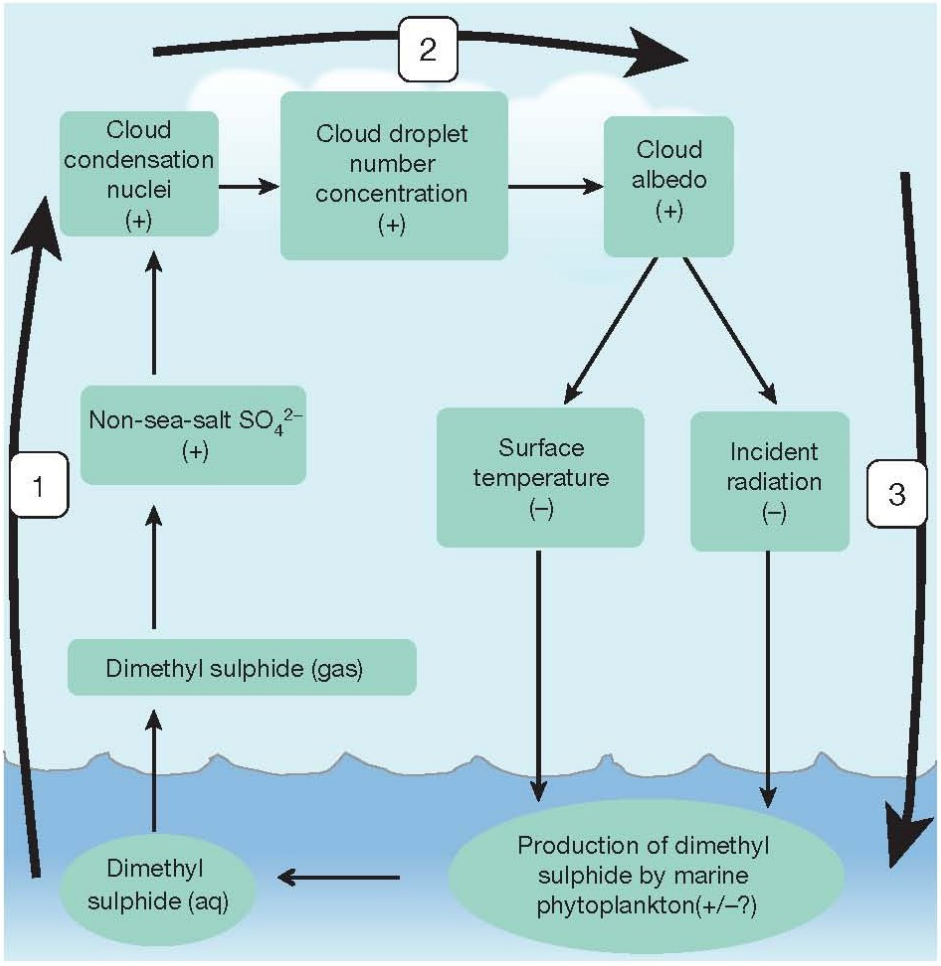

Figure 1. An illustration of the climate regulatory feedback by marine sulphate emissions. Adapted from "The case against climate regulation via oceanic phytoplankton sulphur emissions" by P. K., Quinn, and T. S., Bates, 2011, *Nature*, *480*(7375), 51-56. Copyright 2011 by Macmillan Publishers Limited

2.4 Particulate Matter

Marine biogenic VOCs are an important source of secondary organic particulate matter, or secondary organic aerosols (SOA) (Gibson et al., 2015). Airborne particulate matter is hugely important in mediating climate (formation of clouds), earth ecosystems (wet and dry deposition), and heath (acute and chronic diseases). Particulate matter is a mixture of

organic and inorganic substances derived in primary or secondary forms from anthropogenic and natural sources. It includes solid and liquid particles which are directly emitted to the atmosphere in the form of dust, pollen, smoke, soot, and fine aerosols (Harrison, Deacon, & Jones, 1997; Gibson et al., 2009b). Particulates are categorized into different size fractions and it is suggested that the toxicological effects are determined by PM size, number, and chemical composition (Gibson et al., 2009b), e.g. total suspended particles (TSP), coarse particles, PM_{10}, respirable $PM_{4.0}$, $PM_{2.5}$, PM_1, ultrafine (<0.1 μm). $PM_{2.5}$ and PM_{10} are those with median aerodynamic diameter of less than or equal to 2.5 μm, and less than or equal to 10 μm respectively (Harrison et al., 1997; Gibson et al., 2013b Gibson et al., 2009b). SOA are produced by secondary formation through photochemical reactions of pollution gases such as the byproducts of fuel combustion (SO_2 and NO_X) and NH_3 (Ostro & Chestnut, 1998; Kroll & Seinfeld, 2008). Organic aerosol (OA) is a major component of the fine particulate matter; it comprises both primary and secondary organic aerosol (SOA). SOA accounts for a large fraction of both terrestrial and marine tropospheric aerosol (Robinson et al., 2007). The main source of PM in Nova Scotia is long-range transport (>75% of the PM mass concentration) that originates from the NE US and the Windsor-Québec corridor (Gibson et al., 2015; Gibson et al., 2010). Local sources include combustion of fossil fuels for power, space heating and transport, biomass burning, construction activities, sea salt, re-suspended surface dust, and ship emissions (Gibson et al., 2013b). Wildfires in North America can also subsequently impact downwind atmospheric composition, i.e. surface level of $PM_{2.5}$ (Palmer et al., 2013; Franklin et al., 2014; Gibson et al., 2015). WHO estimates that PM pollutant is ranked the 13th leading cause of mortality in the world with 4.3 million

premature deaths attributable to household air pollution in 2012 (Anderson, Thundiyil, & Stolbach, 2012).

2.5 Measurement of Trace Reactive Gases

2.5.1 Integrated VOC Sample Collection

Volatile organic compounds in ambient air can be collected by three different methods; use of an evacuated canister, passively sampled onto a sorbent bed, or actively by pumping air through sorbent tubes or bubbled through a liquid housed in an impinger device with a liquid that will either trap or react with the VOC of interest. Thermal desorption tubes (TDT) have been used for decades, as an alternative standard method to whole air sample (WAS) canisters (also known as SUMMA canisters), for the sampling of VOCs in air (USEPA, 1999; Brown & Purnell, 1979; Schmidbauer & Oehme, 1988; Wai-mei Sin, Wong, Sham, & Wang, 2001). The advantage of using TDT over WAS canisters is that the tubes are small and can be readily transported to and from Sable Island for long-term monitoring of VOCs. WAS canisters are too bulky to be easily transported by aircraft, and the autosampling instrumentation is too large to make sampling practical on Sable Island. In addition, another advantage of using thermal desorption tubes is that each TDT can be reused at least three hundred times before the sorbent material needs to be replaced, providing a significant cost advantage. In addition, cleaning WAS canisters with helium becomes expensive over the long-term. Storing WAS canisters also becomes an issue as they are bulky. Another advantage of using TDT is that they can be stored in the refrigerator at 4°C for up to 3 years, whereas WAS canisters needs to be analyzed within one week.

2.5.2 Gas Chromatography

There are three types of GC detectors: i) non-specific detectors (e.g. thermal conductivity detectors, TCDs) that respond to everything eluting from the column, ii) semi-specific detectors such as a flame ionization detector (FID) and photoionization detector (PID), and iii) specific detectors, which are element selective, e.g. electron capture detector (ECD) (halogens) and flame photometric detector (FPD). Despite the high sensitivity of some of these detectors, the addition of a mass spectrometer (MS), i.e. GC-MS, provides a better option due to its ability to accurately identify the VOC of interest with sensitive limits of detection. In addition, the GC-MS also uses augmenting features such as chemical ionization (CI), multiple ion monitoring (MIM) or selective ion monitoring (SIM), or MS/MS (Belmont et al., 2011). The single quadruple mass analyzer of the GC-MS uses selective ion monitoring (SIM) mode to easily distinguish between GC co-eluting compounds (with different m/z molecular fragments) or deuterium-labelled and non-labelled analogues, as used in this study. Selective ion monitoring, as the name implies, 'homes in' on a m/z molecular fragment that is specific to the VOC of interest and within the retention time window associated with that compound (Harris, 2007). Moreover, GCs are fitted with capillary columns that come along with the introduction of a technology for producing fused silica replacing packed columns. Previously, packed columns had lengths of 6' to 10'; however, the newer capillary columns are being produced in lengths of 15 to 105 meters. The column internal diameter is very small compared to the 2 to 4 mm i.d. packed columns. The capillary columns have i.d.'s of 0.10 to 0.75 mm. Some of the larger i.d. capillary columns are actually filled with solid support, PLOT columns, but most are simply coated on the inside with a thin film of

stationary phase. The stationary phase is chemically bonded to the inside walls of the fused silica tubing. The outside of the column is coated with a polyamide coating for better durability. Polydimethyl siloxane is a common "backbone" for creating different stationary phases. Replacing methyl groups with other groups changes its polarity and separation capabilities (Dorman & Dawes, 2012).

2.5.3 Near-Real Time Measurement of VOCs

Near real-time VOC measurements include total-VOC measurement by flame ionization or photoionization (e.g. Thermo 55i or ppbRAE), VOC measurement by proton transfer reaction-mass spectrometer (PTR-MS) (Holzinger, Jordan, Hansel, & Lindinger, 1998), or air server-Unity-2 TD-GC-MS (AS-TD-GC-MS) with temporal resolution raging from 6 seconds (PTR-MS) to 1-hr (AS-TD-GC-MS) respectively. The Thermo model 55i is a gas chromatography system that uses (FID) to measure VOCs. A Thermo 55i was previously deployed by Hayes (2014) to measure methane and non-methane hydrocarbons on Sable Island from March 2013 through to December 2014. However, the study has abandoned the 55i instrument for VOC measurement, replacing it with a photoionization detector due to its superior detection limit and that the ppbRAE does not require hydrogen which is problematic to transport to the island by aircraft.

2.6 Source Apportionment

To protect the environment and human health by developing effective pollution reduction methods, the drivers of temporal variation of TRGs emission sources and attribution at a given receptor must be established. The source apportionment process, also known as receptor modelling, provides theoretical and mathematical framework, which aids in quantifying emission source contributions (Anjali, 2004; Guo, Wang, & Louie, 2004;

Hayes, 2014; Kim & Hopke, 2004). It is a multivariate least squares statistically-based model (Ramadan, Eickhout, Song, Buydens, & Hopke, 2003; Gibson et al., 2015). The first step in source apportionment modelling is to find the total VOC concentration and determine the contributing VOC species to total VOCs from the field then use other evidence, e.g. visible satellite images, airmass back trajectories, or long-range chemical transport models, to identify the source (Gibson et al., 2013b; Trivitayanurak, Adams, Spracklen, & Carslaw, 2008). Hence, all applications of those models require in situ active or passive ambient air sampling, with or without the need to conduct post sample laboratory analysis to speciate VOC sample data. In addition, other gases, land use features and weather metrics can prove helpful in the source identification step of the modelling (Johnson, Isakov, Touma, Mukerjee, & Ozkaynak, 2010). After the species are inputted into the model the 'source' of the air pollution is first identified by known source chemical markers found within 'factors'. Next, the source contribution is determined by apportioning the source of the VOC identified in each factor, to the total VOC concentration observed at the receptor, e.g. Sable Island.

Some of the common multivariate least squares factor analysis receptor models used for source apportionment of VOCs and PM include the US Environmental Protection Agency's (USEPA) PMF, APCS, and CMB (Gibson et al., 2015).

2.6.1 Positive Matrix Factorization (PMF)

PMF modelling has been previously used by many studies including a study performed by Song et al., (2001) which looked at apportionment of VOCs to understand the spatial and temporal trends in a rural area. Pires et al. (2007), on the other hand performed source apportionment using a different receptor model, the principal component analysis (PCA),

to monitor air pollution and for efficient air pollution management. The purpose of these receptor models is to simplify a data matrix of observations of a number of objects over a number of sources to develop an understanding of the relationship within the attributes (Hubert, Meulman, & Heiser, 2000; Gibson et al 2015). The PMF model, for instance, consists of speciated data of previously analyzed pollutant chemical constituents and an uncertainty file. After using the model to establish the correlations in the data provided, the data is broken down into two matrices: *source profiles* that outline the fingerprints (chemical species) for the source, and *source contributions* that determine the source contribution in percentage. Finally, by relating previous knowledge of the emission inventories, wind speed and direction, and the source markers to the source profiles, the various emission sources are identified (Norris et al., 2008).

2.7 Air Mass Back Trajectories

Air mass back trajectories are useful in the study as they augment PMF results in pollution source identification; they are used to compute air parcel trajectories for dispersion and deposition simulations model (HYSPLIT - Hybrid Single Particle Lagrangian Integrated Trajectory Model, 2016). The model used for this research is the Hybrid Single-Particle Lagrangian Integrated Trajectory (HYSPLIT) model. HYSPLIT has been used by Gibson et al., 2009b and Gibson et al., 2013b to investigate air mass histories, dispersion, deposition and transport for mapping air pollutant sources.

2.8 Remote Sensing

Moderate Resolution Imaging Spectroradiometer (MODIS) is an instrument operating on NASA Terra and Aqua satellites that provides high radiometric sensitivity in 36 spectral bands. MODIS views the surface of the Earth every 1 to 2 days and it acquires data

related to global aquatic, terrestrial and atmospheric dynamics and processes. Data collected by these satellites is used to develop models of the interactive Earth system and predict accurate global changes, which can play a role in improving policies for the protection of the environment (Geyh, Roberts, Lurmann, Schoell, & Avol, 1999). The visual images generated by Terra and Aqua MODIS can be used for identifying long-range transport of smog or wildfire smoke advecting from the continent or local marine smog during stagnant marine inversions, especially surrounding the oil and gas fields near Sable Island (Waugh et al., 2010; Hayes, 2014). The new NASA Visible Infrared Imaging Radiometer Suite (VIIRS) can also be used to collect visible and infrared imagery and radiometric measurements of the land, atmosphere, cryosphere, and oceans. VIIRS is capable of detecting algal blooms, climate impacts, and assessing primary productivity and ecosystem health in the ocean.

CHAPTER 3 MATERIALS AND METHODS

3.1 Site Description

Sable Island is an isolated and remote island located in the Atlantic Ocean, 290 km southeast of Halifax, Nova Scotia. The island is made up of sand dunes and sand bars, crescent-shaped, and is 42 km long. Figure 2 is a location map for Sable Island showing the distance of the island from Halifax, its size, and its location in the Atlantic Ocean.

Figure 2. Map showing the location of Sable Island. Adapted from "Source apportionment of the air quality on Sable Island" by A. Hayes. Copyright by Alex Hayes, 2014

Sable Island National Park Reserve, managed by Parks Canada, is the 43rd National Park created in Canada (Brauer, Blair, & Vedal, 1996). The island's transitional location between the pollution-influenced North American continent and the clean marine environment makes it an important site for climate monitoring by allowing continuous measurements of polluted airflow of the continent (Inkpen et al., 2009). It is also a good site for assessing biogenic marine emissions and their contribution to air pollution that are mostly resulting from phytoplankton bloom surrounding the Island shown in Figure 3 (Duderstadt et al., 1998). The island is also influenced by local pollution sources such as offshore oil and gas production, long-range transport, passing ships and on-island sources (Waugh et al., 2010).

Figure 3. Phytoplankton bloom around Sable Island. Image captured by NASA MODIS on the Aqua satellite on July 3, 2010. Adapted from *NASA*, retrieved from http://modis.gsfc.nasa.gov/gallery

Travelling to the island by air mainly depends on weather and beach conditions that are crucial for aircraft takeoff and landing. Due to the frequent fluctuations in these conditions, the site was visited only twice in the past year. The first visit to the island was a day trip in June 2015; the visit was strictly for transporting instruments to and from the island, and maintenance check. The second visit was a 5-day trip in September 2015 for instrumentation setup. The instrumentation was housed on the roof of the Parks Canada air chemistry monitoring station. Figure 4 and Figure 5 below are images of Sable Island taken in summer 2015.

Figure 4. Sable Island beach in June 2015

Figure 5. Photo of Sable Island taken from aircraft

3.2 Thermal Desorption Tubes

Thermal desorption tubes (TDT) were the chosen method for remotely and automatically sampling VOCs over a 24-hr and over a 1-month period on Sable Island.

To analyze a broader range of VOCs, a multi-bed TDT, known as 'Soil Vapor Intrusion™' (SVI) tube from PerkinElmer was utilized on Sable Island. The SVI is a 3½" long x ¼" external diameter stainless steel tube sealed with brass Swagelok caps (containing a special GC-MS rated PTFE ferrule) on both ends (Figure 6). The tubes are filled with four sorbents to trap gaseous phase gases in the boiling point range that includes chloroform through to semi-volatile compounds such as pyrene. The four sorbents are patented but are carbonaceous and likely to be similar to a carbon molecular sieve, graphitized carbon black and activated carbon sorbents. Alternately, another TDT from PerkinElmer known as Tenax shown in Figure 7 was used to run test and blank tubes. It is made up of a single, polymeric, hydrophobic, sorbent bed. Being only one sorbent, Tenax is less capable of retaining a wide range of VOCs but is especially good at trapping benzene, toluene, ethylbenzene and xylene boiling point ranges.

Figure 6. SVI thermal desorption tube from PerkinElmer

Figure 7. Tenax thermal desorption tube from PerkinElmer

3.3 Multitube Sequential Sampler (MTS-32)

The VOC samples were collected onto the SVI TDTs via a MTS-32 (Markes International, UK) automated, multitube sequential sampler (the instrument subject to contractual delay). The MTS-32 autosampler holds up to 32 TDT, allowing sequential active sampling onto a series of sorbent tubes by drawing the same volume of air at constant flow rate through each tube for a specified period of time, in our case 1-month of daily samples. The sample flow rate was set to 30 mL/min using a digital flow meter. One capped TDT was also kept in the MTS-32 box as a control. The flow rate was checked at the end of the sampling to determine if there was any sample flow error. To avoid passive sampling and loss of retained samples, the tubes were sealed with diffusion-locking inserts known as DiffLok™ caps (MTS-32 User Manual, 2015). DiffLok caps aid in sealing the tubes at ambient pressure, only allowing gas flow through and onto the TDT when pressure is applied. They consist of a threaded stainless steel cap that has long, multichannel, helical pathways from the ambient air to the TDT sorbent, which in the process eliminate passive diffusion of vapors into and out of the tubes, yet still allowing pumped sampling when a tube is in the sampling port position (TDTS 61 Application

Note, 2009). Figure 8 shows the placement of the MTS-32 on the roof of the air chemistry monitoring station on Sable Island in Figure 9.

Figure 8. MTS-32 on the air chemistry monitoring station on Sable Island

Figure 9. The Air Chemistry Monitoring Station on Sable Island

3.4 Post-Sample Analysis

After sample collection on Sable Island, the TDTs were returned to the laboratory for analysis using both Markes International Unity-2 thermal desorption-Thermo 1300 gas chromatography-Thermo ISQ mass spectrometry systems (TD-GC-MS) (Figure 10).

Figure 10. TD-GC-MS system setup showing the nitrogen and helium gas supplies.

The Unity-2 thermal desorption (TD) unit shown on the far right of both systems in Figure 11, thermally desorbs the VOCs from the sample TDT and then re-traps and focuses the VOCs onto a Markes International air toxics cold trap as illustrated in Figure 12. The air toxics cold trap is then heated in a stream of ultrapure helium that transports the VOCs onto a capillary GC column for chromatographic separation. The Thermo ISQ

single quadrupole MS is finally used for VOC identification and quantification (Woolfenden, 1997).

Figure 11. Markes International Unity-2 thermal desorption-Thermo 1300 gas chromatography-Thermo ISQ mass spectrometry systems (TD-GC-MS)

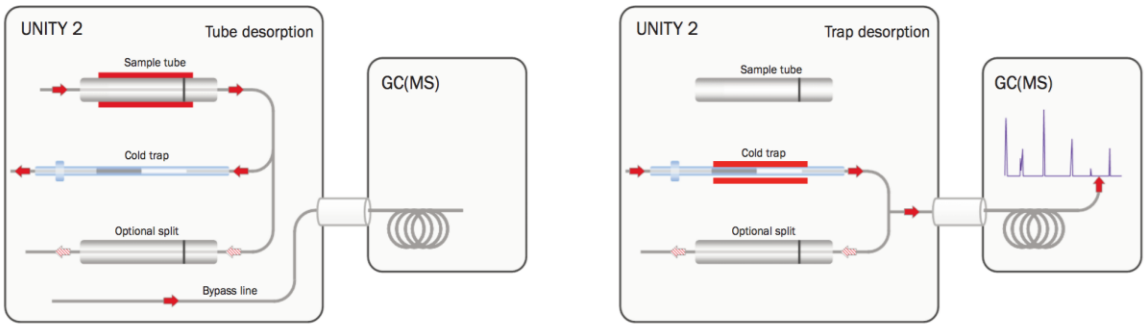

Figure 12. Schematic of carrier gas flow during sample tube (left) and focusing trap (right) thermal desorption on the Unity-2 system. Adapted from *Unity 2 Operators' Manual*, 2012

Each of the Thermo Trace 1300 GCs was fitted with Rtx®-VMS GC capillary column with a proprietary Crossbond® stationary phase. The first GC was fitted with an Rtx®-VMS capillary column of 40 m length, 0.18 mm internal diameter, and 1.0 µm thickness. The second GC was fitted with a 60 m length column, of 0.25 mm internal diameter (i.d.), and 1.0 µm thickness.

3.5 Method Development

Considerable method development was needed in order to optimize the VOC separation, identification and quantification of individual peaks. As the two TD-GC-MS systems were not fully installed properly, or full training given, there were delays in being able to analyze samples. After two service and training visits by Thermo engineers and applications specialists the systems were set up correctly and adequate training provided.

3.5.1 External and Internal Standards Preparation

Seven NIST certifiable, primary VOC external calibration standard mixes (8260B Calibration Mega Mix #1 and 502.2 Calibration Mixes #1-6) and three deuterium labeled internal standards (1,2-dichloroethane-d4, chlorobenzene-d5, and 1,2-dichlorobenzene-d4) were purchased from Restek. The external standard (mega calibration mix) contained 76 compounds ranging from diethyl ether to 1,2,3-trichlorobenzene and was used to identify compound retention times. It was also used to quantify VOCs in samples by calculating response factors. The other six 502.2 calibration standard mixes contained a range of VOCs with the most volatile being dichlorodifluoromethane in Mix #1 and least volatile being 1,2,3-trichlorobenzene in Mix #6. These mixes were used for instrument method development while testing for optimum oven temperatures and oven ramps as well as other GC-MS parameters. The concentration of the mixes was 2000 μg/mL in purge-and-trap grade methanol. Each standard mix ampule was inverted several times before breaking the tip off to re-dissolve gases in the headspace. The primary standard mixes were immediately transferred into 1 ml, pre-cleaned, amber vials. These transferred primary standard mixtures were then dated and either stored at 4°C in the fridge or at 25°C in a freezer. Then, a second set of vials was labeled the same way but with concentrations of 1000 μg/mL. Using the 100 μL syringe, 100 μL of HPLC grade methanol was transferred into the second set of vials. Next, a 100 μL of the calibration standard mixes were added by immersing the syringe into the methanol while making sure methanol and all the vials in use are kept on ice packs to remain cold. A third set of vials was labeled with concentrations of 100 μg/mL, and pipetted with 900 μL of methanol using 1 mL pipette and 100 μL of the 1000 μg/mL mixes. Finally, a fourth set

of vials labeled with 10 µg/mL was pipetted with 900 µL of methanol and 100 µL of the 100 µg/mL mixes. All standard vials were stored in the freezer (Figure 13).

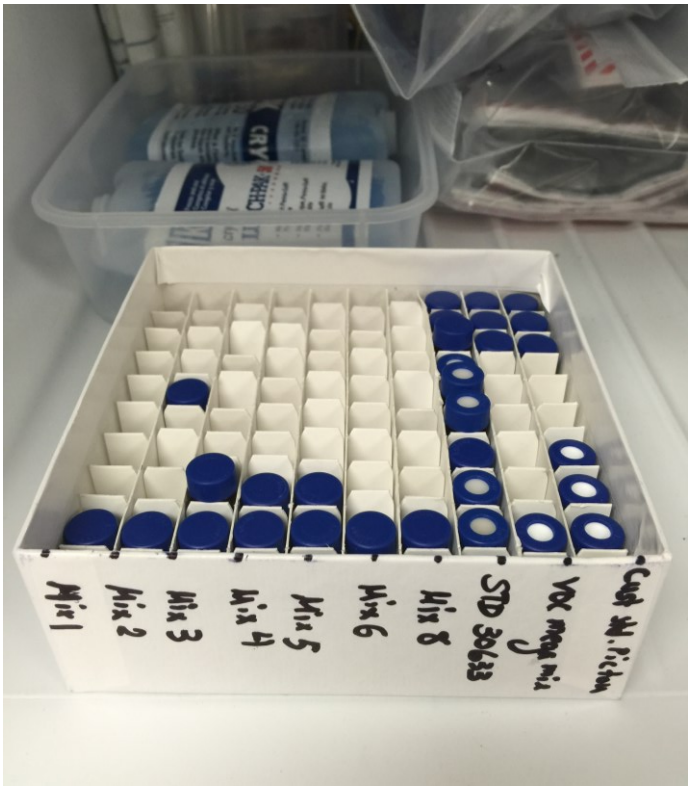

Figure 13. Internal standards and external calibration standards stored in the freezer

A Markes' Calibration Solution Loading Rig (CSLR) connected to helium gas supply was used to load the standards into the sorbent tubes. Conditioned TDT were first placed into the CSLR. Gas flow through the CSLR and TDT was maintained at 50 mL/min using a needle valve, volumes of 2 µL, 5 µL, and 10 µL of the 10 µg/mL calibration standards were individually injected with 10 µL precision syringes onto the attached tubes. The tubes were kept attached to the rig for 3 minutes to allow helium to purge out excess methanol used during the serial dilutions.

3.5.1.1 Deuterium-Labelled Internal Standards

The proposed approach for this research was to use deuterium analogues as internal standards since they are inert to the samples are not found in nature. This was complemented by deploying automated SIM (autoSIM) to monitor two to three selected ion pairs derived from the targeted analytes and their isotopic analogue, i.e. deuterium analogue. Extensive work has been done using AutoSIM, however, due to software complications, manual identification and integration had to eventually be applied. The use of internal standard calibration method aims to correct for errors that might stem from sample preparation, handling, and introduction into the GC. By adding a labelled analogue, deuterated in this case, of known amount, 50 ng, to the daily sequence of samples and standards analyzed on the GC-MS, the deuterated analogue should experience the same changes as the targeted analyte in the external standard (Klee, n.d.). The internal standard would correct for day-to-day changes in MS responses since the resulting pre-determined relative response factors (RRFs) remained constant. In addition, this approach would quantify the unknown concentrations of the sample constituents. By running all three internal standard simultaneously on single TDTs, it was concluded that the least volatile standard, 1,2-dichlorobenzene-d4, was the best potential choice for the analysis. The RRF between the internal standard (Analyte A) and the sample or external standard (Analyte B) is typically determined by analyzing the two analytes simultaneously within the same TDT (Rome & Mcintyre, 2012). Without autoSIM, the approach was not attainable because the deuterium-labelled analogue 1,2-dichlorobenzene is chemically identical to its non-labelled analogue which was collected in our samples. In this case, the analogues would co-elute as a single non-separated peak.

With future improvements to this approach, the analyte response factors would be calculated by determining the peak areas and concentrations of the analytes (Rome & Mcintyre, 2012).

$$Response\ Factor = \frac{Peak\ area}{Concentration}$$

The response factors were then used to calculate the RRF between the two target analytes A and B (Rome & Mcintyre, 2012).

$$Relative\ Response\ Factor = \frac{Reponnse\ Factor\ for\ Analyte\ A}{Response\ Factor\ for\ Analyte\ B}$$

Furthermore, once the RRF is established, an unknown concentration of a targeted sample analyte (Analyte B) can be determined in the presence of a known concentration of (Analyte A) (Rome & Mcintyre, 2012).

$$Concentration\ A = \frac{Peak\ area\ A}{Peak\ area\ B} \times Concentation\ B \times \frac{1}{RRF}$$

3.5.2 GC-MS Instrumental Settings

From the Thermo XCalibur homepage, 'Instrument Method' was selected to adjust the default method settings. For the ISQ series settings as shown in Figure 14 below, the 'Method Type' was set to Acquisition -General, the 'Ionization mode' was set to EI (i.e. Electron Ionization), and the 'Run completion' was set to GC run time. The 'MS transfer line temperature' was to 250°C and 'Ion source temperature' were set to 300°C. By

increasing the temperature in each successive zone of the GC, it was ensured that volatiles in one section remained volatile in the next. This prevented analytes condensing onto the walls of the transfer line or ion source and therefore prevented peak broadening in the resulting chromatograms. In the 'Scans' table, the mass range was set to 35-300 mu at scan time 0.2 seconds for 2.00 minutes.

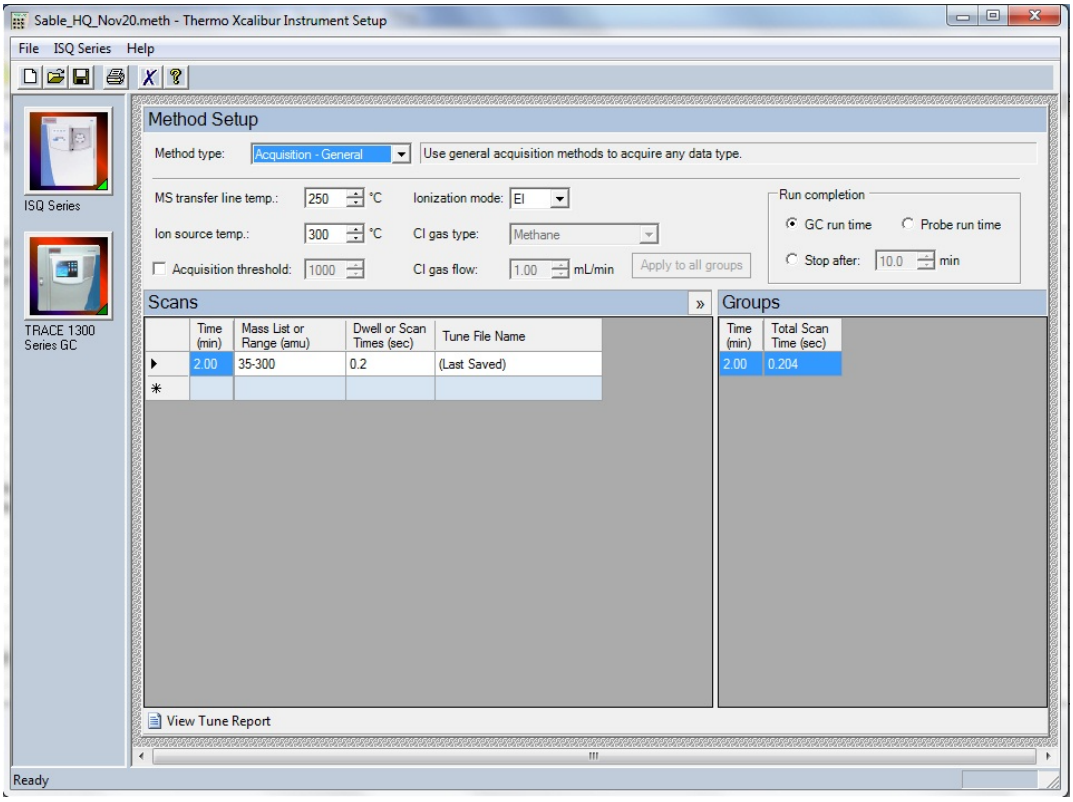

Figure 14. ISQ series instrument settings.

For the Trace 1300 Series GC, the flow rate and the GC oven temperature program for both GC-MS systems were determined using the EZGC Method Translator and Flow Calculator software; this was downloaded from the Restek-Pure Chromatography site (http://www.restek.com/ezgc-mtfc). The Method Translator generates methods based on

selection of “Efficiency”, “Speed”, “Translate”, or “Custom” in Results. For both GC-MS systems, oven temperature program from EPA Method 524.2 was updated through “Efficiency” by assuming that the optimum flow rate for the first system is 1.01 mL/min and 1.4 mL/min for the second. Different methods were compared before selecting the final results by looking at the corresponding chromatograms generated and the run times. Selection depended mostly on the best shape of peaks and most efficient time GC runs to save helium gas and reduce cost.

The GC oven ramps for the 40 m and 60 m columns were set as shown in Table 5 and Table 6 below.

Table 5. Oven ramp settings for GC fitted with the 40 m column

#	Rate (°C/min)	Temperature (°C)	Hold Time (min)
Initial		45.0	6.55
1	8.4	100.0	1.45
2	17.3	240	1.9

Table 6. Oven ramp settings for GC fitted with the 60 m column

#	Rate (°C/min)	Temperature (°C)	Hold Time (min)
Initial		45.0	8.25
1	7.1	100.0	0
2	13.4	240	2.45

As shown in Figure 15, the oven ‘Max. temperature’ was set to 240 °C, the ‘Prep-run timeout’ to 999.0 min, ‘Equilibration time’ to 0.5 min, ‘Ready delay’ to 0.00 min. Next, under the S/SL (front) tab shown in Figure 16, the ‘S/SL mode’ was set to Splitless, and the ‘Carrier mode’ to Constant flow. In the ‘Inlet’ box, the ‘Splitless time was set to 50.0

min. In the ‘Carrier flow’ box, the ‘Flow’ for the first system was set to 1.01 mL/min and 1.4 mL/min for the second. In the ‘Carrier options’ box, the ‘Vacuum compensation’ was checked. In the ‘Septum purge’ box, the Purge flow’ was set to 20.0 mL/min and ‘Constant septum purge’ was checked before finally sending the method to the GC.

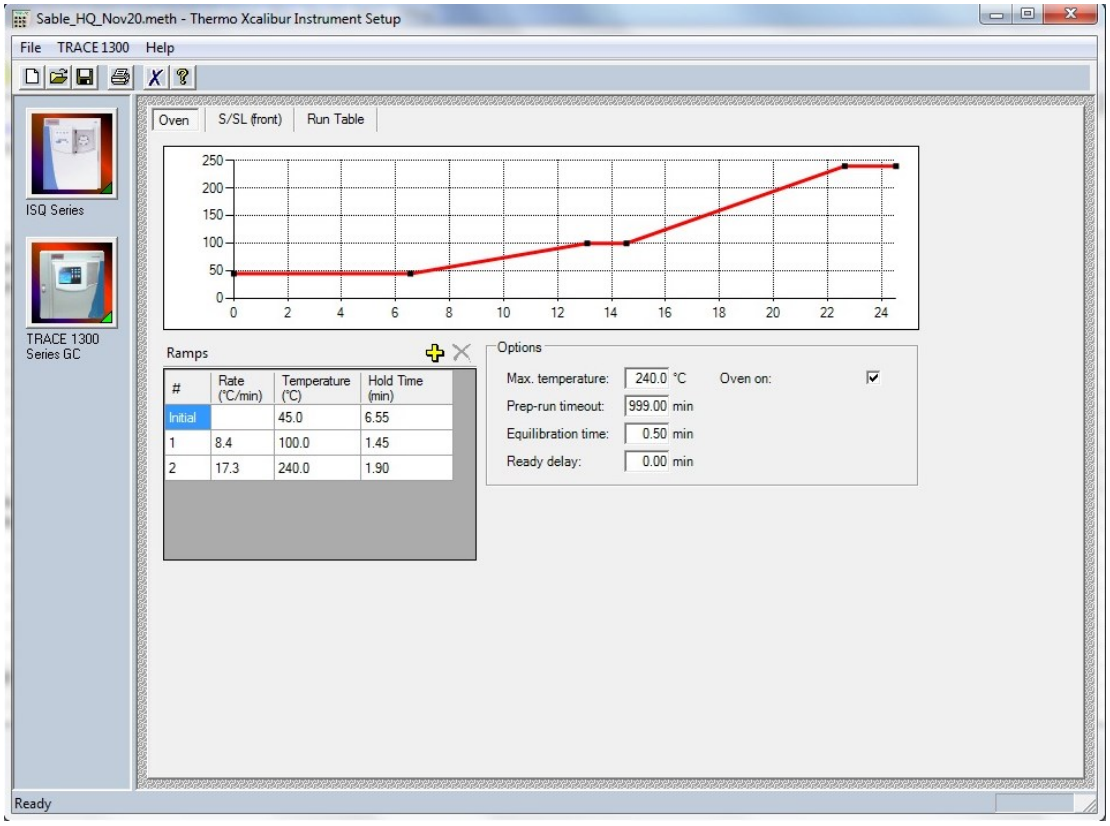

Figure 15. Trace 1300 Series GC oven settings

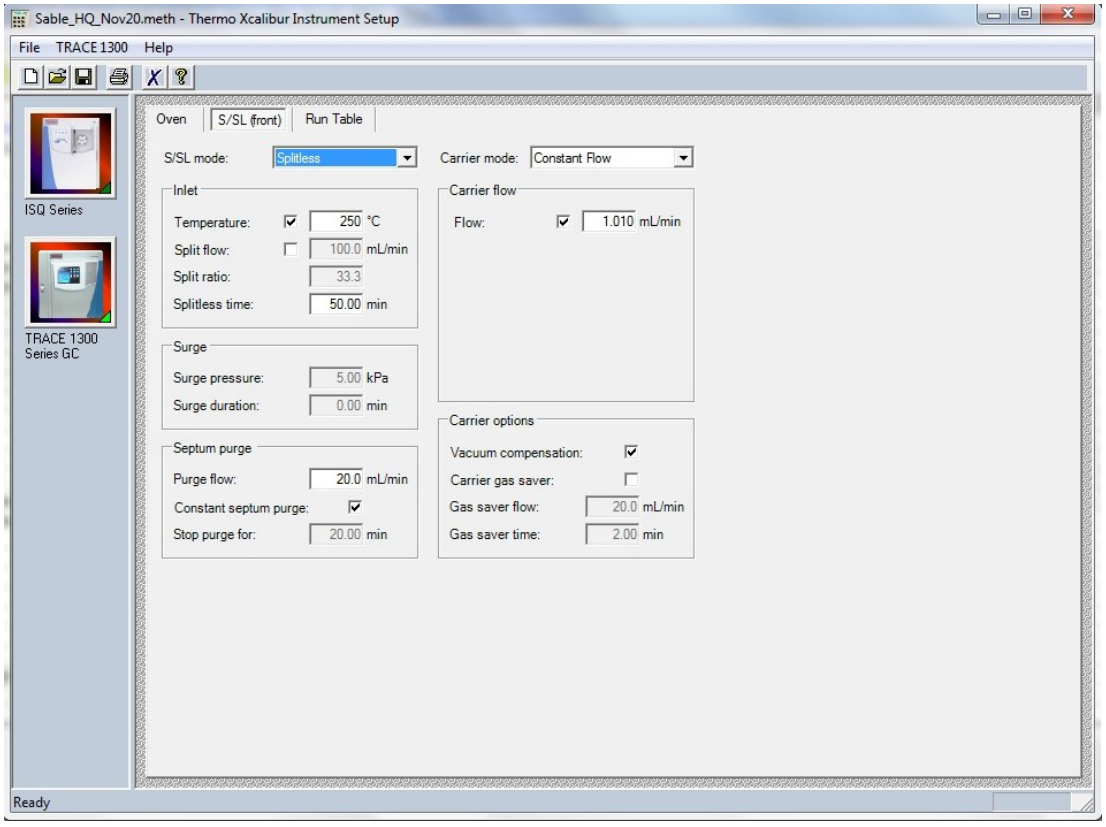

Figure 16. Trace 1300 Series GC Split/Splitless injection settings

3.5.3 Unity-2 Instrumental Settings

Similar to the GC setup, a thermal desorption method was also established using the Markes software as provided in the Figure 17-Figure 19.

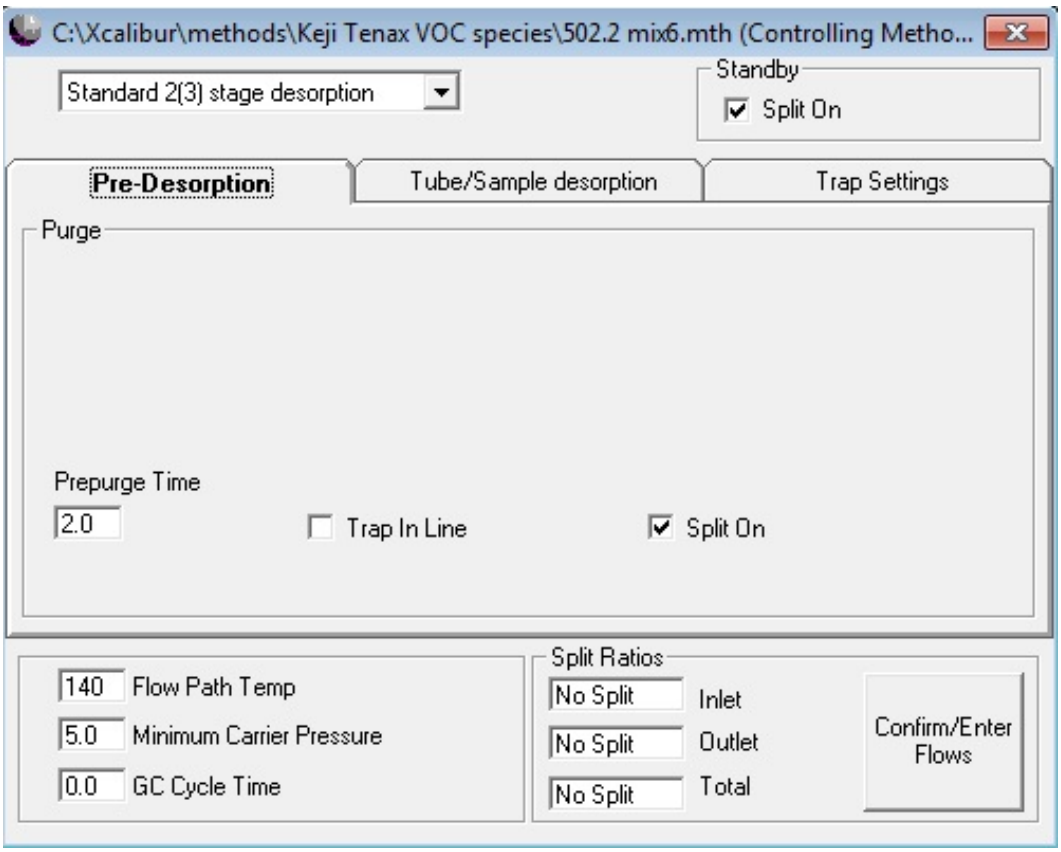

Figure 17. Unity-2 pre-desorption settings

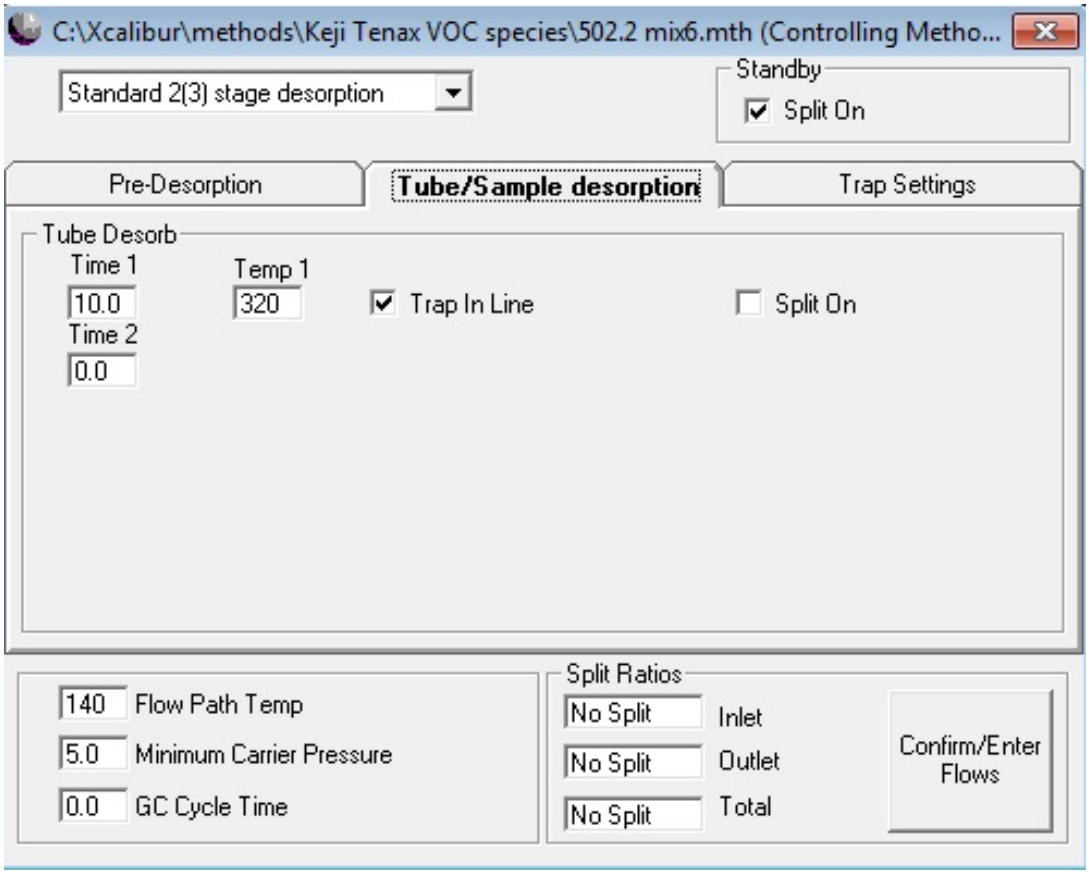

Figure 18. Unity-2 tube desorption settings

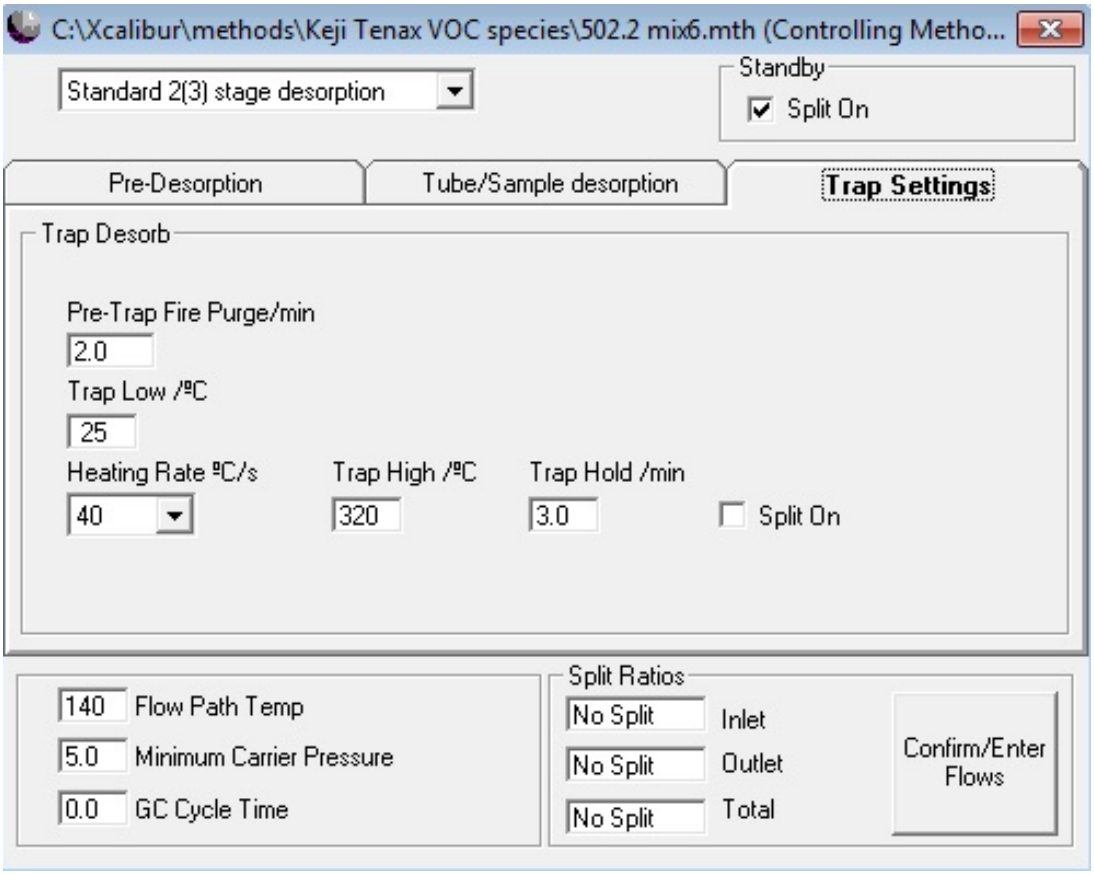

Figure 19. Unity-2 trap settings

3.6 Loading and Running Thermal Desorption Tubes

Both thermal desorption units were purged with Ultra-pure Nitrogen and Helium (carrier gas) set at 50 psi pressure using an attached regulator valve. The first step for loading a tube into the Unity-2 thermal desorber was removing the brass Swagelok caps from both ends of the TDT and loading the tube into the unit with the ringed side of the tube facing the back of the instrument. This allows the flow of the carrier gas to be reversed to the direction of sampling flow in order to desorb the less volatile compounds into the unit first. For every analysis batch of sample and standard TDTs, a new acquisition sequence was set up using the Thermo Xcalibur 'Sequence Setup' module within Xcalibur Software. Each sample/standard row in the sequence was selected individually and processed by clicking the Run Sample button in the toolbar. As soon as the Trace 1300 and ISQ status read 'Waiting for Contact Closure', the run button on the Unity-2 software was then selected. A leak check on the Unity-2 was automatically performed for each tube before desorbing the sample and collecting onto the cold trap. After each run, the TDT was removed from the Unity-2, recapped, and set-aside until conditioned for re-use. At the end of the analysis process, the last tube analyzed was usually left in the Unity-2 to maintain a closed system until the next analysis day. When finally done, the Nitrogen gas toggle valve on the baseplate was turned off.

3.7 Identifying a Compound

In order to build a custom library for our study, compounds in standards had to be identified through the 'Qual Browser' in XCalibur software (Figure 20).

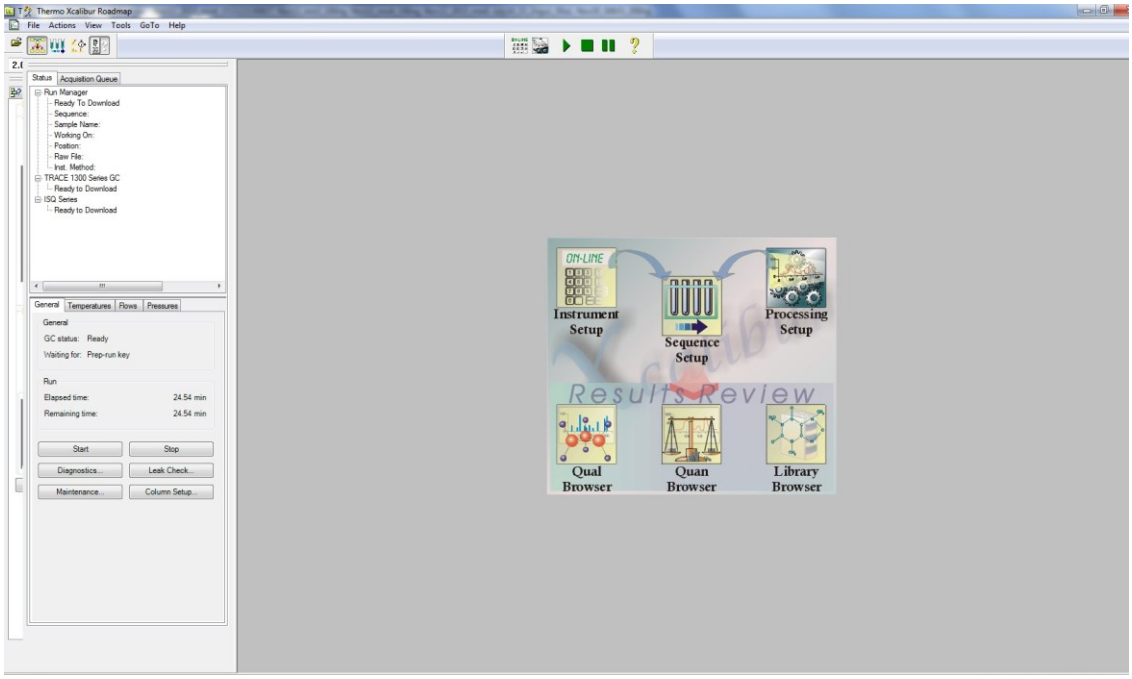

Figure 20. Thermo XCalibur Roadmap page

Six raw data files of different standard tubes that had already been run were used to find the retention times of the VOCs. For each file, the background ranges on the chromatogram were removed by right-clicking on the spectrum window and selecting 'Remove Background' then 'Ranges'. Two areas in the chromatogram window were then selected near the start and end signals of a compound peak. The compound (e.g. Figure 21) was then identified by clicking and dragging the mouse under the peak, approximately 1/3 the peak signal above the baseline, then right-clicking in the spectrum window and selecting 'Library' and 'Search'. The latter step opened a popup window with a list of compounds that matched the spectrum along with the probability of the match as shown in Figure 22. Typically, matches above 25% were considered a good match.

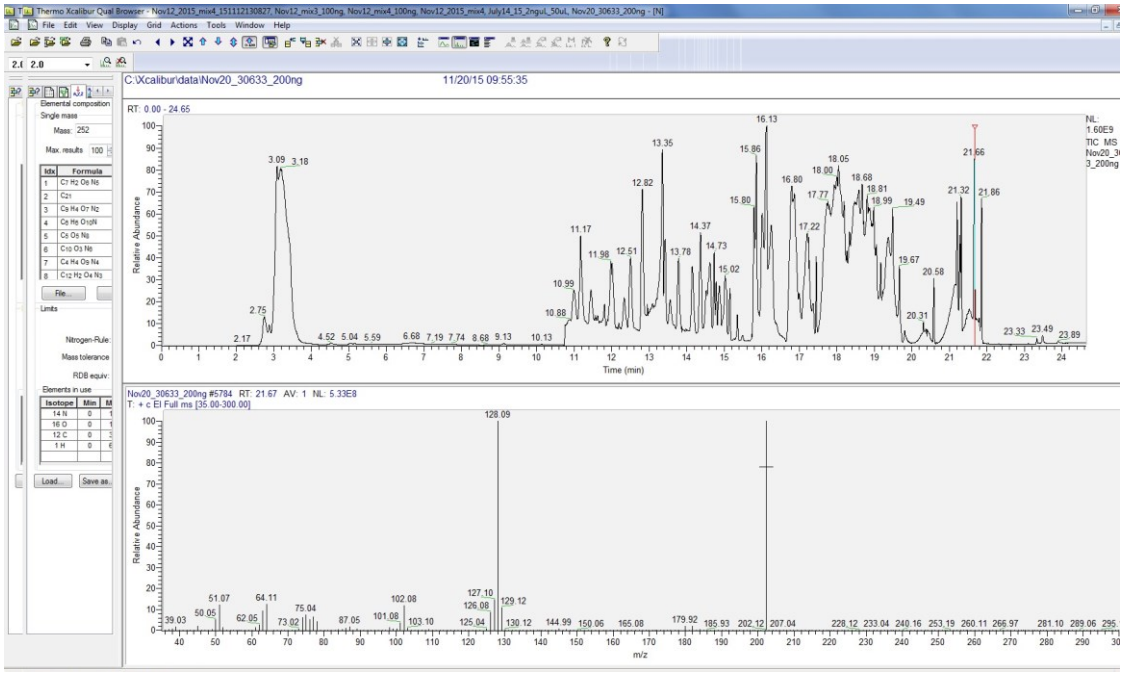

Figure 21. A chromatogram of the mega mix external standard diluted. Mass spectrum from the peak at retention time 21.67 min suggests a compound with molar mass of 128.08 g/mol

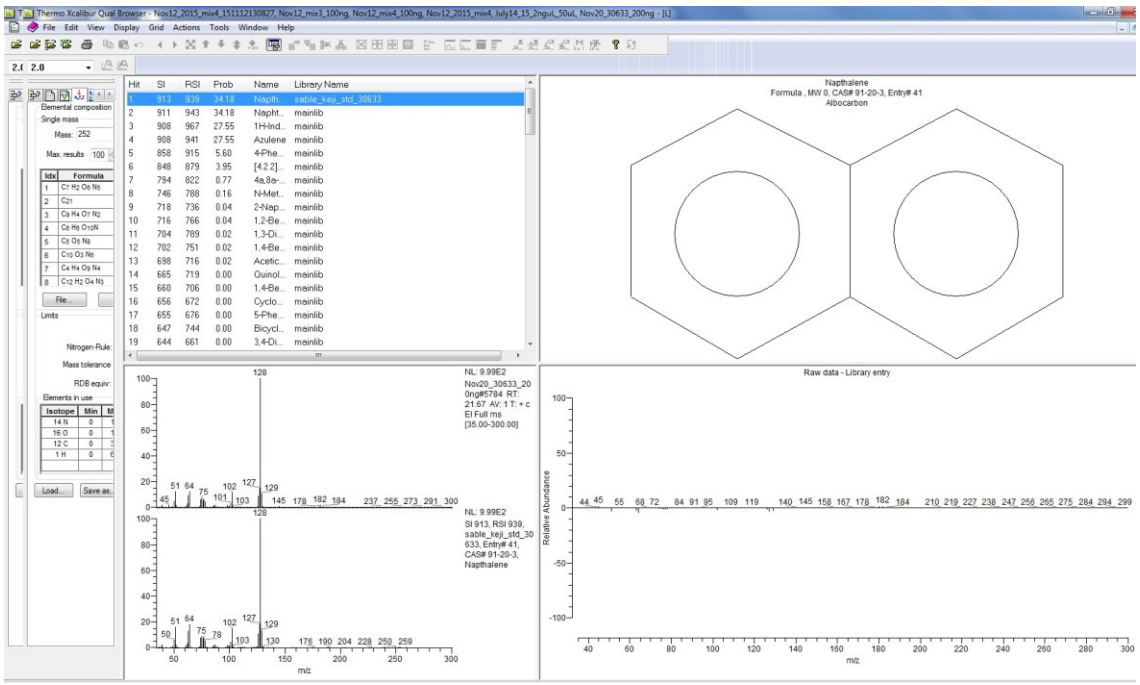

Figure 22. The pre-built library identifies the compound (i.e. Naphthalene) based on its retention time and molar mass

3.7.1 **Creating and Building the Library**

When using a specific protocol repeatedly to look for the same compounds, it is worthwhile to establish a library of those compounds based on that protocol. This way, the spectra used to identify the compounds is more targeted towards the protocol used instead of a general protocol that may result in a lower match frequency. A library for the specific VOCs analyzed over Sable Island was built using built-in libraries in XCalibur software by clicking on 'Library Browser' in the 'Roadmap' screen then on 'Librarian' tab and 'Create Library'. In order to build the library, the chromatograms of the six standards were opened in Qual Browser to import their constituents into the library. The background ranges for each peak in the chromatograms were removed in order to better

identify the spectra of the desired compound using the existing libraries in XCalibur. Once a compound was confirmed as the one desired, it was exported to the library by right-clicking on the spectra window and choosing 'Library' and 'Export to Library Browser' followed by 'Prepend' instead of 'Overwrite' to avoid deleting the original software data. In the 'Library Browser' window, the 'Librarian' tab was selected to find the newly imported spectra from the list of compounds. By clicking on 'Edit Spectra' icon, the relevant information for each compounds was entered (i.e. name, chemical formula, and CAS# to further include metadata such as chemical structure). Once all the compounds are edited, the 'Add to Library' icon was selected to add the spectra to the library created for Sable Island VOCs. The retention times of all the compounds present in the chromatograms of the six standards were recorded prior to establishing a processing method.

3.8 Establishing a Processing Method

In XCalibur homepage, 'Processing Setup' was selected to create a new processing method by clicking on the 'New' button. The chromatogram for each standard mix was imported by clicking on 'Open Raw'. In the identification tab shown in Figure 23, the name of each compound was entered in the 'Name' box by clicking the dropdown menu and selecting '<NEW>'. Based on the chromatogram selected, the retention times retrieved from Qual browser for all the compounds were entered as 'Expected time' in the 'Retention time' box. The figures below show the settings used for yielding the most accurate data. Note that in the 'Detection' tab, 'Genesis Peak Detection' selection was based on what detected the best peak area. For instance, 'Spectrum' was selected to identify the peak area for naphthalene, while 'Highest Peak' was selected for benzene,

and ‘Nearest RT’ for the more volatile compounds such as iodomethane. An example of the processing method settings for naphthalene is shown in Figure 23-Figure 27 below.

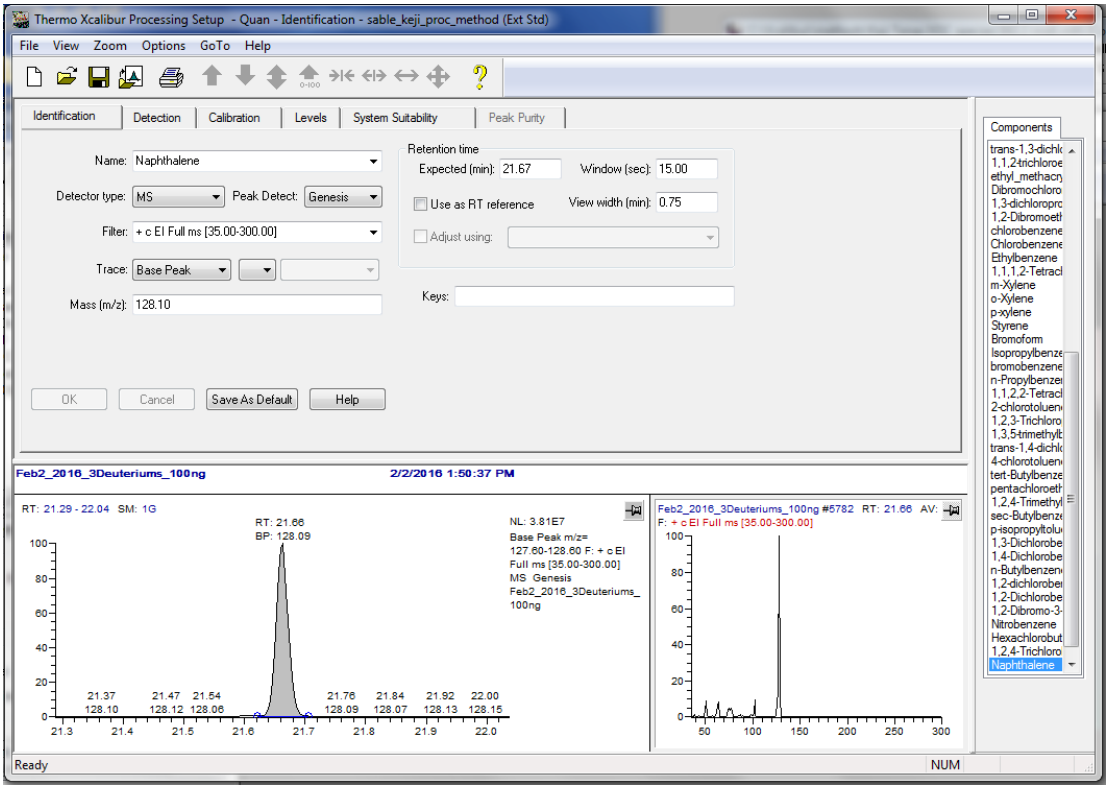

Figure 23. Identification settings for Naphthalene entered in the ‘Processing Setup’ page in XCalibur

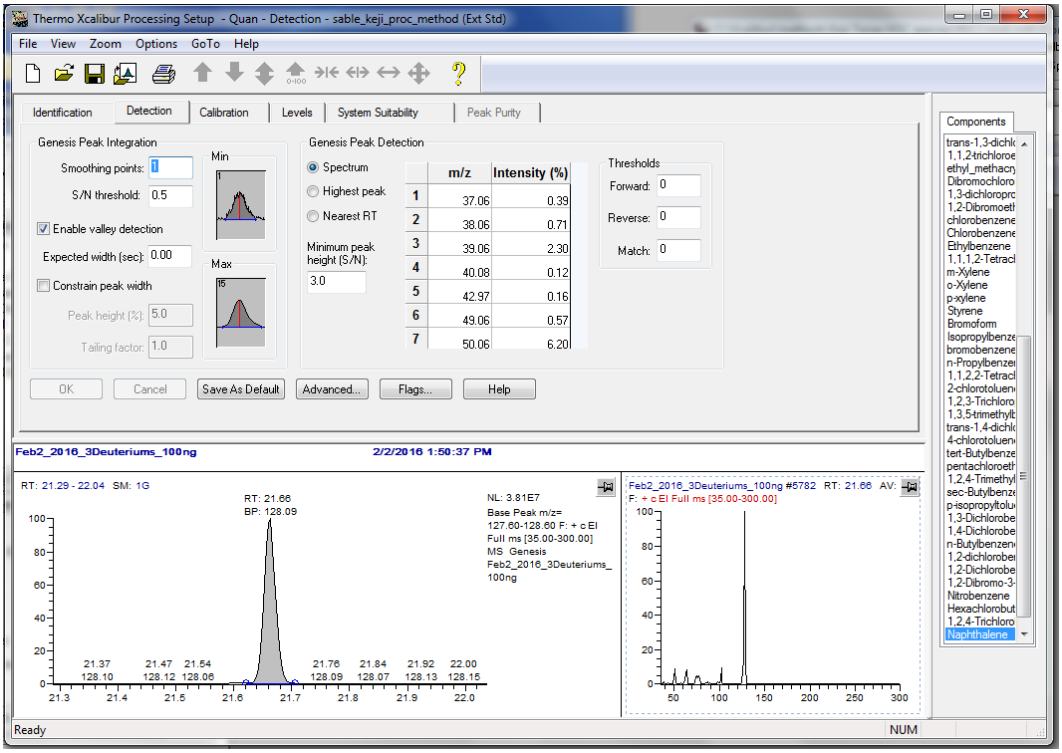

Figure 24. Detection settings for Naphthalene entered in the ‘Processing Setup’ page

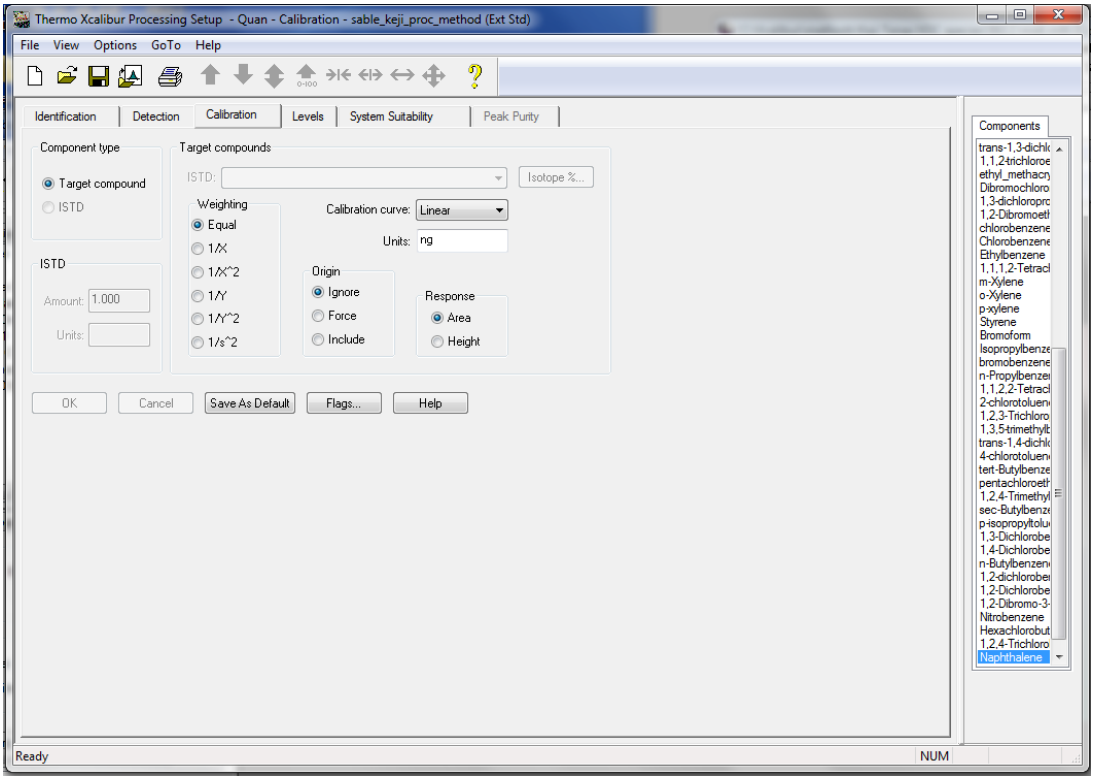

Figure 25. Calibration settings for all the compounds in the calibration mix entered in the 'Processing Setup' page in XCalibur

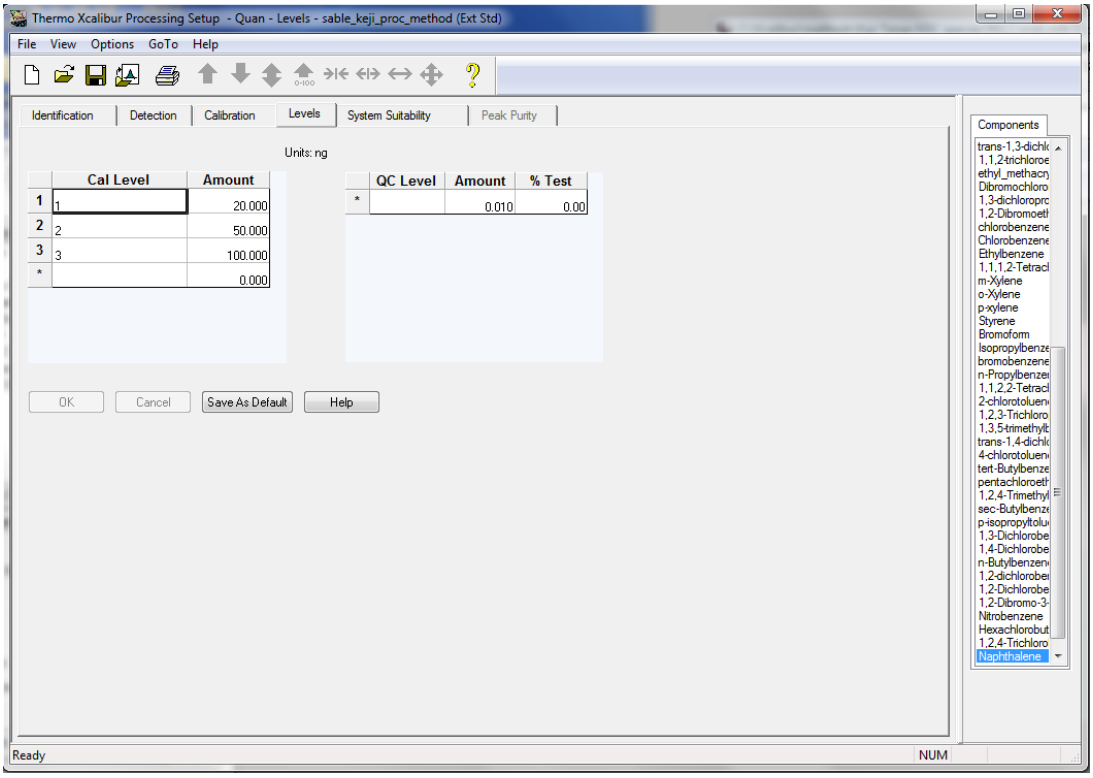

Figure 26. Calibration levels setup for all the compounds in the calibration mix

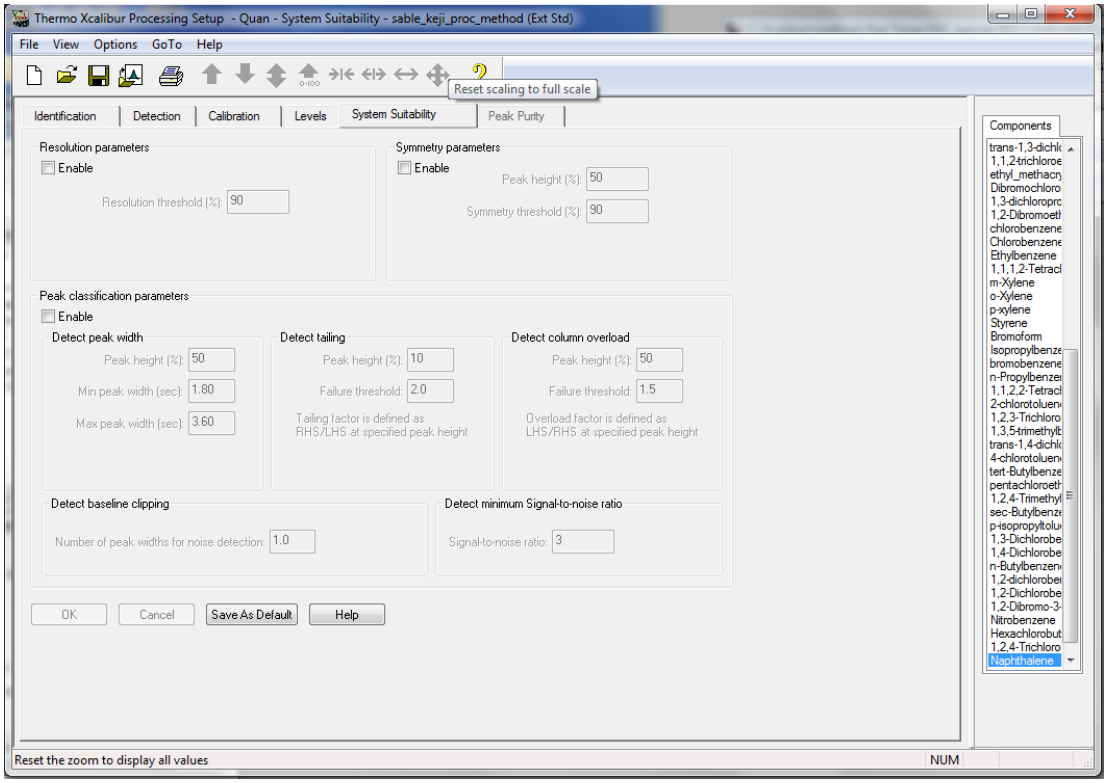

Figure 27. The ‘System Sustainability’ settings were left unchanged

3.9 Quantifying VOCs

After running a sequence of blank, standards, and samples, the data files in the sequence were reprocessed by selecting the 'Batch Reprocess' icon in the Sequence Editor Toolbar. This step aided in processing result files for quantifying and calibrating data as shown in Figure 28.

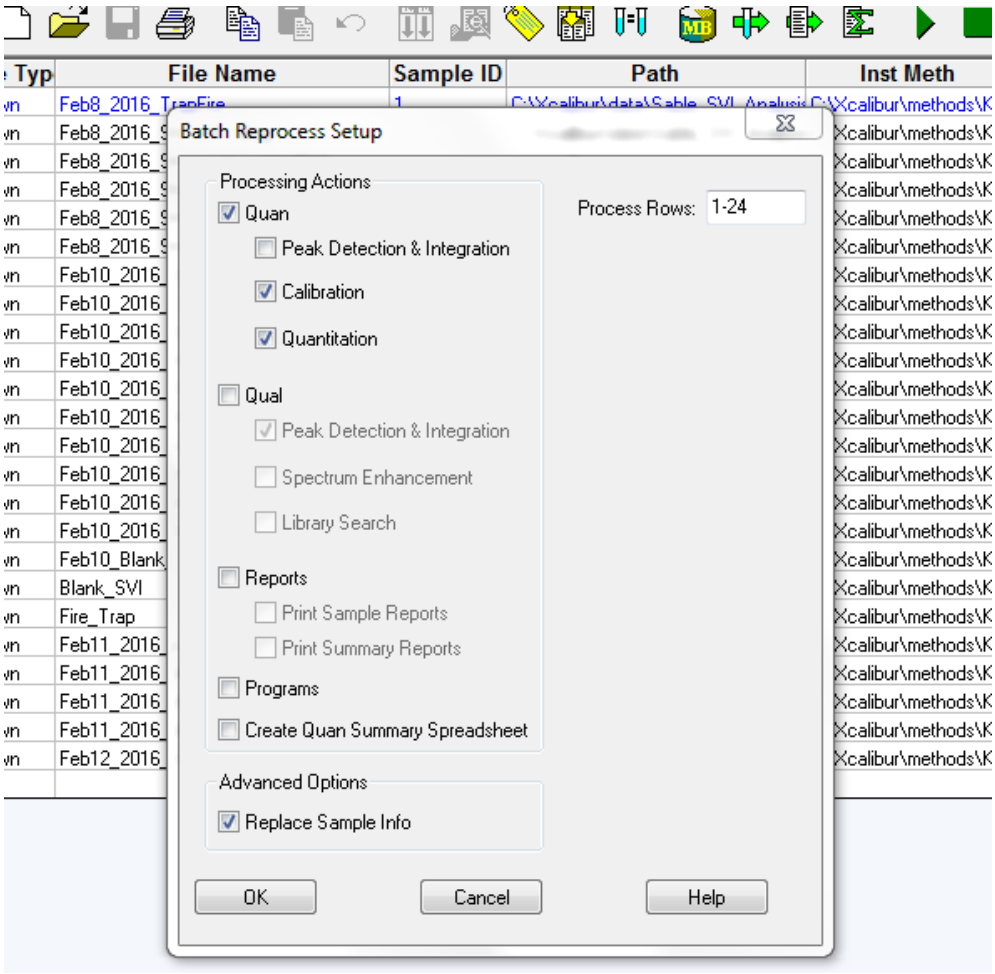

Figure 28. Batch reprocessing setup for a sequence of samples

Quan browser was used then to create calibration curves from standards run on the GC-MS and to quantify the compounds present in samples of unknown concentrations. By specifying the levels of the standards (i.e. '1' for 20 ng, '2' for "50" ng, and '3' for 100 ng), a calibration curve was automatically created as shown in Figure 29.

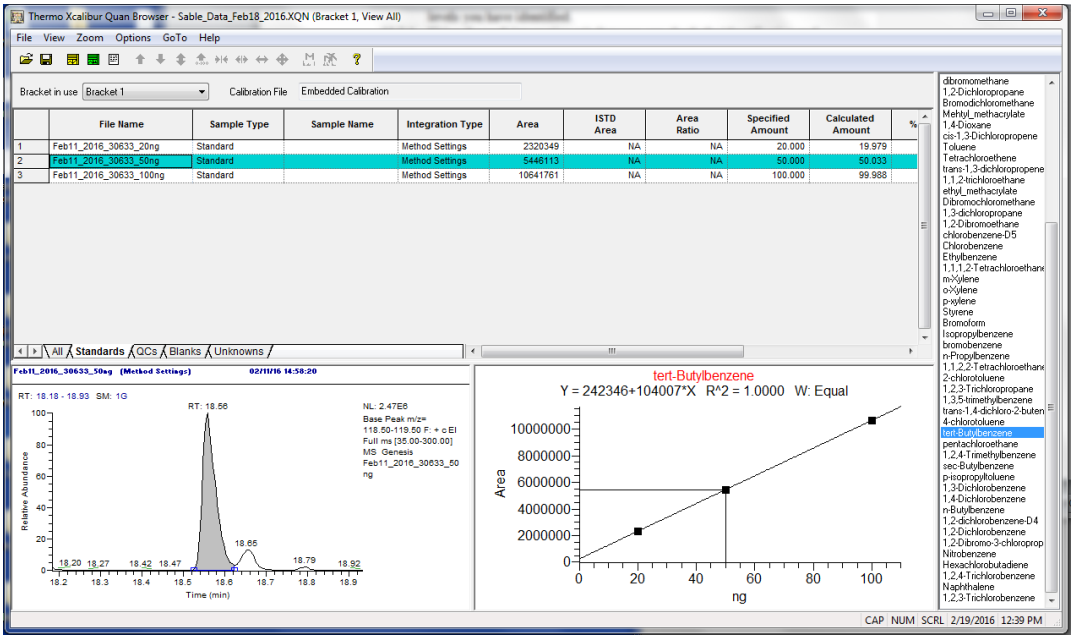

Figure 29. Integration curve of tert-butylbenzene of 50 ng of the calibration standard (lower right window) its calibration curve (lower left window)

The identity and integration of the compounds were confirmed in the peak integration window shown in the tert-butylbenezene example in Figure 30.

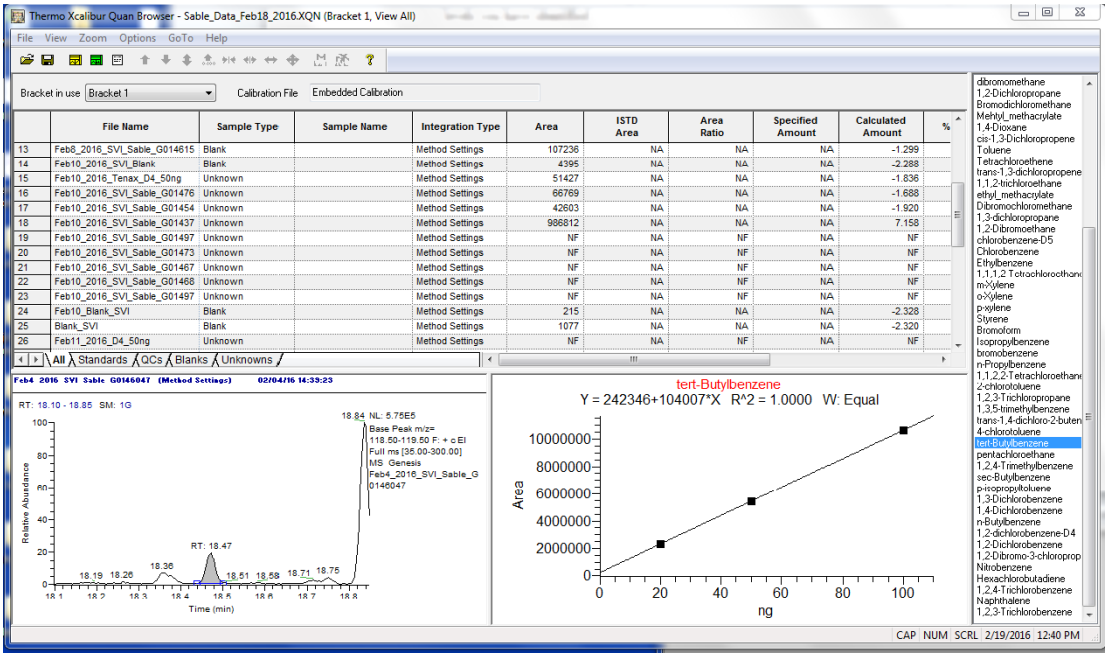

Figure 30. Integration curve of tert-butylbenzene from a sample (lower right window) and calibration curve of the three calibration standard levels '1' for 20 ng, '2' for "50" ng, and '3' for 100 ng (lower left window)

Finally, the metadata was exported to Microsoft Excel for further processing.

3.10 Equipment Malfunctions

3.10.1 Mass Spectrometer Ion Source Cleaning

Due to poor peak sensitivity, the ion source in one of our systems had to be removed and cleaned. The ion source cartridge was disassembled (Figure 31) and only the metal portion of the following Repeller assembly, Ion Volume, Lens 1, Lens 2, and Lens 3/RF Lens scrubbed with aluminum oxide slurry using a cotton-tipped applicator. The components were then rinsed with a toothbrush under a stream of running tap water to remove aluminum oxide slurry. Next, they were placed in a beaker with warm detergent solution and sonicated for 5 minutes, then rinsed with tap water and sonicated again with

de-ionized water for 5 minutes. Sonication was repeated with fresh deionized water until the water was clear – twice in this case. The components were sonicated in acetone for a minute and then transferred using clean forceps to another beaker with acetone and sonicated for another minute and left on a Kimwipe to dry. The Locking Ring, Repeller Spring, and Cartridge Sleeve were scrubbed with a warm detergent solution, rinsed with tap water, deionized water, and methanol respectively. The ion source cartridge components were then reassembled and fitted back into the ion source block of the instrument shown in Figure 32 (ISQ User Guide, 2012).

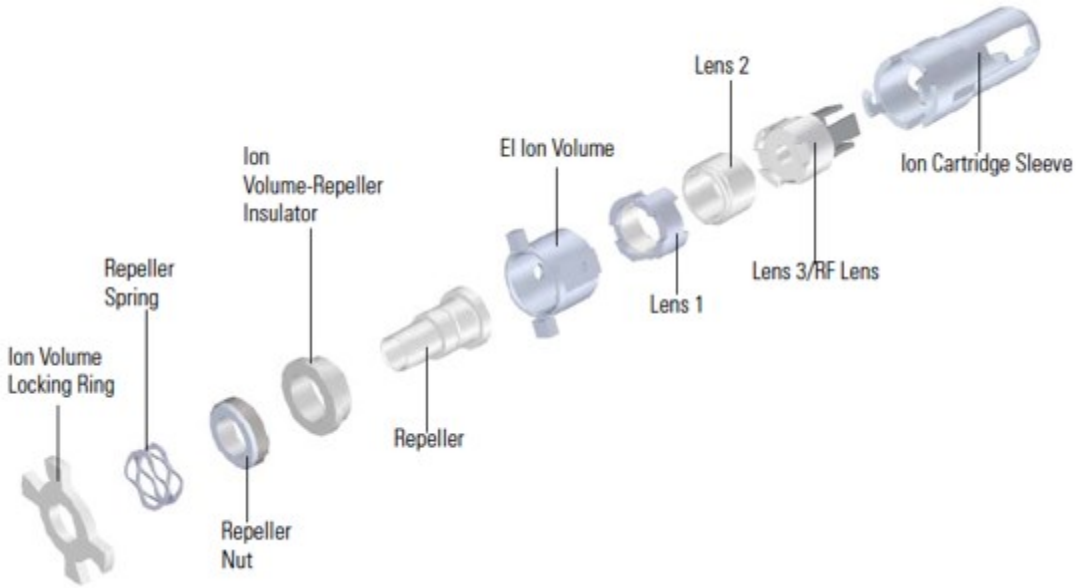

Figure 31. Ion source cartridge assembly. Adapted from *Thermo Fisher Scientific ISQ Hardware Manual*, 2012

Figure 32. Ion source block in the ISQ mass spectrometer.

3.10.2 Changing Tube Seals and Filters

It is common for tube seals and filters to wear out after extensive use. The O-rings should typically last for around 1000 tube-sealing operations and must be replaced in the event of failure. On February 11th 2016, the Unity-2 system failed the leak test, therefore, sample analysis had to be suspended until the issue was resolved. The Unity-2 operator manual was referred for the method to replace the O-rings and PTFE filters which sit behind the

O-rings in both sample tube seals in the instrument. After switching off the Unity system, the O-Ring extraction tool was used to hook out the O-rings and filter disks (Figure 33). New, clean filters followed by new O-rings were then pushed in with the O-Ring insertion tool shown in Figure 34.

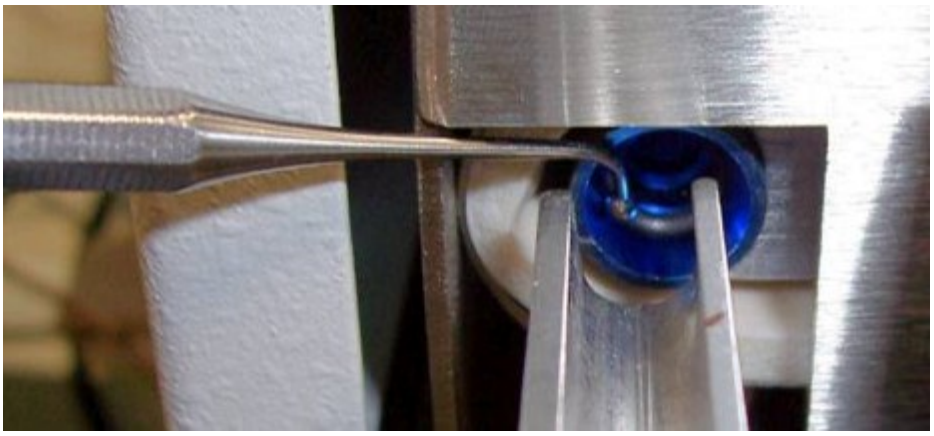

Figure 33. O-ring extraction tool used for pulling out O-rings fitted in the Unity-2 system. Adapted from *Unity-2 Operators Manual*, 2012

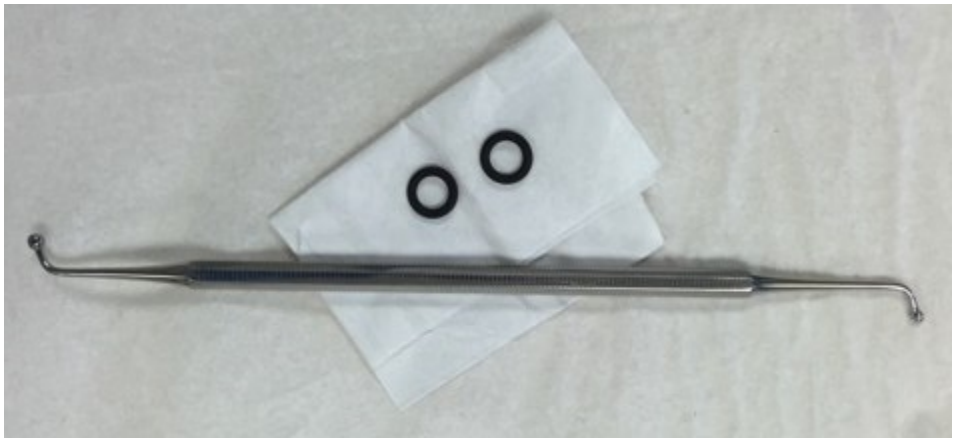

Figure 34. O-Ring insertion tool and O-ring.

Figure 35 shows the process of changing the O-rings in the Unity-2 instrument.

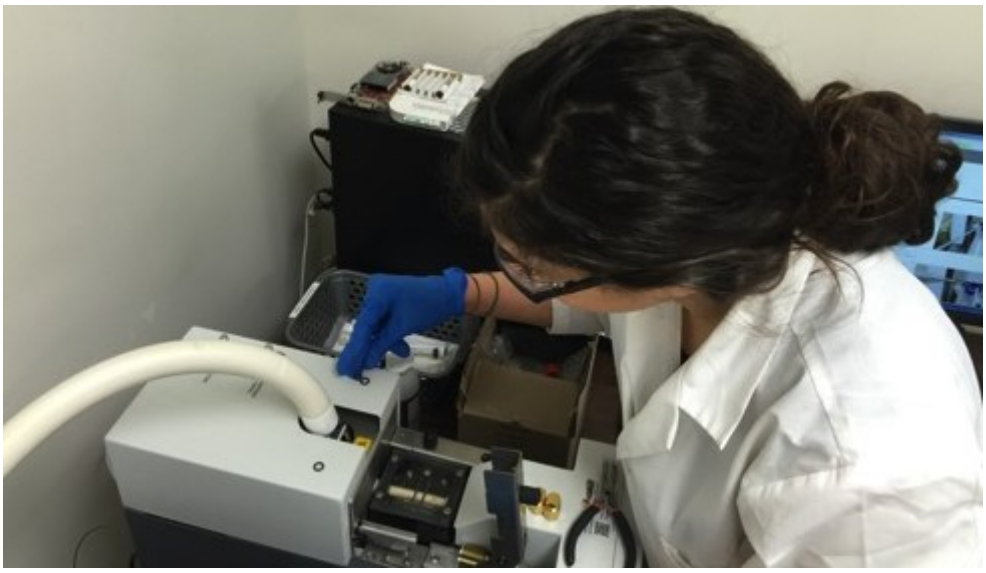

Figure 35. Replacement process of worn out O-rings in the Unity-2 (Photo courtesy of Codey Barnett)

CHAPTER 4 RESULTS AND DISCUSSION

4.1 Instrumentations on Sable Island

Table 7 provides detail of the gas emission monitoring equipment and instruments on Sable Island.

Table 7. Operating gas emission monitoring equipment on Sable Island

Equipment Name	Temporal Resolution	Installed	Operating	Operator	Original Sensor Funding/Replaced by (Date)
Original ESRF Funded Project (2003-2015)					
Equipment Shed	-	yes	yes	Dalhousie (2016 onwards)	ESRF
NO_x, Teledyne, Continuous Analyzer	1-hr	removed	no	NSE[1]>AFRG[2]	NAPS
SO_2 Teledyne Continuous Analyzer	1-hr	removed	no	NSE>AFRG	NAPS
O_3, Teledyne, Continuous Analyzer	1-hr	removed	no	NSE>AFRG	NAPS
H_2S, Teledyne, Continuous Analyzer**	1-hr	removed	no	NSE>AFRG	Encana
Current ESRF Funded Project (through to March 1 2017)					
VOC species auto tube samplers, Markes MTS-32 sequential sampler	24-hr integrated	yes	yes	AFRG	ESRF
ppbRAE	15-min	yes	yes	AFRG	AFRG
Data display website, data archive and threshold warnings	N/A	yes	yes	AFRG	ESRF

[1]Nova Scotia Environment, [2]Atmospheric Forensics Research Group

From Table 7 it can be seen that the temporal resolution for the majority of the instruments was 1-hour, apart from the ppbRAE that was 15 minutes. The VOC species were sampled as an average mass collected actively over 24-hours starting at 00:00 and running until 23:59.

4.2 General Air Quality

4.2.1 Meteorological Data

Table 8 below provides the descriptive statistics for the hourly meteorological variables from Sable Island for 2015.

Table 8. Descriptive statistics and data completeness for hourly 2015 meteorological variables from Sable Island

Variable	Temperature *[°C]*	Wind Direction *[°]*	Wind Speed *[km/h]*
n	8443	8760	8711
n missing	317	0	49
Mean	9.04	201.36	25.39
St Dev	7.20	98.96	12.60
Min	-11.4	0	0
25 pct	4.1	130	17
Median	8.9	220	24
75 pct	14.9	280	34
Max	53.8	360	84
IQR	10.8	150	17
Data Completeness (annual)	96.38%	100.00%	99.44%

From Table 8 it can be seen that the data completeness for the annual temperature, wind direction and wind speed was 96.38%, 100.00% and 99.44% respectively, which can be considered excellent data completeness. It can also been seen from Table 8 that the mean (min:max *units*) temperature and wind speed was found to be 9.04 (-11.4:53.8°C) and 25.39 km/h (0:84 km/h). The maximum temperature of 53.8°C seems unlikely, and may be a result of excess solar radiation heating from a nearby surface or the temperature sensor is faulty. It is recommended that the meteorological sensors be checked to determine if they require calibration or replacement.

4.2.2 Wind Roses

Figure 36 below provides a 2015 annual wind rose for Sable Island.

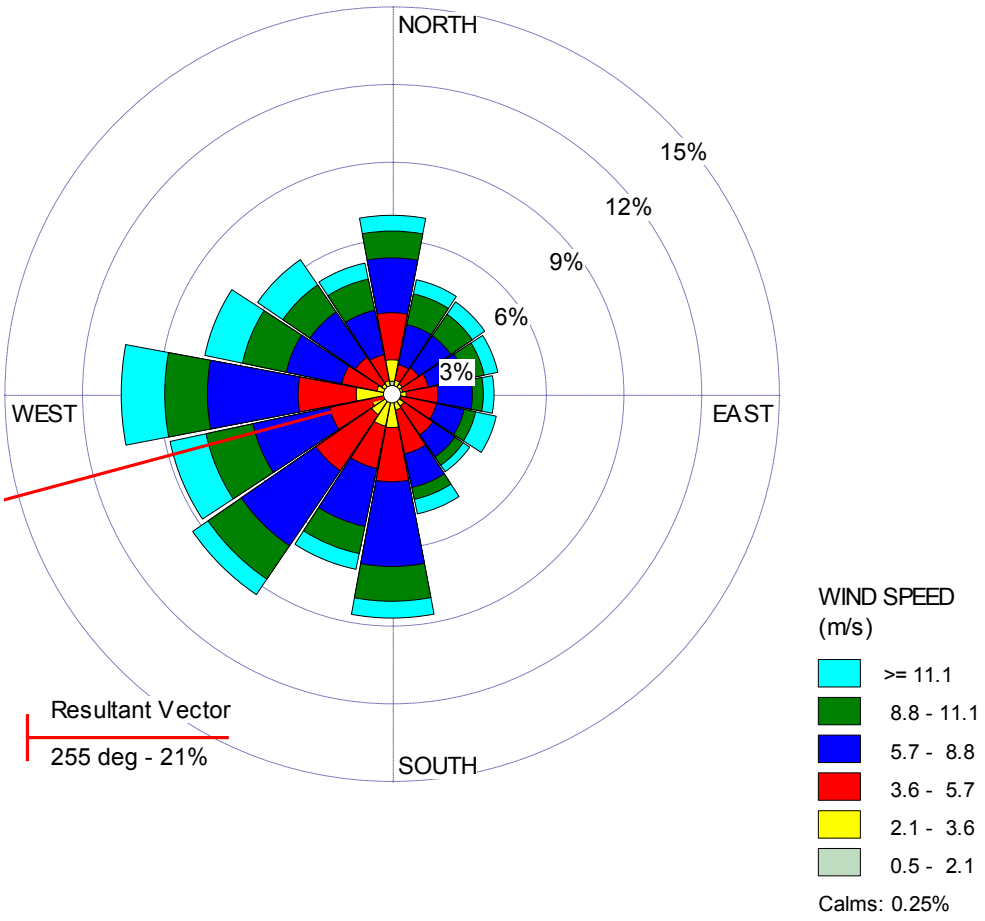

Figure 36. Sable Island 2015 annual wind rose

It can be seen from the resultant vector shown in Figure 36 that the annual average wind direction was blowing from 255°, which is consistent with the known prevailing wind in Atlantic Canada (Waugh, 2006).

Figure 37 is a wind rose for Sable Island during the sampling period between October 1st to October 31st, 2015.

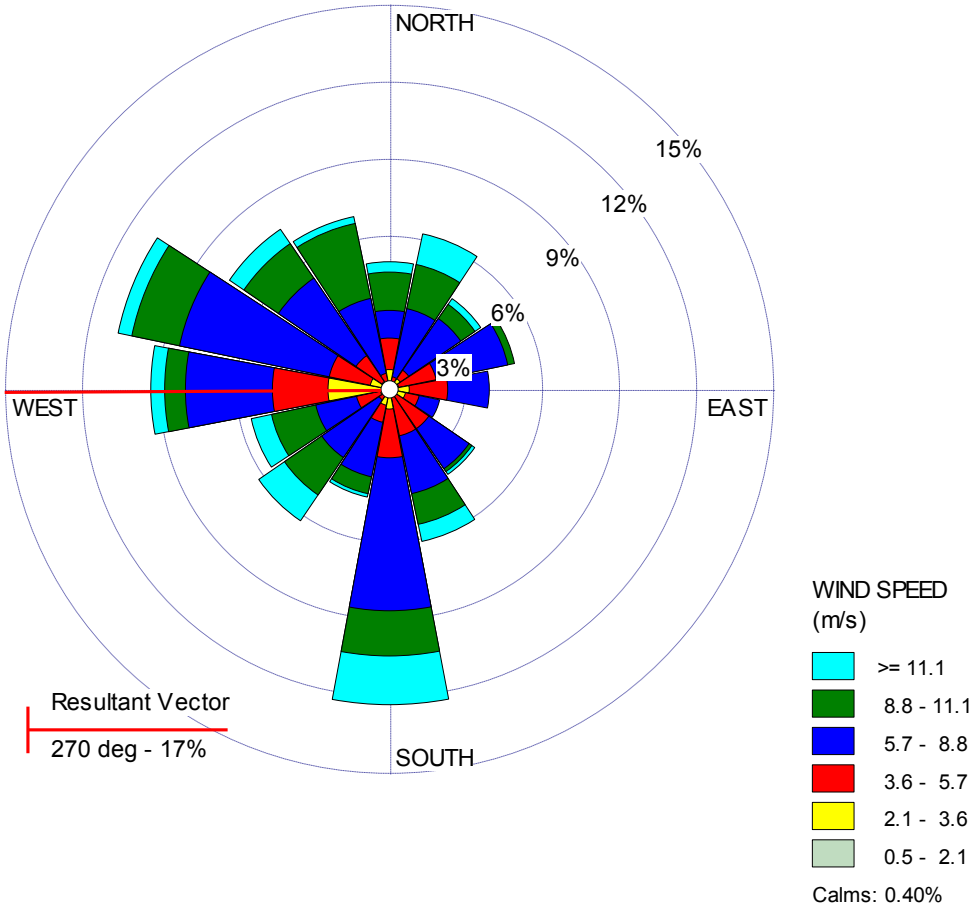

Figure 37. Sable Island wind rose covering the sampling period from October 1st to October 31st, 2015

It can be seen from the resultant vector shown in Figure 37 that the average wind direction for the month of October was blowing from 270°. As can be seen in Figure 37, when compared to the annual wind rose, there was a significant airflow from the South

between October 1st and October 31st, with winds above 11.1 m/s blowing for 1.5% of the time.

4.3 NOAA HYSPLIT Air Mass Back Trajectory Source Regions

In order to identify local and long-range upwind source regions, 5-day air mass back trajectories were run twice per day for the whole month of October. These appear in the Appendix. National Oceanic and Atmospheric Administration (NOAA) HYSPLIT runs were completed online at the following link http://ready.arl.noaa.gov/hysplit-bin/trajasrcm.pl. The trajectories are classified into 3 regions: North West North (NWN), North, and Marine.

Table 9 shows the likely emission sources of VOCs based on the 5-day HYSPLIT air mass back trajectories in Figure 58 in the Appendix. The trajectories are classified into 3 regions: North West North (NWN), North, and Marine.

Table 9. Trajectory source regions identified at the source location Sable Island based on the HYSPLIT model

Date ***[mm-dd-yyyy]***	**Trajectory Source Region**
10-01-2015	Marine
10-02-2015	Marine
10-03-2015	Marine
10-04-2015	North
10-05-2015	NWN
10-06-2015	NWN
10-07-2015	NWN
10-08-2015	NWN
10-09-2015	NWN
10-10-2015	NWN
10-11-2015	Marine
10-12-2015	Marine
10-13-2015	NWN
10-14-2015	NWN
10-15-2015	NWN
10-16-2015	North
10-17-2015	NWN
10-18-2015	North
10-19-2015	North
10-20-2015	North
10-21-2015	North
10-22-2015	North
10-23-2015	NWN
10-24-2015	North
10-25-2015	North
10-26-2015	NWN
10-27-2015	NWN
10-28-2015	NWN
10-29-2015	North
10-30-2015	NWN

4.4 Remote Sensing

Figure 38 and Figure 39 below provide Aqua and Terra MODIS, and VIIRS true colour, chlorophyll-a and sea surface temperature satellite images, retrieved from http://oceancolor.gsfc.nasa.gov/cgi/browse.pl, showing phytoplankton bloom activity on October 22nd and October 28th, 2015 around Sable Island. These visual and chlorophyll-a images and graphics are powerful tools to help us make the link between phytoplankton presence, phytoplankton bloom mass and the presence of biogenic VOCs know to be associated with these blooms.

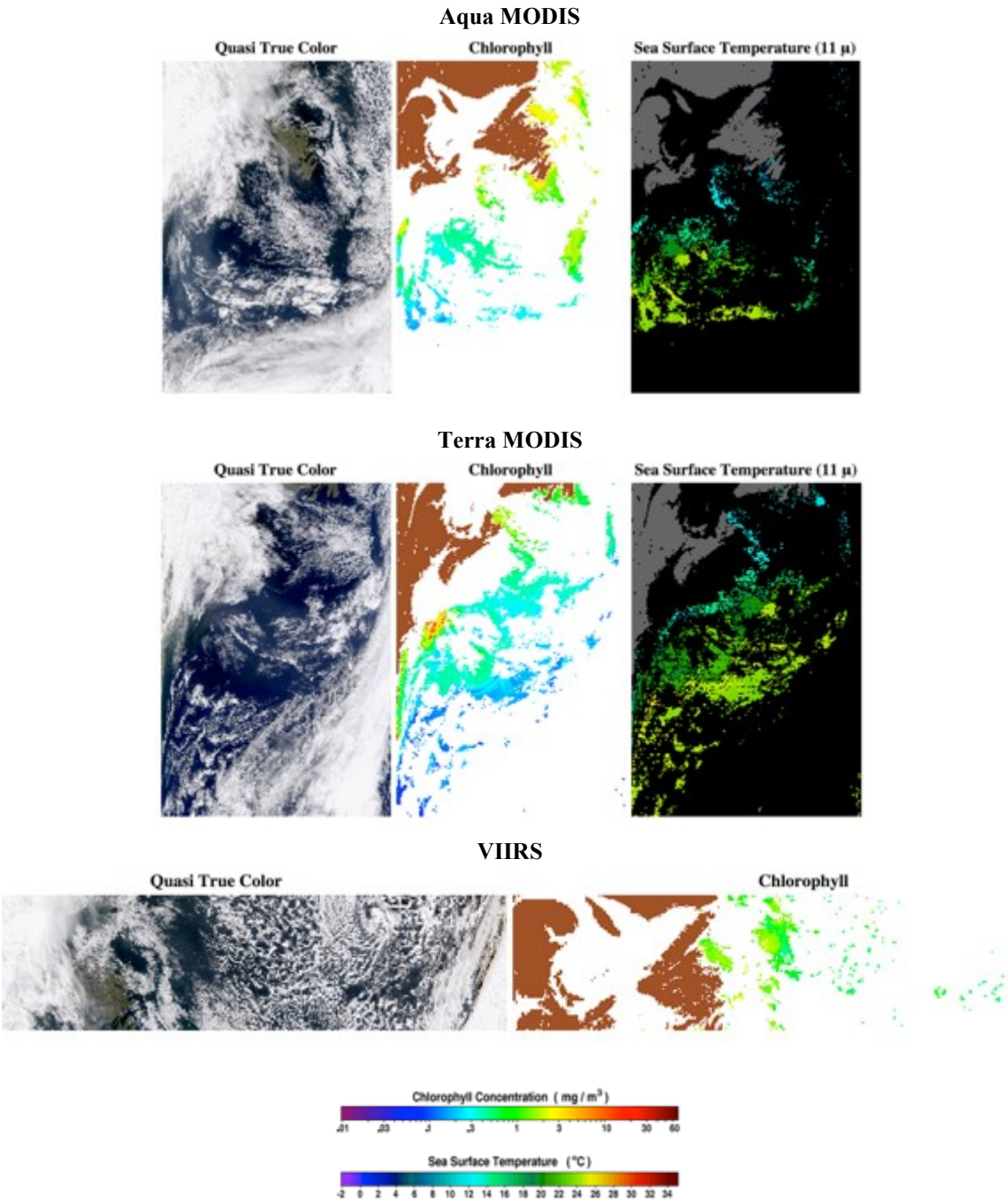

Figure 38. NASA Aqua and Terra MODIS plots of true colour, chlorophyll-a, and sea surface satellite images; and VIIRS true colour and chlorophyll-a satellite image for October 22nd, 2015. Adapted from *NASA OceanColor Web*, retrieved from http://oceancolor.gsfc.nasa.gov/cms/

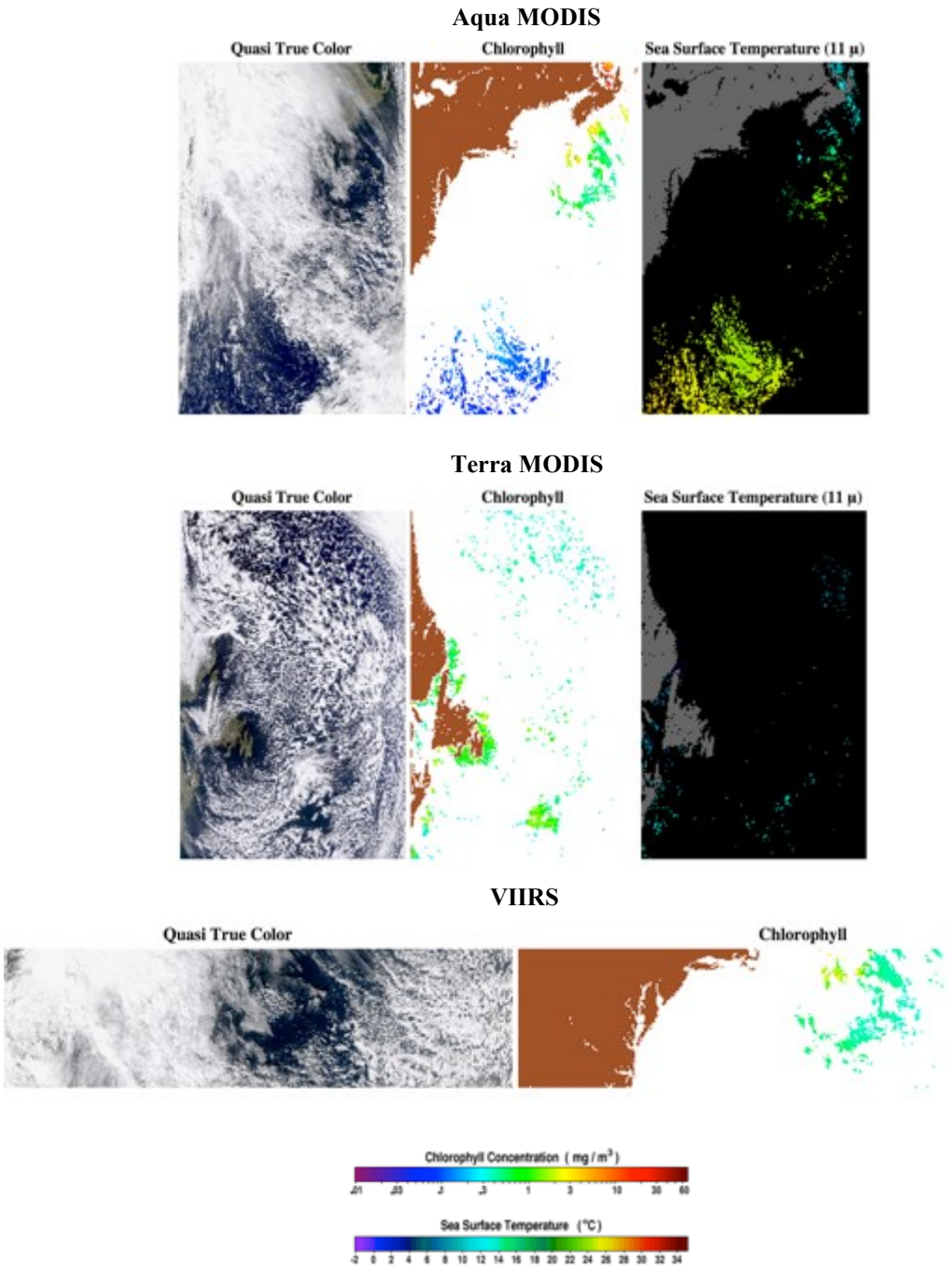

Figure 39. NASA Aqua and Terra MODIS plots of true colour, chlorophyll-a, and sea surface satellite images; and VIIRS true colour and chlorophyll-a satellite image for October 28th, 2015. Adapted from *NASA OceanColor Web*, retrieved from http://oceancolor.gsfc.nasa.gov/cms/

4.5 VOC Data

The data analyzed between October 1st and October 31st, 2015 was divided into trace, micro, macro, and gross VOCs for visualization purposes, where the descriptive statistics of the trace and micro VOCs were reported in *[ng/m^3]* and macro and gross VOCs in *[µg/m^3]*.

4.5.1 Trace VOCs on Sable Island

Table 10 provides the descriptive statistics for the trace VOCs chloroform, 1,1,1-trichloroethane, 1,2-dichloropropane, bromoform, and trans-1,2-dichloroethene measured over the sampling period October 1st to October 31st.

Table 10. Descriptive statistics for trace VOCs *[ng/m^3]*

Compound	Count	Mean	Std Dev	C.I. of Mean	Max	Min	Median	IQR
Chloroform	19	2.29	8.68	4.19	38.1	0.000401	0.0867	0.42339
1,1,1-Trichloroethane	4	0.474	0.269	0.428	0.739	0.192	0.482	0.457
1,2-Dichloropropane	3	3.789	4.044	10.046	8.134	0.136	3.096	5.999
Bromoform	3	0.928	1.042	2.588	2.072	0.0332	0.679	1.529
trans-1,2-Dichloroethene	15	0.0148	0.0115	0.00636	0.0332	0.000058	0.0134	0.01914

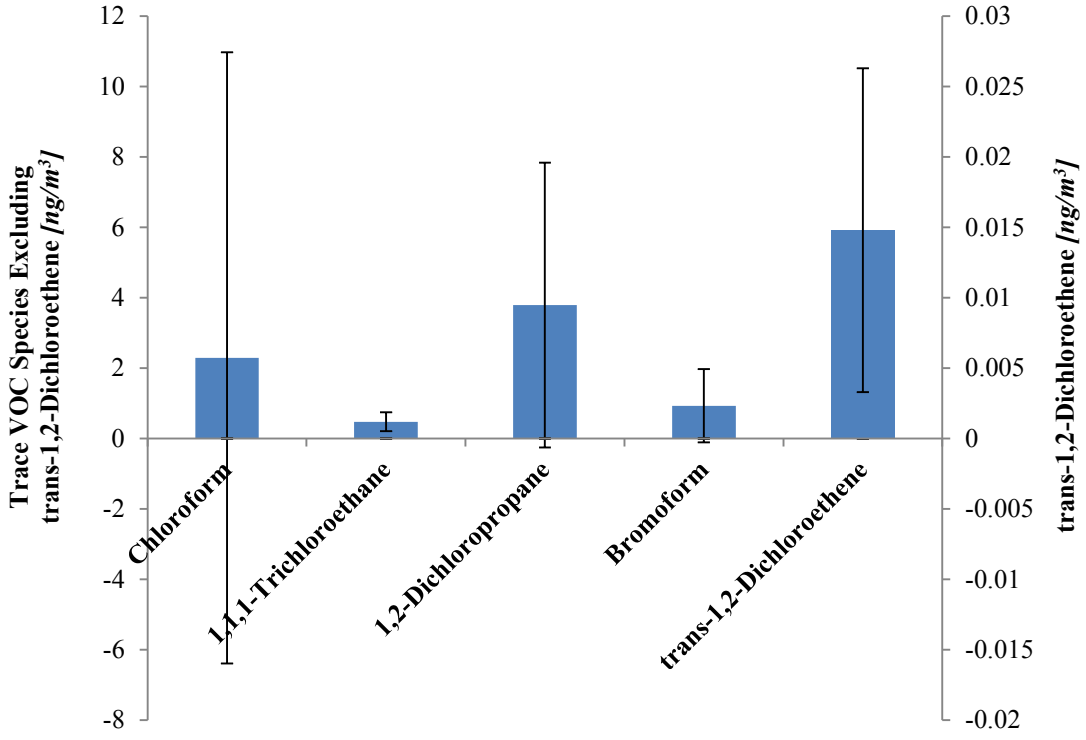

Figure 40. A 95% confidence interval plot of chloroform, 1,1,1-trichloroethane, 1,2-dichloropropane, bromoform, and trans-1,2-dichloroethene measured over the sampling period October 1st to October 31st, 2015

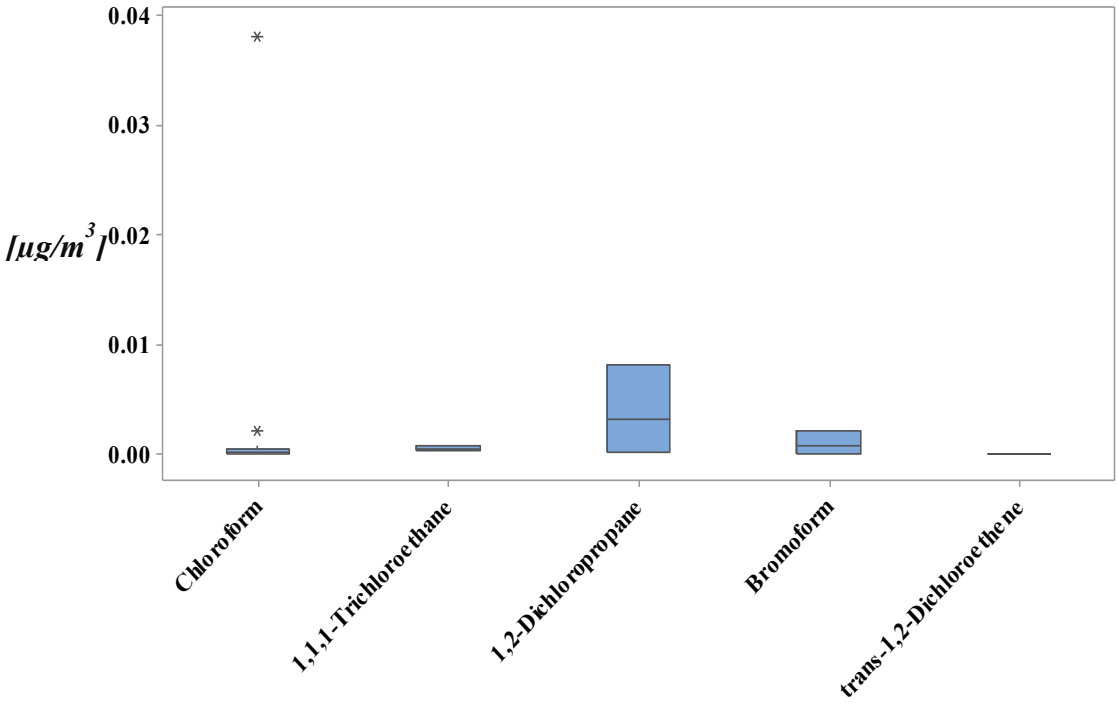

Figure 41. Box plot of chloroform, 1,1,1-trichloroethane, 1,2-Dichloropropane, bromoform, and trans-1,2-dichloroethene measured over the sampling period October 1st to October 31st, 2015

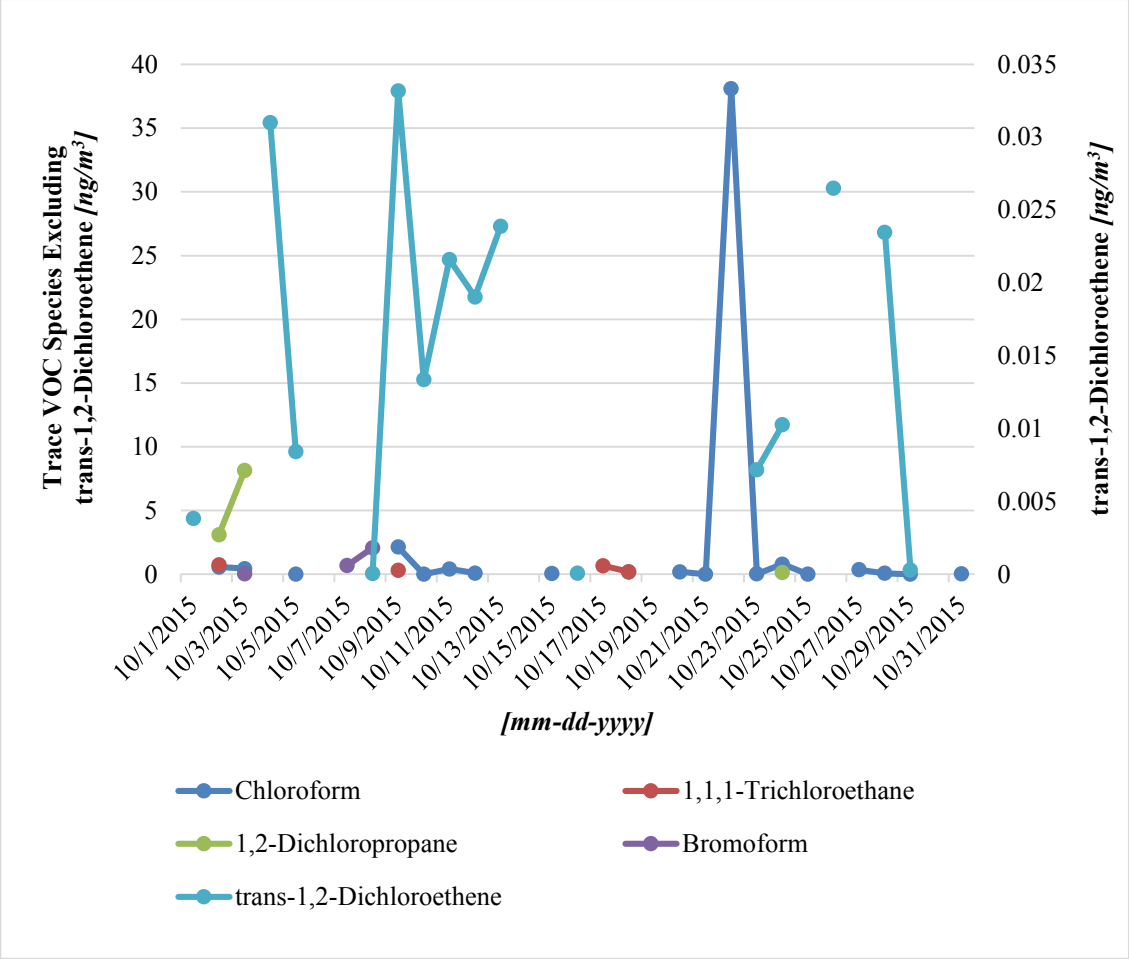

Figure 42. Time series plot of chloroform, 1,1,1-trichloroethane, 1,2-Dichloropropane, bromoform, and trans-1,2-dichloroethene measured over the sampling period October 1st to October 31st, 2015

The mean (min:max ng/m^3) of chloroform was found to be 2.29 (0.000401:38.1 ng/m^3). Table 1 shows that chloroform production is associated with several algal species including the coccolithophore *Emiliania huxleyi* that is located in the Atlantic Ocean (Colomb et al., 2008). Kladi, et al. (2004), also reported chloroform ($CHCl_3$) production from marine red algae listed in Table 2-Table 4. Bromoform ($CHBr_3$) with mean 0.928 (0.0332:2.072 ng/m^3) has also been reported to be produced by several marine algae species as shown in Table 1-Table 4. According to Moore and Tokarczyk (1993), elevated concentrations of halomethanes is an indication of a macroalgal source in the region (Moore & Tokarczyk, 1993; Paul & Pohnert, 2011).

Moreover, 1,1,1-trichloroethane, trans-1,2-dichloroethene, and 1,2-dichloropropane, are used as soil fumigants, in chlorination process and in chemical industries (Howard, 1990). Previous studies have concluded that the primary sources of chlorinated hydrocarbons (CHCs) in the environment are anthropogenic sources which are carried into marine environments via rivers (Howard, 1990; Dewulf & Langenhove, 1977). Therefore, only chloroform and bromoform from the trace halogenated (halo)-VOCs listed in Table 10 are likely to be associated with phytoplankton.

The wide confidence intervals (C.I.'s) for chloroform and trans-1,2-dichloroethene in Figure 40 are due to the high variability in collected data. However, the wide C.I. for 1,2-dichloropropane is likely due to the low count of data available for this compound, which was found to be only 3. Moreover, the source of VOCs contained in the box plot in Figure 41 is as for the C.I. plot.

In Figure 42, a spike in chloroform is visible on October 22nd at 38.0837 ng/m^3. The 5-day HYSPLIT air mass back trajectories associated with the daily spike on October 22nd are from the NWN, hence the low possibility of continental, industrial or anthropogenic

sources of VOCs. This suggests that the chloroform, known as a marker for phytoplankton emission, came from the ocean (Moore & Tokarczyk, 1993; Moore et al., 1995; Moore, Oram, & Penkett, 1994). Moreover, the NASA Aqua and Terra MODIS, and VIIRS satellite true colour and chlorophyll-a images in Figure 38 show blooms of phytoplankton around Sable Island, further supporting the argument that chloroform emission was linked to phytoplankton on October 22nd. A significant spike can also be seen for trans-1,2,-dichloroethene on October 9th and the air mass back trajectories associated with the daily spike on this day were from the NWN, again a region of few anthropogenic emissions and therefore the trans-1,2,-dichloroethene is likely from the ocean as the air mass passed from the mainland across the ocean en route to Sable Island. In addition, this compound has a relatively short half-life in the atmosphere due to the presence of a double bond in the molecule, which can be easily attacked by OH radicals. Therefore, it is unlikely to have come from a source region a few days prior to reaching the ocean.

4.5.2 Micro VOCs on Sable Island

Table 11 provides the descriptive statistics for the micro VOCs 1,1-dichloroethane, acrylonitrile, cis-1,2-dichloroethene, 2,2-dichloropropane, bromochloromethane, tetrachloromethane, tetrahydrofuran, 1,4-Dioxane, cis-1,3-dichloropropene, tert, butylbenzene, hexachlorobutadiene, 1,2,3-trichloropropane, benzene, and isopropylbenzene over the sampling period October 1st to October 31st, 2015. Figure 43, Figure 44, and Figure 45 correspond to the parametric visualization, non-parametric visualization, and time series plot of the micro VOC species, respectively.

Table 11. Descriptive statistics for micro VOCs *[ng/m^3]*

Compound	Count	Mean	Std Dev	C.I. of Mean	Max	Min	Median	IQR
1,1-Dichloroethane	8	9.647	12.162	12.162	37.546	0.102	6.058	9.638
Acrylonitrile	6	221.78	6.377	6.377	233.922	216.99	219.8	5.054
cis-1,2-Dichloroethene	14	20.6	37.6	21.7	119	0.0699	1.11	19.972
2,2-Dichloropropane	4	19.793	20.178	20.178	38.002	0.0545	20.557	34.771
Bromochloromethane	12	24.5	69.7	44.3	245	0.219	2.48	6.106
Tetrachloromethane	13	10.505	31.863	31.863	116.149	0.0174	1.358	2.078
Tetrahydrofuran	1	25.228			25.228	25.228	25.228	0
1,4-Dioxane	3	10.62	5.93	5.93	16.894	5.107	9.858	8.84
cis-1,3-Dichloropropene	5	179.71	60.491	60.491	267.488	134.50	141.849	95.487
tert-Butylbenzene	8	57.321	67.205	67.205	195.761	4.468	28.757	78.694
Hexachlorobutadiene	10	27.625	35.927	35.927	124.959	1.731	16.733	14.481
1,2,3-Trichloropropane	2	81.5	88.2	792	144	19.2	81.5	124.8
Benzene	8	127	357	298	1010	0.017	0.472	3.186
Isopropylbenzene	10	177.58	185.805	132.917	562.939	8.738	114.487	224.05

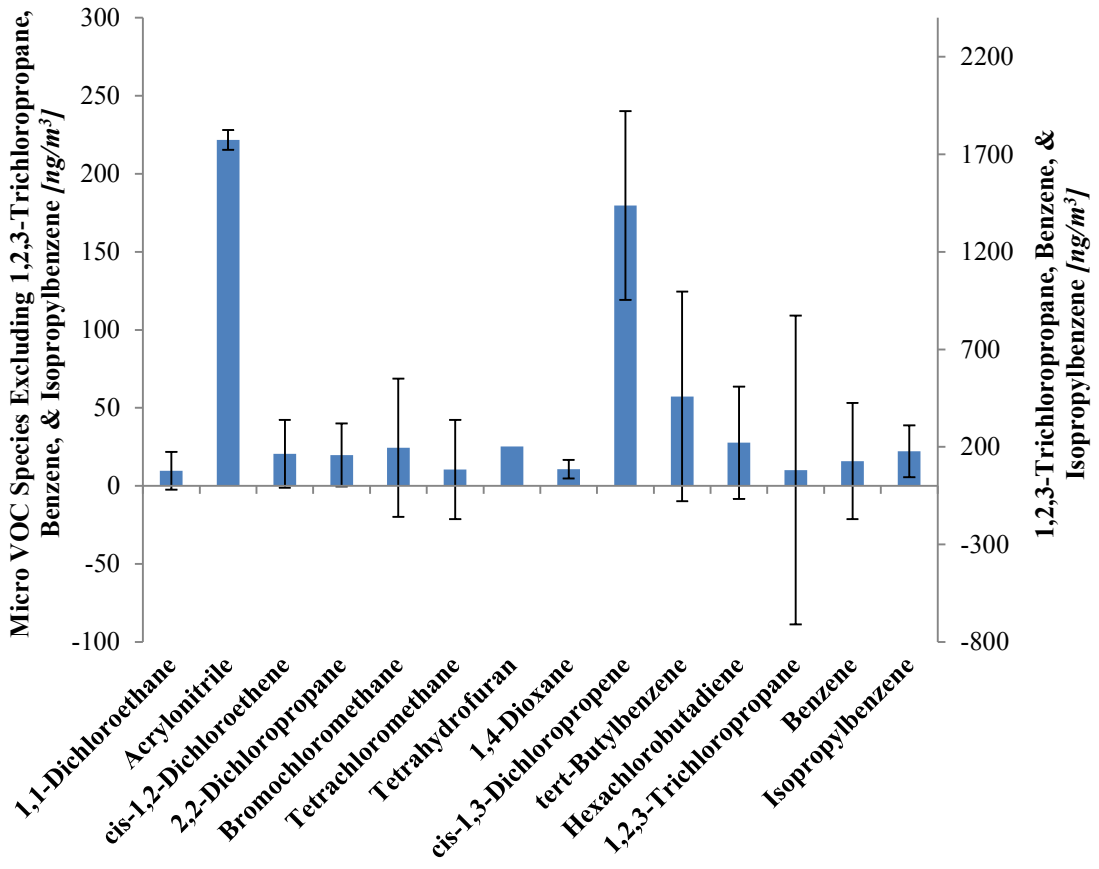

Figure 43. A 95% confidence interval plot of 1,1-dichloroethane, acrylonitrile, cis-1,2-dichloroethene, 2,2-dichloropropane, bromochloromethane, tetrachloromethane, tetrahydrofuran, 1,4-Dioxane, cis-1,3-dichloropropene, tert, butylbenzene, hexachlorobutadiene, 1,2,3-trichloropropane, benzene, and isopropylbenzene measured over the sampling period October 1st to October 31st, 2015

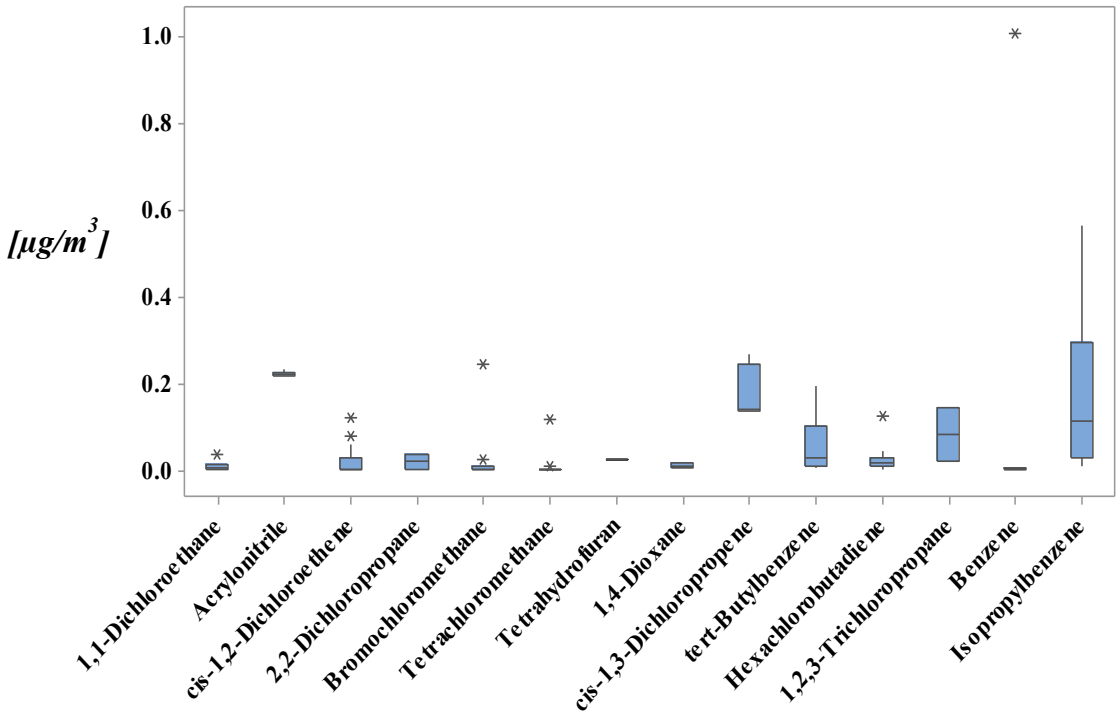

Figure 44. Box plot of 1,1-dichloroethane, acrylonitrile, cis-1,2-dichloroethene, 2,2-dichloropropane, bromochloromethane, tetrachloromethane, tetrahydrofuran, 1,4-dioxane, cis-1,3-dichloropropene, tert-butylbenzene, hexachlorobutadiene, 1,2,3-trichloropropane, benzene, and isopropylbenzene measured over the sampling period October 1st to October 31st, 2015

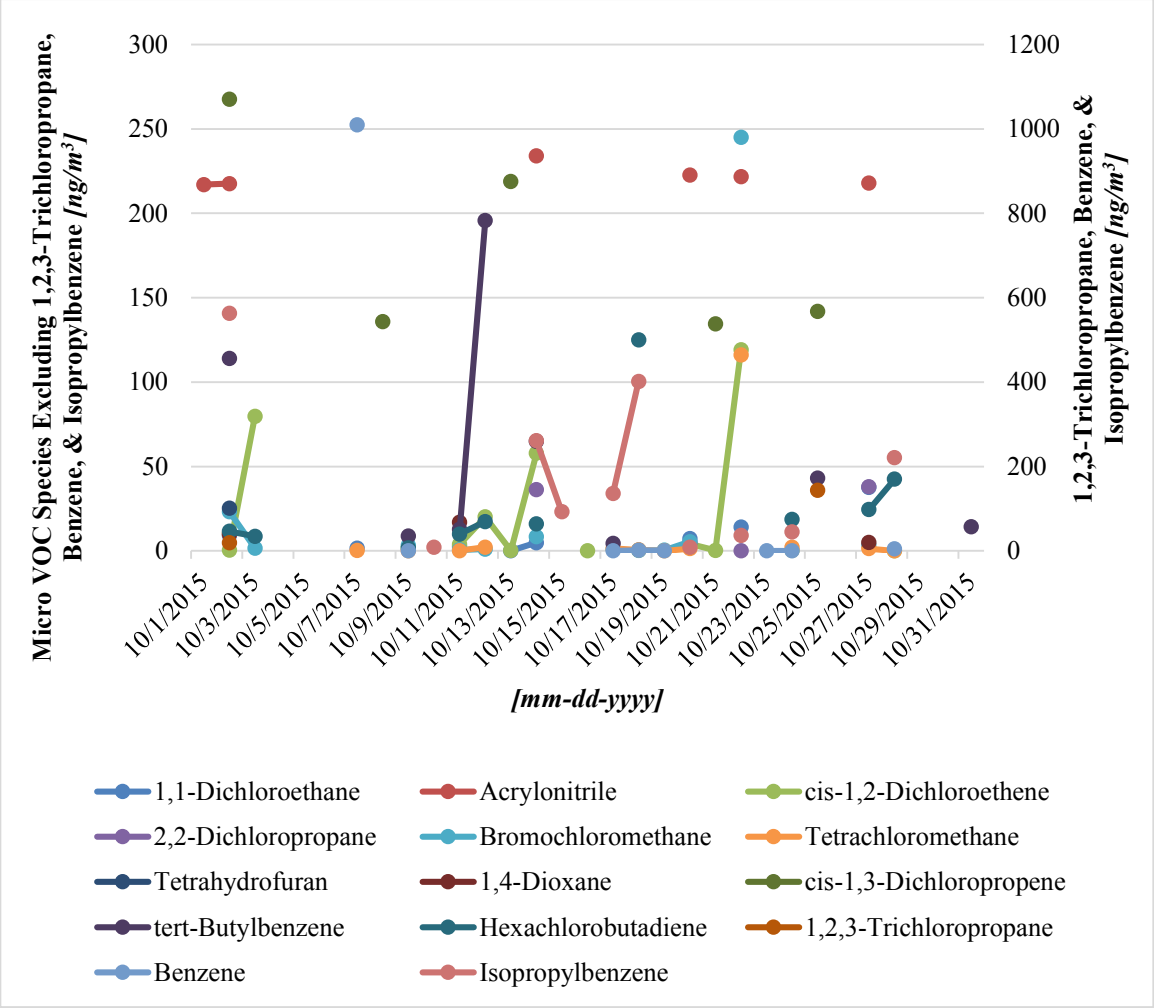

Figure 45. Time series plot of 1,1-dichloroethane, acrylonitrile, cis-1,2-dichloroethene, 2,2-dichloropropane, bromochloromethane, tetrachloromethane, tetrahydrofuran, 1,4-Dioxane, cis-1,3-dichloropropene, tert-butylbenzene, hexachlorobutadiene, 1,2,3-trichloropropane, benzene, and isopropylbenzene measured over the sampling period October 1st to October 31st, 2015

From Table 11, the mean (min:max ng/m^3) of 1,1-dichloroethane was found to be 9.647 (0.102:37.546 ng/m^3); production of this compound from phytoplankton was reported in several studies listed in Table 1. Moreover, Table 2 shows that bromochloromethane (CH_2BrCl), found at mean 24.5 (0.219:245 ng/m^3), is also produced by marine red alga

Phycodrys quercifolia, *Gymnogongrus antarcticus*, *Georgiella confluens*, *Asparagopsis armata*, and the tetrasporophyte form of *A. taxiformis*, *Falkenbergia rufolanosa*. According to Kladi et al. (2004), tetrachloromethane (CCl_4) is also a halogenated volatile metabolite of *Asparagopsis armata* as reported in Table 3. Red and brown macroalgae typically produce longer C2-C9 chain-length hydrocarbons. (Paul & Pohnert, 2011; Scarratt, & Moore, 1999; Kladi et al., 2004). However, the other chlorinated micro VOCs cis-1,2-dichloroethene, 2,2-dichloropropane, cis-1,3-dichloropropene, hexachlorobutadiene, and 1,2,3-trichloropropane are usually associated with anthropogenic sources and are primarily used in the chlorination of water as well as in manufacturing and plastic compounds, and as pesticides (WHO, 2003; Howard, 1990; Dewulf & Langenhove, 1977).

It can also be seen from Table 11, that the mean (min:max ng/m^3) concentration for acrylonitrile was 221.718 (216.99:233.922 ng/m^3), concluding that it was the most abundant compound amongst the measured micro VOCs. Acrylotnitrile and 1,4-dioxane are synthetic chemicals and their main source is plastic industries (WHO, 2002). Furthermore, tetrahydrofuran, tert-butylbenzene, benzene, and isopropylbenzene are markers for emissions from combustion of fossil fuels for power, space heating and transport, or industrial emissions in continental outflow (Elbir, Cetin, Cetin, Bayram, & Odabasi, 2006).

The C.I. for tetrahydrofuran Figure 43 is missing due to having only one data point. The wide C.I. for cis-1,3-dichloropropene is explained by low data count of 5 in this case. The source of the VOCs contained in the box plot in Figure 44 is as for the C.I. plot in Figure 43.

Despite the discontinuity of time series from Figure 45, spikes in bromochloromethane and tetrachloromethane can be seen on October 22nd at around 255 ng/m^3 and 116.14 ng/m^3, respectively. Evidence of phytoplankton blooms is shown in Figure 38 by MODIS and VIIRS satellite true colour, chlorophyll-a and sea surface temperature images. This supports the argument that phytoplankton emission markers, bromochloromethane and tetrachloromethane most likely came from phytoplankton on October 22nd. Moreover, the air mass back trajectories associated with the daily spike on this day were from the NWN (Figure 46) (source regions low in anthropogenic emissions), supporting the evidence of phytoplankton source.

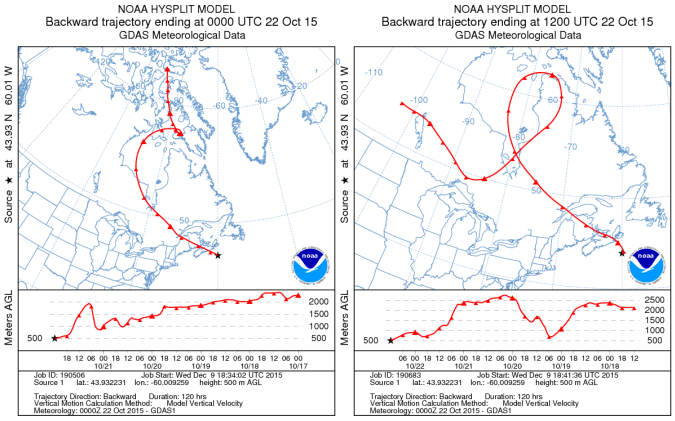

Figure 46. HYSPLIT back trajectories on October 22nd originating from the NWN region

Spikes for benzene on October 7th and hexachlorobutadiene and isopropylbenzene on October 18th can also be identified. However, there is little evidence linking them to anthropogenic sources since the air mass back trajectories were coming from the NWN on October 7th and from the North on October 18th. This provides further evidence that

VOC spikes seen on October 7th and October 18th were linked to oceanic source as the air mass leaves the mainland and crosses over the Scotian shelf.

4.5.3 Macro VOCs on Sable Island

Table 12 provides the descriptive statistics for the macro VOCs trichloroethene, bromodichloromethane, methyl methacrylate, 1,1,2-trichloroethane, ethyl methacrylate, 1,2-dibromoethane, chlorobenzene, styrene, bromobenzene, n-propylbenzene, 1,3,5-trimethylbenzene, trans-1,4-dichloro-2-butene, 4-chlorotoluene, p-isopropyltoluene, n-butylbenzene, 1,2-dichlorobenzene, 1,2-dibromo-3-chloropropane, nitrobenzene, 1,2,4-trichlorobenzene, naphthalene, and 1,2,3-trichlorobenzene measured over the sampling period October 1st to October 31st, 2015. Figure 47, Figure 48, and Figure 49 correspond to the parametric visualization, non-parametric visualization, and time series plot of the macro VOC species, respectively.

Table 12. Descriptive statistics for macro VOCs *[$\mu g/m^3$]*

Compound	Count	Mean	Std Dev	C.I. of Mean	Max	Min	Median	IQR
Trichloroethene	8	0.393	0.000138	0.000115	0.393	0.393	0.393	0
Bromodichloromethane	21	0.33	0.0554	0.0252	0.572	0.316	0.317	0.003
Methyl methacrylate	12	1.556	3.205	2.036	11.384	0.302	0.316	0.425
1,1,2-Trichloroethane	3	0.487	0.282	0.702	0.812	0.31	0.337	0.377
Ethyl methacrylate	10	0.47	0.256	0.183	0.932	0.273	0.342	0.366
1,2-Dibromoethane	3	1.019	1.246	3.095	2.457	0.265	0.334	1.644
Chlorobenzene	14	0.408	0.498	0.287	2.066	0.211	0.238	0.054
Styrene	9	0.399	0.0469	0.036	0.521	0.371	0.383	0.025
Bromobenzene	6	0.35	0.409	0.429	0.897	0.0444	0.13	0.8082
n-Propylbenzene	8	2.206	1.527	1.277	5.06	0.0225	2.171	1.754
1,3,5-Trimethylbenzene	15	0.532	0.688	0.381	1.973	0.00403	0.157	0.7735
trans-1,4-Dichloro-2-butene	5	0.386	0.484	0.601	1.248	0.122	0.185	0.356
4-Chlorotoluene	17	1.971	2.527	1.299	8.872	0.0406	1.283	1.814
p-Isopropyltoluene	10	1.65	3.703	2.649	11.523	0.019	0.0486	0.4845
n-Butylbenzene	10	0.676	0.847	0.606	2.851	0.00283	0.585	0.6446
1,2-Dichlorobenzene	6	1.208	1.243	1.305	3.31	0.096	0.81	1.742
1,2-Dibromo-3-chloropropane	3	0.272	0.0254	0.0631	0.297	0.246	0.274	0.038
Nitrobenzene	1	0.765			0.765	0.765	0.765	0
1,2,4-Trichlorobenzene	6	0.497	0.618	0.649	1.754	0.194	0.252	0.14
Naphthalene	13	0.703	1.553	0.939	5.776	0.0185	0.228	0.357
1,2,3-Trichlorobenzene	26	0.398	1.029	0.416	5.394	0.00433	0.168	0.2882

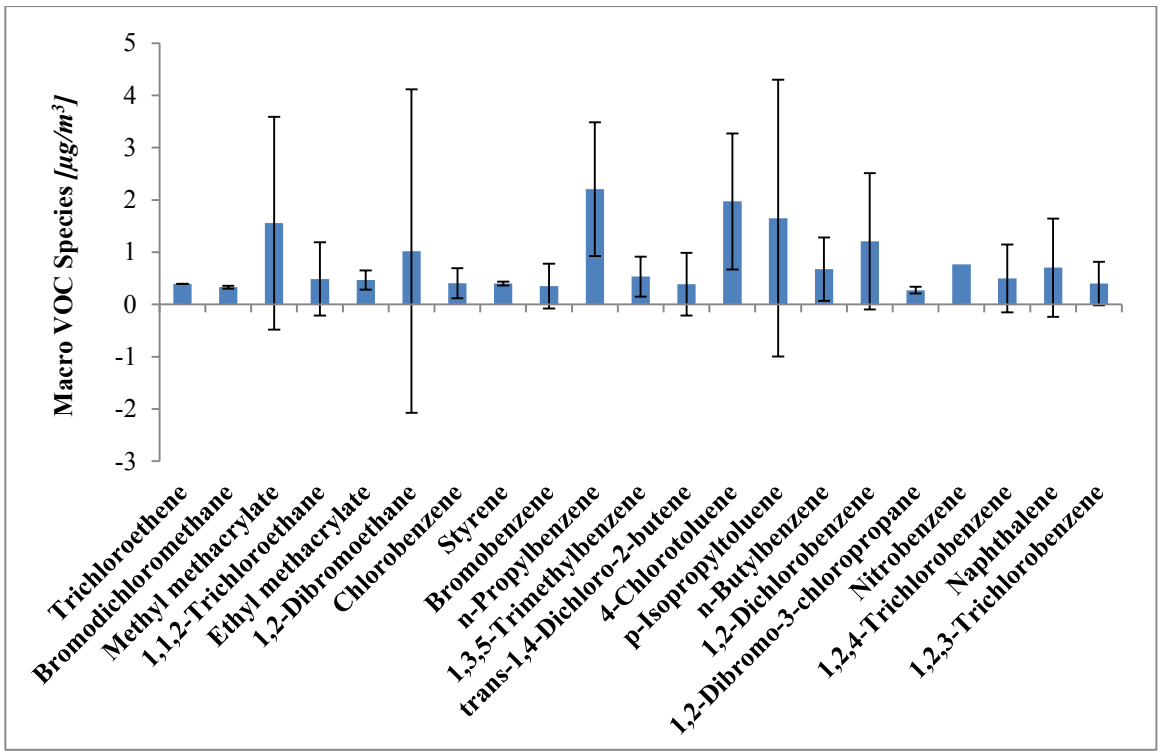

Figure 47. A 95% confidence interval plot of trichloroethene, bromodichloromethane, methyl methacrylate, 1,1,2-trichloroethane, ethyl methacrylate, 1,2-dibromoethane, chlorobenzene, styrene, bromobenzene, n-propylbenzene, 1,3,5-trimethylbenzene, trans-1,4-dichloro-2-butene, 4-chlorotoluene, p-isopropyltoluene, n-butylbenzene, 1,2-dichlorobenzene, 1,2-dibromo-3-chloropropane, nitrobenzene, 1,2,4-trichlorobenzene, naphthalene, and 1,2,3-trichlorobenzene measured over the sampling period October 1st to October 31st, 2015

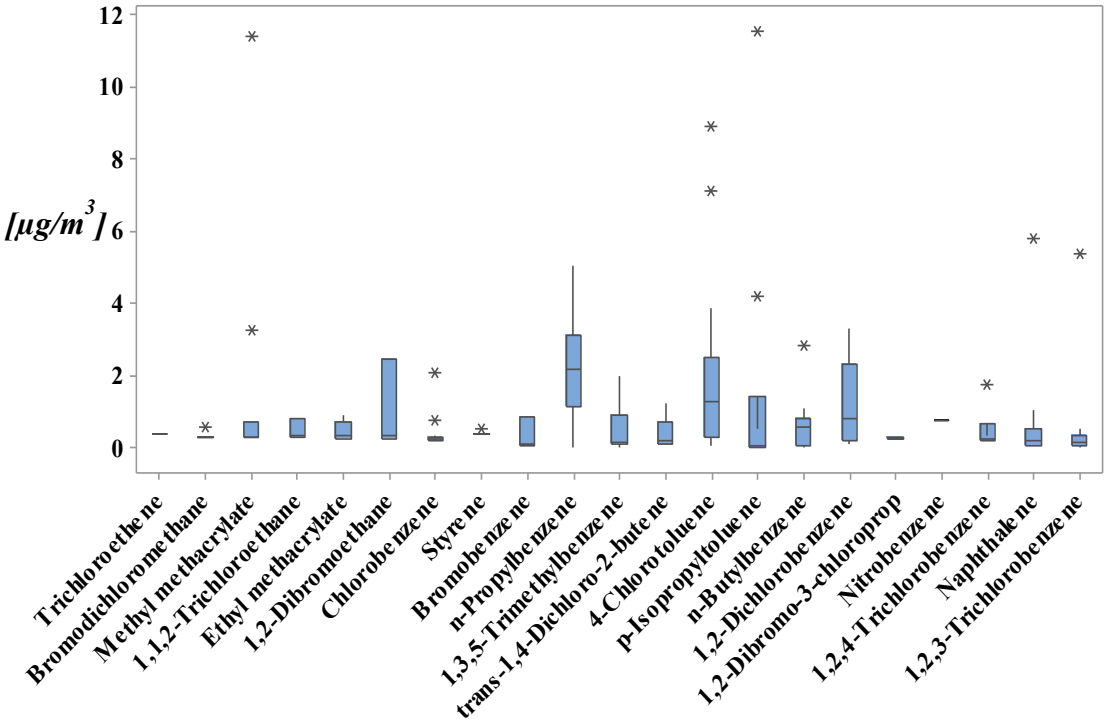

Figure 48. Box plot of trichloroethene, bromodichloromethane, methyl methacrylate, 1,1,2-trichloroethane, ethyl methacrylate, 1,2-dibromoethane, chlorobenzene, styrene, bromobenzene, n-propylbenzene, 1,3,5-trimethylbenzene, trans-1,4-dichloro-2-butene, 4-chlorotoluene, p-isopropyltoluene, n-butylbenzene, 1,2-dichlorobenzene, 1,2-dibromo-3-chloropropane, nitrobenzene, 1,2,4-trichlorobenzene, naphthalene, and 1,2,3-trichlorobenzene measured over the sampling period October 1st to October 31st, 2015

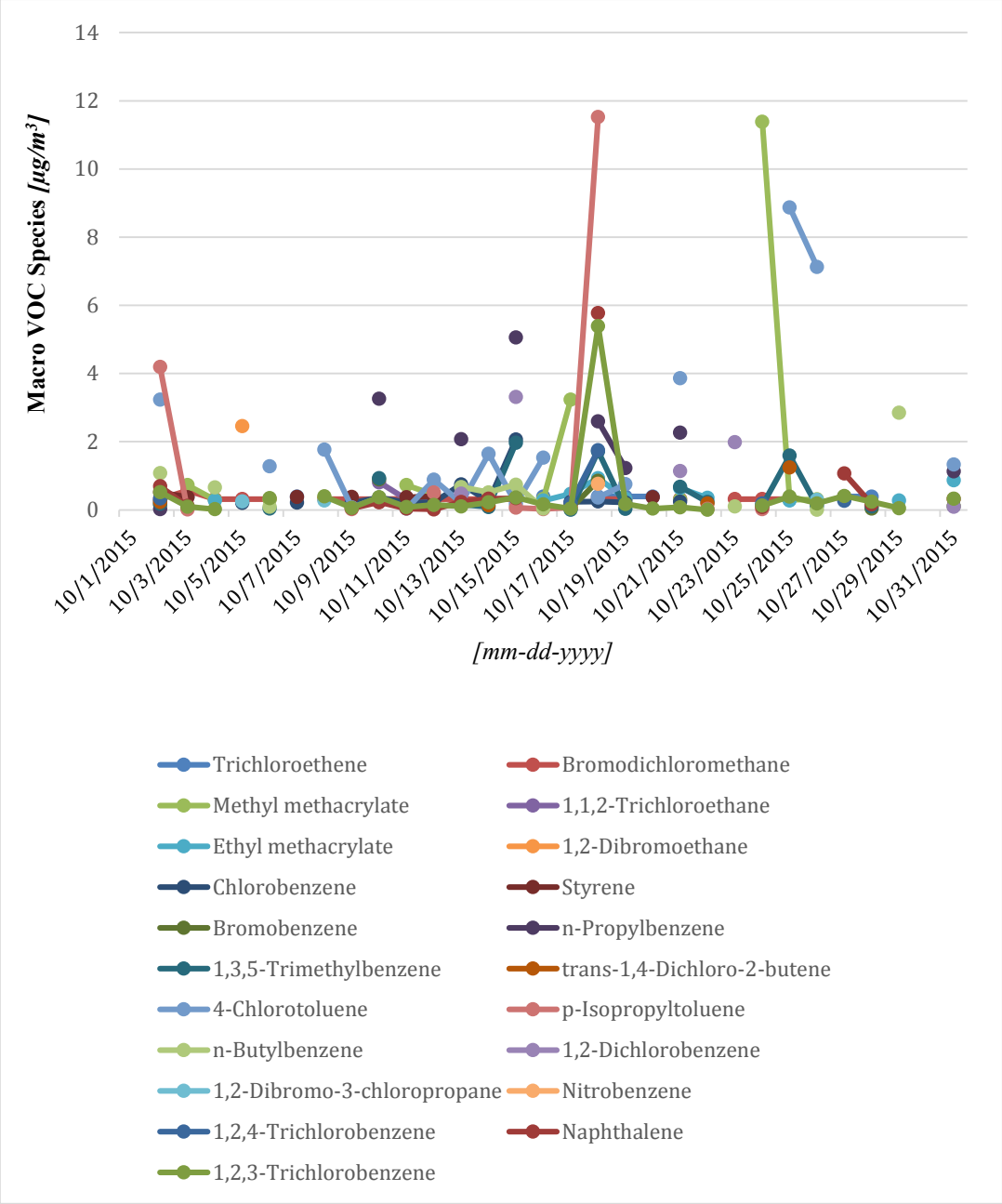

Figure 49. Time series plot of trichloroethene, bromodichloromethane, methyl methacrylate, 1,1,2-trichloroethane, ethyl methacrylate, 1,2-dibromoethane, chlorobenzene, styrene, bromobenzene, n-propylbenzene, 1,3,5-trimethylbenzene, trans-1,4-dichloro-2-butene, 4-chlorotoluene, p-isopropyltoluene, n-butylbenzene, 1,2-dichlorobenzene, 1,2-dibromo-3-chloropropane, nitrobenzene, 1,2,4-trichlorobenzene, naphthalene, and 1,2,3-trichlorobenzene measured over the sampling period October 1st to October 31st, 2015

Trichloroethene with mean (min:max μg/m^3) found at 0.393 (0.3927:0.3931 μg/m^3) is identified as vehicle exhaust emission (Elbir et al., 2006), however it was also reported as a product from phytoplankton as shown in Table 1. Bromodichloromethane ($CHBrCl_2$) was found to have a mean of 0.33 (0.316:0.572 μg/m^3); its productions from red marine algae was reported in Table 2-Table 3. Table 2 also lists the red marine algae that emit 1,2-dibromoethane (1,2-$C_2H_4Br_2$). According to Sabolis (2010), the water samples collected from coastal zones of the NW Atlantic Ocean contained 0.3-0.6 ng/L bromodichloromethane which presented a sign of macroalgal source. Sabolis (2010) also reported the emission of bromodichloromethane from phytoplankton in Table 1. The mean of chlorobenzene in this study was found to be 0.408 (0.221:2.066 μg/m^3). Chlorobenzene is normally considered an anthropogenic air pollutant, e.g., Elbir et al. (2006) found that chlorobenzene was highly contributed by paint production and application emissions. Although, Colomb et al. (2008) found the first evidence of chlorobenzene emission by phytoplankton; they identified chlorobenzene in the headspace above various phytoplankton cultures where *D. tertiolecta* was the strongest emitter of chlorobenzene followed by *C. leptoporus* and *P. tricornutum*. The concentration of 1,2-dichlorobenzene was found at mean 1.208 (0.096:3.31 μg/m3), and according to Euro Chlor (2001), this compound is flushed into marine environments from anthropogenic uses e.g. deodorant in toilet blocks and as a moth repellent. Naphthalene emission is also associated with wildfires which could sometimes exceed anthropogenic emissions, however, given that the samples were taken in the winter, it is unlikely to be associated with wildfires but could be associated with fuel combustion. Moreover, waste disposal as main source of trichlorobenzenes i.e. 1,2,4-trichlorobenzene found at 0.497

(0.194:1.754 $\mu g/m^3$) and 1,2,3-trichlorobenzene at 0.398 (0.0043:5.394 $\mu g/m^3$), in marine environments (Elbir et al., 2006; Jia & Batterman, 2010; Naeher et al., 2007).

It can be seen from Figure 47 that the C.I. for nitrobenzene is missing due to having only one count of data for this compound. The wide C.I. for 1,2-dibromoethane is also likely due to the low data count of 3 for this compound. However, the wide C.I.'s for the other compounds such as methyl methacrylate and p-isopropyltoluene are likely due to having large standard deviations of 3.205 $[\mu g/m^3]$ and 3.703 $[\mu g/m^3]$, respectively. Moreover, the box plot in Figure 48 provides a similar interpretation.

It is most likely that bromodichloromethane, and 1,2-dibromoethane from the range of macro VOCs over Sable Island come from phytoplankton. Methyl methacrylate, 1,1,2-trichloroethane, ethyl methacrylate, chlorobenzene, styrene, bromobenzene, n-propylbenzene, 1,3,5-trimethylbenzene, trans-1,4-dichloro-2-butene, 4-chlorotoluene, p-isopropyltoluene, n-butylbenzene, 1,2-dichlorobenzene, 1,2-dibromo-3-chloropropane, nitrobenzene, 1,2,4-trichlorobenzene, naphthalene, and 1,2,3-trichlorobenzene are strictly associated industrial or fossil fuel combustion emissions continental outflow (Elbir et al., 2006; Jia & Batterman, 2010; Naeher et al., 2007).

In Figure 49, it can be seen that p-isopropyltoluene, naphthalene, and 1,2,3-trichlorobenzene spike on October 18th. The air mass back trajectories are shown to have come from the NWN (a low anthropogenic VOC source region) on October 7th and from the North on October 18th. This provides little evidence of long-range transport of VOCs from the continent. The spikes are therefore likely explained by a local source on the island or from ocean as the air mass crosses over the Scotian shelf en route to Sable Island. Methyl methacrylate measures the highest concentration on October 24th at 11.384 $\mu g/m^3$ and drops to 0.3024 $\mu g/m^3$ on October 25th. Again, the HYSPLIT plots in Figure 50

show air mass back trajectories coming from the North on that day, hence supporting the evidence of an oceanic source.

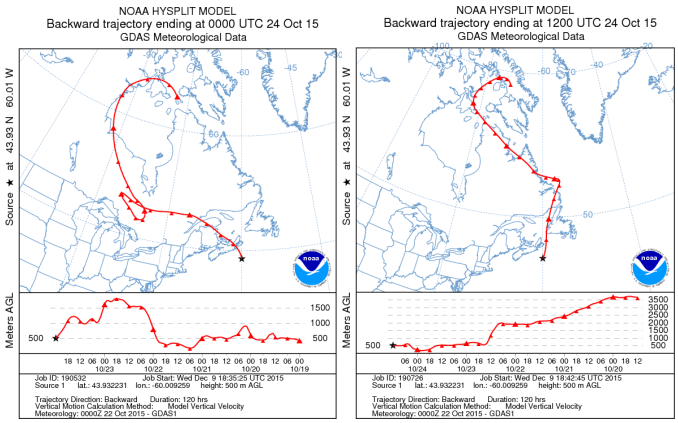

Figure 50. HYSPLIT back trajectories on October 24th originating from the North region

4.5.4 Gross VOCs on Sable Island

Table 13 below provides the descriptive statistics for the gross VOCs 1,1-dichloropropene, 1,2-dichloroethane, toluene, tetrachloroethene, trans-1,3-dichloropropene, 1,3-dichloropropane, ethylbenzene, 1,1,1,2-tetrachloroethane, m-xylene, o-xylene, p-xylene, 1,1,2,2-tetrachloroethane, 2-chlorotoluene, 1,2,4-trimethylbenzene, sec-butylbenzene, dibromochloromethane, and dibromomethane measured over the sampling period October 1st to October 31st, 2015. Figure 51, Figure 52, and Figure 53 correspond to the parametric visualization, non-parametric visualization, and time series plot of the gross VOC species, respectively.

Table 13. Descriptive statistics for gross VOCs *[$\mu g/m^3$]*

Compound	Count	Mean	Std Dev	C.I. of Mean	Max	Min	Median	IQR
1,1-Dichloropropene	1	9.621			9.621	9.621	9.621	0
1,2-Dichloroethane	4	17.523	29.778	47.383	61.81	0.00838	4.137	35.0099
Toluene	3	10.923	18.853	46.833	32.692	0.0119	0.0642	24.5101
Tetrachloroethene	7	14.1	36.93	34.154	97.849	0.126	0.127	0.068
trans-1,3-Dichloropropene	2	5.934	7.806	70.136	11.454	0.414	5.934	11.04
1,3-Dichloropropane	7	47.282	68.132	63.011	169.096	0.334	3.143	95.914
Ethylbenzene	2	10.259	1.319	11.855	11.192	9.326	10.259	1.866
1,1,1,2-Tetrachloroethane	3	2.638	1.554	3.861	4.392	1.431	2.092	2.221
m-Xylene	4	30.417	25.829	41.099	57.47	7.321	28.439	44.156
o-Xylene	5	13.944	14.317	17.777	32.016	0.341	5.924	24.269
p-Xylene	3	10.948	5.285	13.129	14.756	4.914	13.174	7.381
1,1,2,2-Tetrachloroethane	6	8.119	9.578	10.051	26.825	0.885	5.311	5.639
2-Chlorotoluene	13	2.782	3.095	1.87	8.134	0.0628	1.39	5.158
1,2,4-Trimethylbenzene	13	2.53	3.16	1.91	10.657	0.0412	1.505	3.439
sec-Butylbenzene	13	3.609	6.081	3.674	20.771	0.00867	1.173	3.6618
Dibromochloromethane	3	69.567	119.872	297.778	207.983	0.312	0.407	155.754
Dibromomethane	1	377.856			377.856	377.856	377.856	0

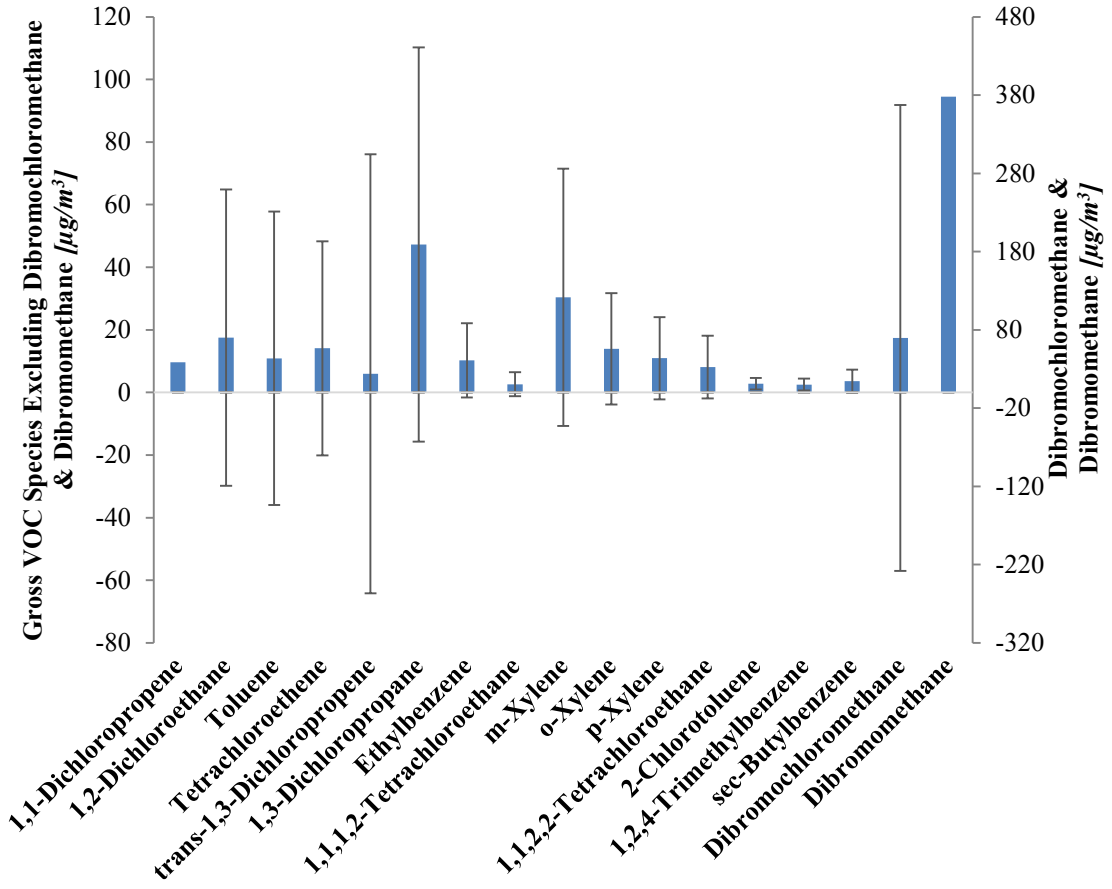

Figure 51. A 95% confidence interval plot of 1,1-dichloropropene, 1,2-dichloroethane, toluene, tetrachloroethene, trans-1,3-dichloropropene, 1,3-dichloropropane, ethylbenzene, 1,1,1,2-tetrachloroethane, m-xylene, o-xylene, p-xylene, 1,1,2,2-tetrachloroethane, 2-chlorotoluene, 1,2,4-trimethylbenzene, sec-butylbenzene, dibromochloromethane, and dibromomethane measured over the sampling period October 1st to October 31st, 2015

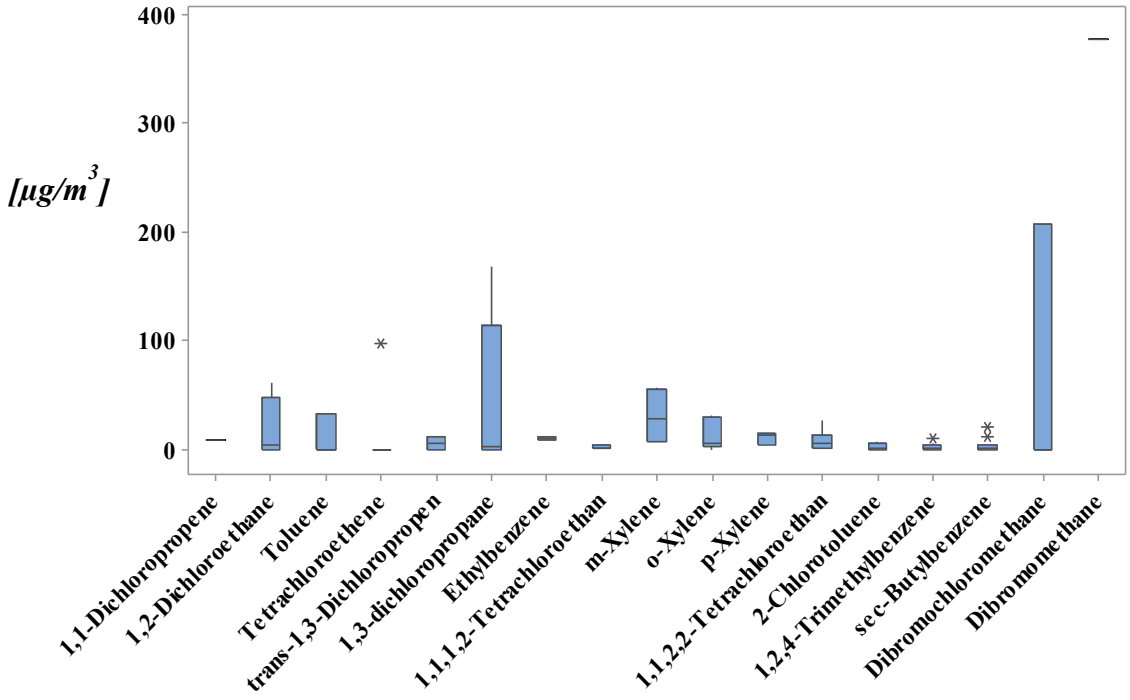

Figure 52. Box plot of 1,1-dichloropropene, 1,2-dichloroethane, toluene, tetrachloroethene, trans-1,3-dichloropropene, 1,3-dichloropropane, ethylbenzene, 1,1,1,2-tetrachloroethane, m-xylene, o-xylene, p-xylene, 1,1,2,2-tetrachloroethane, 2-chlorotoluene, 1,2,4-trimethylbenzene, sec-butylbenzene, dibromochloromethane, and dibromomethane measured over the sampling period October 1st to October 31st, 2015

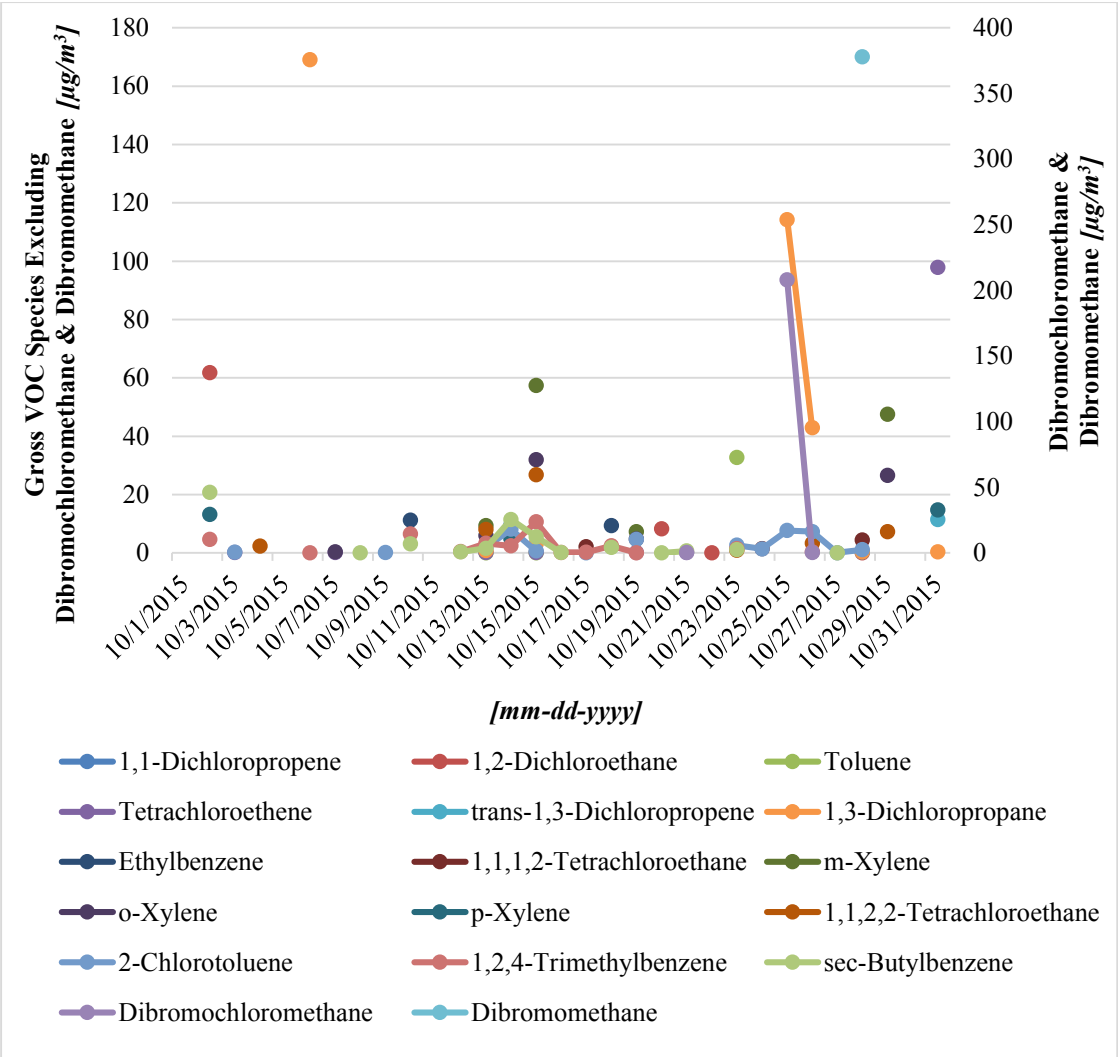

Figure 53. Time series plot of 1,1-dichloropropene, 1,2-dichloroethane, toluene, tetrachloroethene, trans-1,3-dichloropropene, 1,3-dichloropropane, ethylbenzene, 1,1,1,2-tetrachloroethane, m-xylene, o-xylene, p-xylene, 1,1,2,2-tetrachloroethane, 2-chlorotoluene, 1,2,4-trimethylbenzene, sec-butylbenzene, dibromochloromethane, and dibromomethane measured over the sampling period October 1st to October 31st, 2015

In Table 13, the mean of 1,2-dichloroethane and tetrachloroethene are reported at (0.0084:61.81 $\mu g/m^3$) and 14.1 (0.126:97.85 $\mu g/m^3$). From Table 1, *Emiliania huxleyi, Calcidiscus leptoporus* and other algae listed are reported to produce those two

compounds. Table 3 also shows that tetrachloroethene is emitted by the red marine algae *Asparagopsis armata*. Moreover, Table 1-Table 4 list marine algae contributing to the emission of dibromochloromethane and dibromomethane which were found at mean 69.567 (0.312:207.98 $\mu g/m^3$) and 377.86 (377.86:377.86 $\mu g/m^3$), respectively.

It is likely that only dibromochloromethane and dibromomethane from the range of gross VOCs actually come from phytoplankton. Benzene, toluene, ethylbenzene, m,o,p-xylenes (BTEX) are associated with gasoline and diesel vehicle exhaust emissions (Elbir et al., 2006; Lee, Chiu, Ho, Zou, & Wang, 2002). The remaining gross VOCs 1,1-dichloropropene, trans-1,3-dichloropropene, 1,3-dichloropropane, 1,1,1,2-tetrachloroethane, 1,1,2,2-tetrachloroethane, 2-chlorotoluene, 1,2,4-trimethylbenzene, sec-butylbenzene either come from surface runoff, atmospheric deposition or riverine sources (Naeher et al., 2007).

From Figure 51, it can be seen that the C.I.'s for 1,1-dichloropropene and dibromomethane are missing due to having only one count of data. The wide C.I. for dibromochloromethane, 1,2-dichloroethane, toluene, tetrachloroethene, trans-1,3-dichloropropene, 1,3-dichloropropane, are likely due to having both large standard deviations and low count of data. Moreover, the source of the VOCs contained in the box plot in Figure 52 is as for the C.I. plot in Figure 51.

In Figure 45, m-xylene, o-xylene and 1,1,2,2-tetrachloroethane are shown to spike on October 15th (NWN). Dibromochloromethane spikes on October 25th with concentration 207.98 $\mu g/m^3$ and drops to 0.407 $\mu g/m^3$ on October 26th; the drop is likely explained by a sudden bloom crash that can be caused by wind events that are not uncommon during the fall season. Dibromomethane also shows a spike on October 28th measured at 377.86 $\mu g/m^3$. The HYSPLIT plots support the evidence of marine source on October 25th and

October 28th by showing that air masses were coming from the North and NWN, respectively.

4.6 Positive Matrix Factorization Results

The USEPA Positive Matrix Factorization (PMF) v5.0 (the most up to date version) was used to first identify the source of the daily samples of VOC species and then to quantify their mass contribution to the total daily VOC species concentration observed on Sable Island. The recommended PMF model default settings were used, e.g. 20 random start dates model runs. After a number of iterations (50+ model runs), three factors (associated with a source) were chosen based upon *a priori* knowledge of local emissions sources (marine environment, e.g. phytoplankton emissions) and long-range transport of VOCs from the continent.

Figure 54 provides the percentage of the total VOC species mass from all of the samples that appeared in Factor 1.

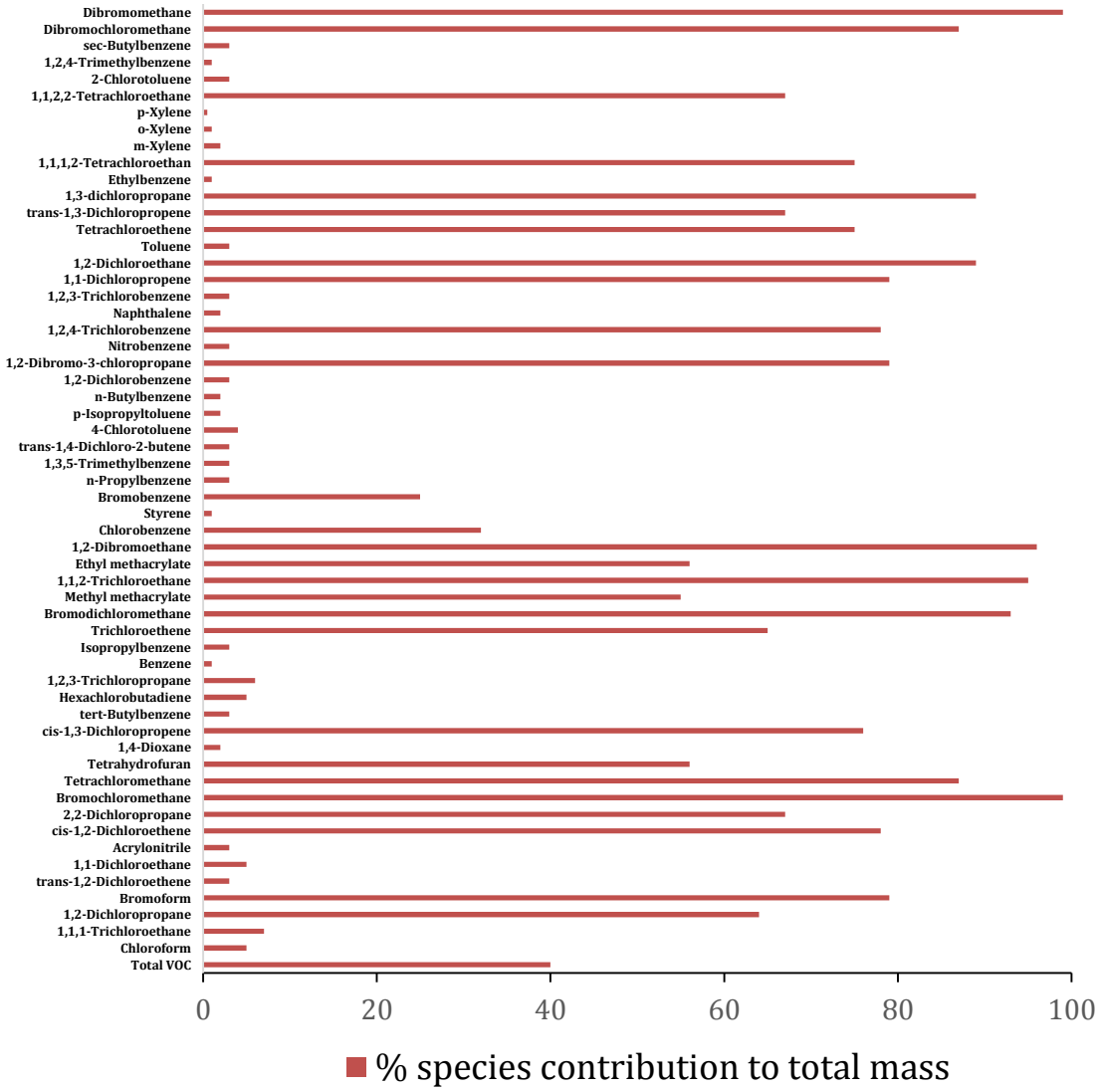

Figure 54. The percentage of the total VOC species mass from all samples associated with Factor 1

After scrutiny of the percentage factor species contained in Figure 54 this factor was identified as marine biogenic phytoplankton emissions. This is due to the high abundance (in some cases almost 100%) of VOCs known to be associated with phytoplankton, e.g. dibromochloromethane and bromochloromethane. In addition, there is low percent contributions from VOCs such as benzene, naphthalene and m,o,p-xylenes that are known

to be associated with long-range transport combustion sources; Therefore, it is highly probable that this factor is related to marine phytoplankton VOC emissions.

Figure 55 also provides the percentage of the total VOC species mass from all samples associated with Factor 2.

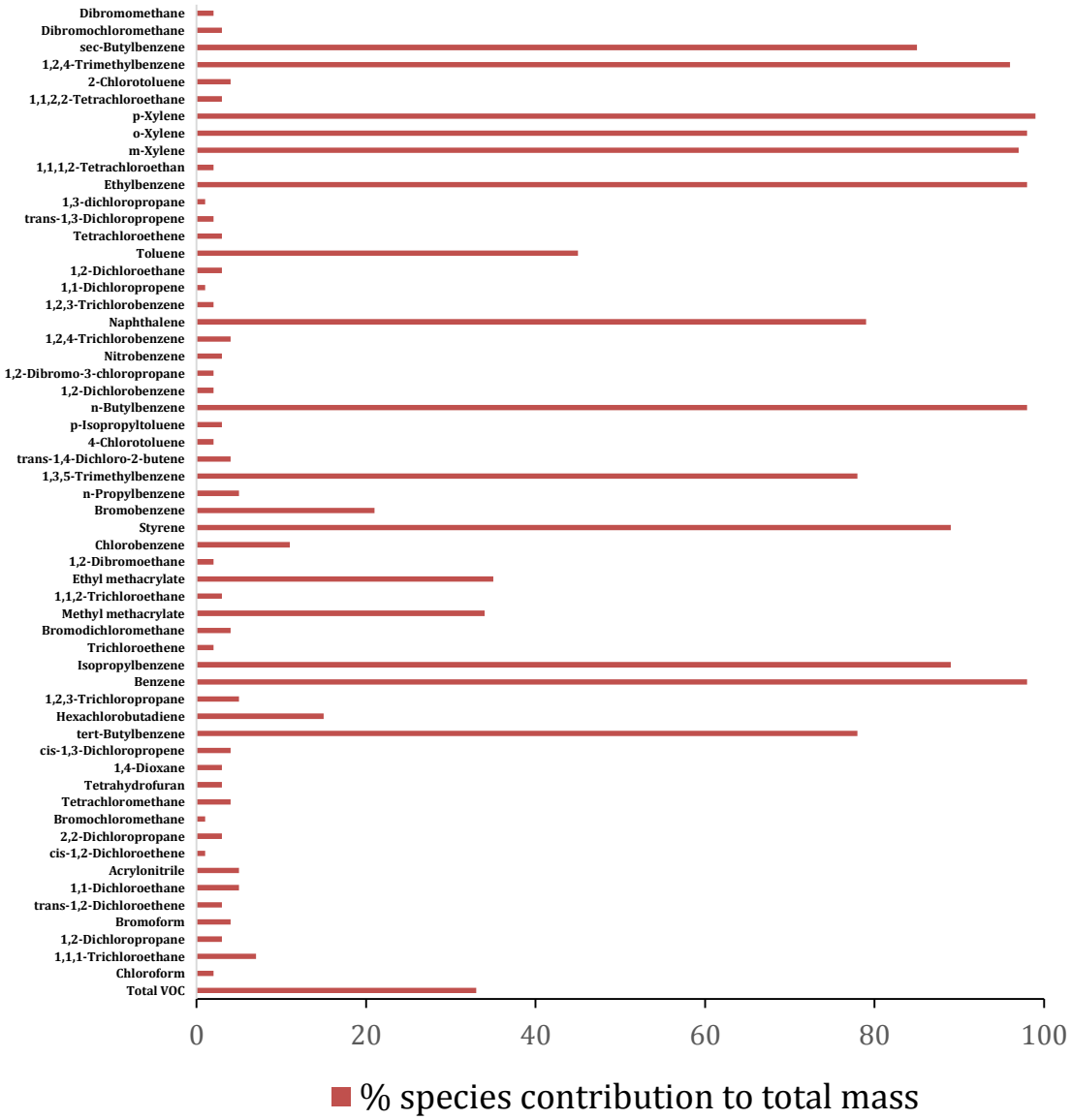

Figure 55. The percentage of the total VOC species mass from all samples associated with Factor 2

Scrutiny of Figure 55 shows high percentage mass abundance of known long-range transport carbonaceous combustion markers associated with Factor 2. These VOC markers are either from the combustion of fossil fuels for power, space heating and transport, or from biomass burning or industrial emissions (Naeher et al., 2007). Given that the samples were taken in the winter the source of the VOCs are unlikely to be associated with wildfires but could be associated with residential wood combustion or biomass heating plant combustion emissions (Naeher et al., 2007).

Finally, the percentage of the total VOC species mass from all samples associated with Factor 3 provided by Figure 56.

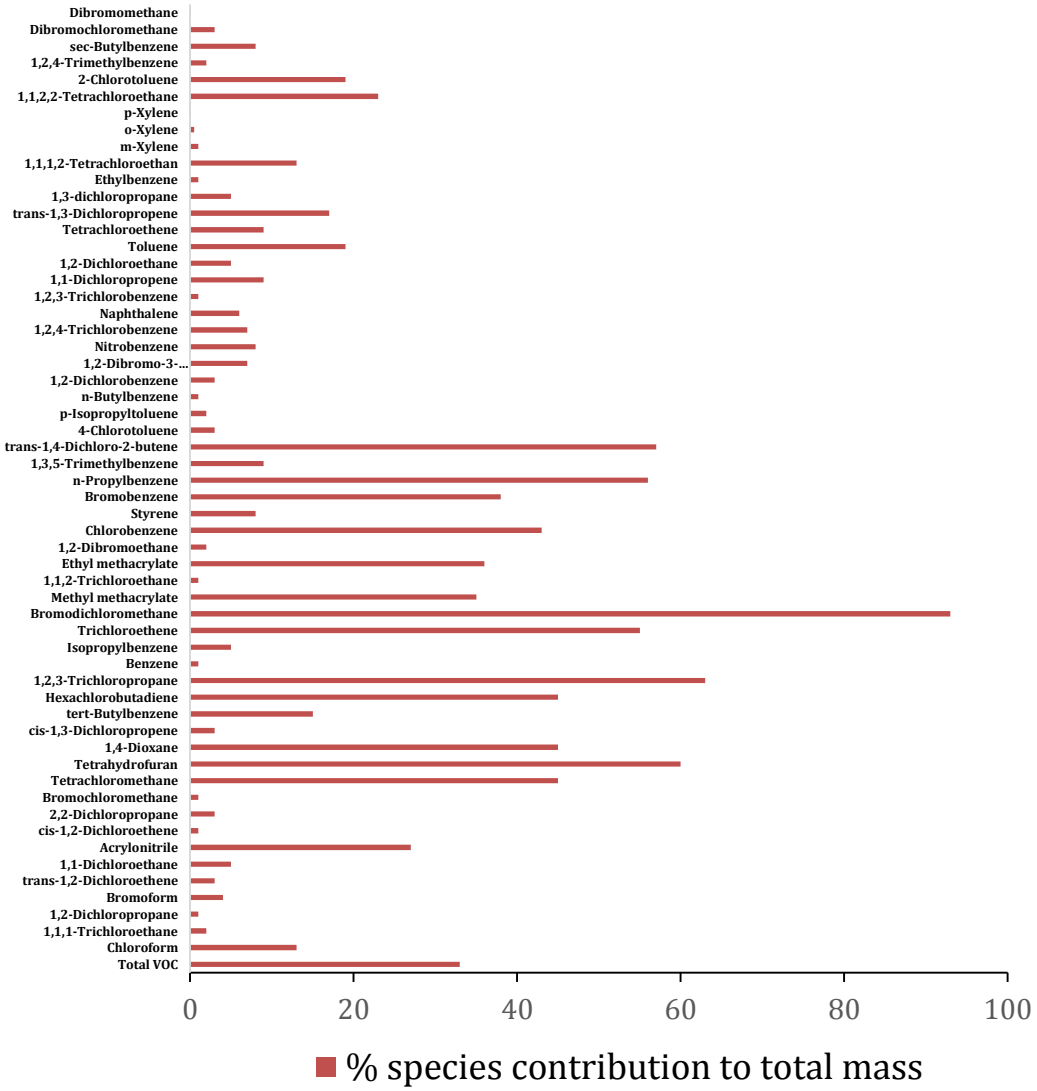

Figure 56. The percentage of the total VOC species mass from all samples associated with Factor 3

Scrutiny of Figure 56 shows high percentage mass abundance of known long-range transport chemical markers associated with Factor 3. These VOC markers are likely linked to industrial emissions in North America (Anjali, 2004; Brown et al., 2007; Cetin, Odabasi, & Seyfioglu, 2003).

4.7 Source Apportionment

Figure 57 provides the source apportionment of the three VOC sources identified.

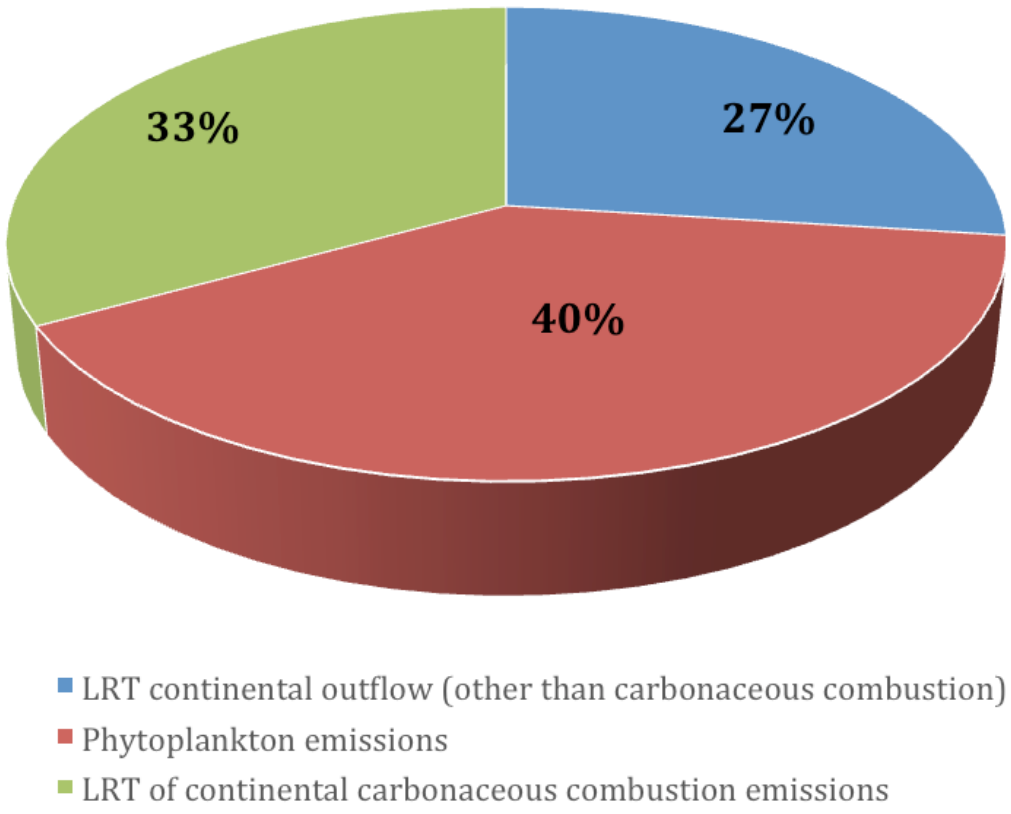

Figure 57. Source apportionment of VOC on Sable Island between October 1st and October and 31st, 2015

From Figure 57, it can be seen that LRT continental outflow (other than carbonaceous combustion) contributed 27% to the overall total VOC mass concentration sampled over the duration of the study, 40% contribution from phytoplankton emissions to the total mass and 33% from the LRT of combustion products from the North American continent.

It would be anticipated that these source attributions would change through the seasons with increases in phytoplankton blooms in the Spring and late Fall, wild fires over the spring, summer and Fall, less reliance on space heating in the summer and LRT smog events impacting Sable Island and the Scotian shelf.

CHAPTER 5 CONCLUSION AND RECOMMENDATIONS

5.1 Conclusion

An extremely valuable data set comprising 31 contiguous days of VOC species data was sampled on Sable Island. From this data set it was possible to conduct source apportionment of the VOC species. It was found that 27% of the total VOCs observed was associated with continental outflow, 40% of the VOCs were associated with marine phytoplankton emissions and 33% of the VOCs were associated with the combustion of carbonaceous material on the North American mainland. This study, and further associated research by the AFRG, will help augment the NASA North Atlantic Aerosols and Marine Ecosystem Study that is running coincident with this study on Sable Island over the next 5-years. This study lays the foundation for the next several years of research investigating the drivers of the temporal variation in VOC species observed on Sable Island, their sources, atmospheric dynamics and contribution to the total VOC observed on Sable Island. These data contained in this thesis will eventually help to better understand the formation of fog and clouds on the Scotian shelf, ultimately helping to improve climate models in the NW Atlantic.

5.2 Recommendations

It is recommended that the flow rate for the MTS-32 be increased to 100 mL/min for future sampling to roughly triple the method detection limit. If further funding were available, it would be worthwhile deploying either a PTR-MS or a Fourier transform-infrared (FT-IR) spectroscopy instrument for the real-time (<15-mins) measurement of C1 halocarbons, e.g. chloromethane. This would allow investigations of diurnal trends in

these phytoplankton associated VOC species. Bench-scale tests of phytoplankton VOC species at temperatures that would simulate future predicted ocean temperatures would be useful to determine if certain phytoplankton produce less or more VOCs during a warming ocean.

BIBLIOGRAPHY

Anderson, J. O., Thundiyil, J. G., & Stolbach, A. (2012). Clearing the air: a review of the effects of particulate matter air pollution on human health. *J Med Toxicol, 8*(2), 166-175. doi:10.1007/s13181-011-0203-1

Anjali, S. (2004). Source apportionment of ambient VOCS in Mumbai city. *Atmospheric Environment, 38*(39), 6829-6843. doi:10.1016/j.atmosenv.2004.09.009

Behrenfeld, M. J., Randerson, J. T., McClain, C. R., Feldman, G. C., Los, S. O., Tucker, C. J., . . . Pollack, N. H. (2001). Biospheric primary production during an ENSO transition. *Science, 291*(5513), 2594-2597. doi: 10.1126/science.1055071

Belmont, M., Steiniger, D., Phillips, E., Guazzotti, S., O'Brian, P., & Semyonov, A. (2013). Determination of 1,4-Dioxane in Drinking Water by Gas Chromatography/Mass Spectrometry (GC/MS) with Selected Ion Monitoring (SIM): Thermo Fisher Scientific Application Note 52295

Brauer, M., Blair, J., & Vedal, S. (1996). Effect of ambient ozone exposure on lung function in farm workers. *American Journal of Critical Care Medicine, 154*, 981-987.

Brown, R. H., Purnell, C. J., (1979). Collection and analysis of trace organic vapour pollutants in ambient atmospheres. The performance of a Tenax-GC adsorbent tube. *Journal of Chromatography, 178*, 79–90.

Brown, S. G., Frankel, A., & Hafner, H. R. (2007). Source apportionment of VOCs in the Los Angeles area using positive matrix factorization. *Atmospheric Environment, 41*(2), 227-237. doi:10.1016/j.atmosenv.2006.08.021

Buckley, F. S. E., & Mudge, S. M. (2002). Dimethylsulphide and ocean–atmosphere interactions. *Chemistry and Ecology, 20*(2), 73-95. doi: 10.1080/02757540410001670209

Butler, J. H., King, D. B., Lobert, J. M., Montzka, S. A., Yvon-Lewis, S. A., Hall, B., . . . D., Elkins, J. W. (2007), Oceanic distributions and emissions of short-lived halocarbons. *Global Biogeochem. Cycles, 21*, GB1023, doi:10.1029/2006GB002732.

Cetin, E., Odabasi, M., & Seyfioglu, R. (2003). Ambient volatile organic compound (VOC) concentrations around a petrochemical complex and a petroleum refinery. *The Science of the Total Environment, 312*, 103-112. doi:10.1016/S0048-9697(03)00197-9

Colomb, A., Yassaa, N., Williams, J., Peekan, I., & Lochte, K. (2008). Screening volatile organic compounds (VOCs) emissions from five marine phytoplankton species by head space gas chromatography/mass spectrometry (HS-GC/MS). *Journal of Environmental Monitoring, 10*, 325-330.

Craig, S. E., Jones, C. T., Li, W. K. W., Lazin, G., Horne, E., Caverhill, C., & Cullen, J. J. (2012). Deriving optical metrics of coastal phytoplankton biomass from ocean colour. *Remote Sensing of Environment, 119*(0), 72-83. doi:10.1016/j.rse.2011.12.007

Craig, S. E., Lohrenz, S. E., Lee, Z. P., Mahoney, K. L., Kirkpatrick, G. J., Schofield, O. M., & Steward, R. G. (2006). Use of hyperspectral remote sensing reflectance for detection and assessment of the harmful alga, Karenia brevis. *Applied Optics., 45*, 5414-5425.

Dewulf, J., & Van Langenhove, H. (1997). Chlorinated C_1- and C_2-hydrocarbons and monocyclic aromatic hydrocarbons in marine waters: an overview on fate processes, sampling, analysis and measurements, *Water Res., 31,* 1825–1838.

Dorman, F. L., & Dawes, P. (2012). Chapter 3 - Column Technology: Open Tubular Columns. In C. F. Poole (Ed.), *Gas Chromatography*, 79–96. Amsterdam: Elsevier, doi:10.1016/B978-0-12-385540-4.00003-1

Duderstadt, K. A., Carroll, M. A., Sillman, S., Wang, T., Albercook, G. M., Feng, L., & Forbes, G. (1998). Photochemical production and loss rates of ozone at sable island, Nova Scotia during the north atlantic regional experiment (NARE) 1993 summer intensive. *Journal of Geophysical Research: Atmospheres, 103*(D11), 13531-13555. doi:10.1029/98JD00397

Elbir, T., Cetin, B., Cetin, E., Bayram, A., & Odabasi, M. (2006). Characterization of Volatile Organic Compounds (VOCs) and Their Sources in the Air of Izmir, Turkey. *Environmental Monitoring and Assessment*, *133*(1), 149–160.

Environment Canada: Fossil Fuels. (2013). Retrieved November from http://www.ec.gc.ca/energie-energy/default.asp?lang=En&n=1F4E5D8A-1

Environment Canada: Pollution Sources. (2012). Retrieved from http://www.ec.gc.ca/Air/default.asp?lang=En&n=F963E49C-1

Environment Canada: Smog. (2014). Retrieved from https://www.ec.gc.ca/air/default.asp?lang=En&n=13D0EDAA-1

Euro Chlor (2001). Risk assessment for the maritime environment—1,4-dichlorobenzene. Retrieved from http://www.eurochlor.org/chlorine/science/risk12.htm

Franklin, J. E., Drummond, J. R., Griffin, D., Pierce, J. R., Waugh, D. L., Palmer, P. I., . . . Saha, A. (2014) A case study of aerosol depletion in a biomass burning plume over Eastern Canada during the 2011 BORTAS field experiment. *Atmospheric Chemistry and Physics Discussions*. acp-2014-31

Geyh, A. S., Roberts, P. T., Lurmann, F. W., Schoell, B. S., & Avol, E. L. (1999). Initial field evaluation of the Harvard active ozone sampler for personal ozone monitoring. *J. Environ. Anal. Environ. Epidemiol, 2*, 143-149.

Gibson, M. D., Guernsey, J. R., Beauchamp, S., Waugh, D., Heal, M. R., Brook, J. R., Terashima, M. (2009a). Quantifying the spatial and temporal variation of ground-level ozone in the rural Annapolis Valley, Nova Scotia, Canada using nitrite-impregnated passive samplers. *Journal of the Air & Waste Management Association, 59*(3), 310-320. doi:10.3155/1047-3289.59.3.310

Gibson, M. D., Haelssig, J., Pierce, J. R., Parrington, M. P., Franklin, J. E., Hopper, J.T., Li, Z. & Ward, T. J. (2015). A comparison of four receptor models used to quantify the boreal wildfire smoke contribution to surface PM2.5 in Halifax, Nova Scotia during the BORTAS-B experiment. *Atmospheric Chemistry and Physics, 15*, 815-827

Gibson, M. D., Heal, M. R., Bache, D. H., Hursthouse, A. S., Beverland, I. J., Craig, S. E., Clark, C. F., Mike, H. J., Guernsey, J. R., & Jones, C. (2009b). Using Mass Reconstruction along a Four-Site Transect as a Method to Interpret PM10 in West-Central Scotland, United Kingdom. *Journal of the Air & Waste Management Association, 59*(12), 1429-1436. doi:Doi 10.3155/1047-3289.59.12.1429

Gibson, M. D., Heal, M. R., Li, Z., Kuchta, J. S., Hayes, A., King, G. H., & Lambert, S. (2013a). The spatial and seasonal variation of nitrogen dioxide and sulphur dioxide in Cape Breton Highlands National Park, Canada, and the association with lichen abundance. *Atmospheric Environment, 64,* 303-311. doi:10.1016/j.atmosenv.2012.09.068

Gibson, M. D., Pierce, J. R., Waugh, D., Kuchta, J. S., Chisholm, L., Duck, T. J., Palmer, P. I. (2013b). Identifying the sources driving observed PM2.5 variability over Halifax, Nova Scotia, during BORTAS-B. *Atmospheric Chemistry and Physics,* (13), 4491-4533. doi:10.5194/acpd-13-4491-2013

Gibson, M. D., Ward, T. J., Wheeler, A. J., Guernsey, J. R., Seaboyer, M. P., Bazinet, P., . . . Stieb, D. M. (2010). Woodsmoke source apportionment in the Rural Annapolis Valley, Nova Scotia, Canada. *Conference Proceedings of the 103rd Annual Conference of the Air and Waste Management Association, Calgary*(June 22-25).

Guenther, A., Karl, T., Harley, P., Wiedinmyer, C., Palmer, P. I., & Geron, C. (2006). Estimates of global terrestrial isoprene emissions using MEGAN (Model of Emissions of Gases and Aerosols from Nature). *Atmos. Chem. Phys., 6*(11), 3181-3210. doi:10.5194/acp-6-3181-2006

Guidelines for the quantitative gas chromatography of volatile flavouring substances, from the Working Group on Methods of Analysis of the International Organization of the Flavor Industry (IOFI). (2011). *Flavour and Fragrance Journal*, doi:10.1002/ffj.2061

Guigard, S., Kindzierski, W., Purtill, C., Schulz, J., Treissman, D., & Vidmar, J. (2006). Assessment Report on Formaldehyde for Developing Ambient Air Quality Objectives. Alberta Environment. Edmonton, Alberta.

Guo, H., Wang, T., & Louie, P. K. K. (2004). Source apportionment of ambient non-methane hydrocarbons in Hong Kong: Application of a principal component analysis/absolute principal component scores (PCA/APCS) receptor model. *Environmental Pollution, 129*(3), 489-498.

Harris, D. C. (2007). *Quantitative chemical analysis*. New York, NY: W.H. Freeman and Co.

Harrison, R. M., Deacon, A. R., & Jones, M. R. (1997). Sources and processes affecting concentrations of PM10 and PM2.5 particulate matter in Birmingham (U.K.). *Atmospheric Environment, 31(*24), 4103-4117. doi:1352-2310/97

Hatakeyama, S., Izumi, K., & Akimoto, H. (1985). Yield of SO2 and formation of aerosol in the photo-oxidation of DMS under atmospheric conditions. *Atmospheric Environment (1967), 19*(1), 135-141.

Hayes, A. (2014). *Source apportionment of air quality on Sable Island*. Unpublished Master of Applied Science Thesis, Dalhousie University, Halifax, NS.

Holzinger, R., Jordan, A., Hansel, A., & Lindinger, W. (2001). Methanol measurements in the lower troposphere near Innsbruck (047°16′N; 011°24′E), Austria. *Atmospheric Environment, 35*(14), 2525-2532.

Hopke, P. K. (1991). An introduction to Receptor Modeling. *Chemom. Intell. Lab. System, 10*(1-2), 21-43.

Howard P. H. (1990). *Handbook of Environmental Fate and Exposure Data for Organic Chemicals*, Lewis Publishers, Chelsea, Michigan.

Hubert, L., Meulman, J., & Heiser, W. (2000). Two purposes for matrix factorization: A historical appraisal. *Siam Review, 42*(1), 68-82. doi:10.1137/S0036144598340483

HYSPLIT – Hybrid single particle lagrangian integrated trajectory model. (2016). Retrieved from http://www.arl.noaa.gov/HYSPLIT_info.php

Inkpen, T., Hingston, M., Waugh, D., Keast, S., McPherson, J., Worthy, D., & Forbes, G. (2009). Sable Island Air Monitoring Program Report: 2003-2006. *Meteorological Service of Canada, Atlantic Region Science Technical Report (*In press).

IPCC, 2007. (2007). *Climate Change 2007: Synthesis Report* (Contribution of Working Groups I, II and III to the Fourth Assessment Report of the Intergovernmental Panel on Climate Change) (p. 104). Geneva, Switzerland: IPCC

ISQ User Guide. (2012). Thermo Fisher Scientific. Retrieved from http://www.thermoscientific.com/content/dam/tfs/ATG/CMD/cmd-support/isq/operations-and-maintenance/operators-manuals/ISQ-User.pdf

Jia, C., & Batterman, S. (2010). A Critical Review of Naphthalene Sources and Exposures Relevant to Indoor and Outdoor Air. *International Journal of Environmental Research and Public Health*, *7*(7), 2903–2939, doi:10.3390/ijerph7072903

Johnson, M., Isakov, V., Touma, J. S., Mukerjee, S., & Ozkaynak, H. (2010). Evaluation of land-use regression models used to predict air quality concentrations in an urban area. *Atmospheric Environment, 44*(30), 3660-3668.

Kim, E., & Hopke, P. K. (2004). Source Apportionment of Fine Particles in Washington, DC, Utilizing Temperature-Resolved Carbon Fractions. *Air & Waste Management Association, 54*, 773–785.

Kladi, M., Vagias, C., & Roussis, V. (2004). Volatile halogenated metabolites from marine red algae. *Phytochemistry Reviews*, *3*(3), 337–366, doi:10.1007/s11101-004-4155-9

Klee, M. (n.d.). GC Solutions #20: Calibration Curves – Part 2, Internal Standard Approach. Retrieved from http://www.sepscience.com/Techniques/GC/Articles/189-/GC-Solutions-20-Calibration-Curves--Part-2-Internal-Standard-Approach

Kroll, J. H., & Seinfeld, J. H. (2008). Chemistry of secondary organic aerosol: Formation and evolution of low-volatility organics in the atmosphere. *Atmospheric Environment, 42*(16), 3593-3624. doi: Doi 10.1016/J.Atmosenv.2008.01.003

Lee, S. C., Chiu, M. Y., Ho, K. F., Zou, S. C., & Wang, X. (2002). Volatile organic compounds (VOCs) in urban atmosphere of Hong Kong. *Chemosphere*, *48*(3), 375–382, doi:10.1016/S0045-6535(02)00040-1

Lindsey, R., & Scott, M. (2010). What are Phytoplankton? Retrieved from http://earthobservatory.nasa.gov/Features/Phytoplankton/

Liss, P. S. (2007). Trace gas emissions from the marine biosphere. *Philosophical Transactions of the Royal Society A: Mathematical, Physical and Engineering Sciences, 365*(1856), 1697-1704. doi:10.1098/rsta.2007.2039

Liu, Y., Shao, M., Fu, L., Lu, S., Zeng, L., & Tang, D. (2008). Source profiles of volatile organic compounds (VOCs) measured in China: Part I. *Atmospheric Environment, 42*(25), 6247-6260. doi:10.1016/j.atmosenv.2008.01.070

McCombs, J. D., Blunt, J. W., Chambers M. V., Munro, M. H. G., & Robinson, W. T. (1988). Novel2(5H)-furanones from the red marine alga Delisea elegans (Lamouroux). *Tetrahedron, 44,* 1489–1502

Monks, P. S., Granier, C., Fuzzi, S., Stohl, A., Williams, M. L., Akimoto, H., . . . Von Glasow, R. (2009). Atmospheric composition change – global and regional air quality. *Atmospheric Environment, 43,* 5268-5350.

Moore, R. M., Geen, C. E., & Tait, V. K. (1995). Determination of Henry's Law constants for a suite of naturally occurring halogenated methanes in seawater. *Chemosphere, 30*(6), 1183-1191.

Moore, R. M., Oram, D. E. and Penkett, S. A. (1994), Production of isoprene by marine phytoplankton cultures. *Geophys. Res. Lett., 21*: 2507–2510. doi:10.1029/94GL02363

Moore, R. M., & Tokarczyk, R. (1993). Volatile biogenic halocarbons in the northwest Atlantic. Global Biogeochem. *Cycles, 7*(1), 195-210. doi:10.1029/92gb02653

MTS-32 User Manual. (2015). Markes International. Retrieved from http://www.restek.com/pdfs/26464_mts-32_user_manual.pdf

Muir, R. M. (2000). *The Geochemistry and source apportionment of selected VOCs in Renfrewshire*. PhD Thesis, University of Paisley, Scotland, UK.

Naeher, L. P., Brauer, M., Lipsett, M., Zelikoff, J. T., Simpson, C. D., Koenig, J. Q., & Smith, K. R. (2007). Woodsmoke Health Effects: A Review. *Inhalation Toxicology, 19*(1), 67-106.

Nightingale, P., Malin, G., & Liss, P. (1995). Production of chloroform and other low molecular-weight halocarbons by some species of macroalgae. *Limnology and Oceanography, 40*(4), 680-689.

Norris, G., Vedantham, R., Wade, K., Schmidbauer, S., Prouty, J., & Foley, C. (2008). EPA positive Matrix Factorization (PMF) 3.0 fundamentals & user guide. U.S. Environmental Protection Agency

O'Dowd, C. D., Aalto, P., Hmeri, K., Kulmala, M. & Hoffmann, T. (2002). Aerosol formation: Atmospheric particles from organic vapours. *Nature, 416*(6880), 497-498.

O'Dowd, C. D., & de Leeuw, G. (2007). Marine aerosol production: a review of the current knowledge. *Phil. Trans. R. Soc. A, 365,* 1753-1774. doi:10.1098/rsta.2007.2043

O'Dowd, C. D., Facchini, M. C., Cavalli, F., Ceburnis, D., Mircea, M., Decesari, S., . . . Putaud, J.P. (2004). Biogenically driven organic contribution to marine aerosol. *Nature, 431*(7009), 676-680. doi:10.1038/nature02959

Ostro, B., & Chestnut, L. (1998). Assessing the health benefits of reducing particulate matter air pollution in the United States. *Environ Res, 76*(2), 94-106. doi:Doi 10.1006/Enrs.1997.3799

Paatero, P., & Hopke, P. K. (2003). Discarding or downweighting high-noise variables in factor analytic models. 8th International Conference on Chemometrics and Analytical Chemistry. *Analytica Chimica Acta, 490*(1-2), 277-289.

Palmer, P., & Shaw, S. (2005). Quantifying global marine isoprene fluxes using MODIS chlorophyll observations. *Geophysical Research Letters, 32*(9), L09805. doi:10.1029/2005gl022592

Palmer, P. I., Parrington, M., Lee, J. D., Lewis, A. C., Rickard, A. R., Bernath, P. F., . . . Young, J. C. (2013). Quantifying the impact of BOReal forest fires on Tropospheric oxidants over the Atlantic using Aircraft and Satellites (BORTAS) experiment: design, execution and science overview. *Atmos. Chem. Phys., 13*(13), 6239-6261. doi:10.5194/acp-13-6239-2013

Paul, C., & Pohnert, G. (2011). Production and role of volatile halogenated compounds from marine algae. *Natural Product Reports, 28*(2), 186-195.

Pires, J. C. M., Sousa, S. I. V., Pereira, M. C., Alvim-Ferraz, M. C. M., & Martins, F. G. (2007). Management of air quality monitoring using principal component and cluster analysis—Part I: SO2 and PM10. *Atmospheric Environment., 42,* 1249-1260. doi:10.1016/j.atmosenv.2007.10.044

Quinn, P. K., & Bates, T. S. (2011). The case against climate regulation via oceanic phytoplankton sulphur emissions. Nature, 480(7375), 51-56. doi: Doi 10.1038/Nature10580

Ramadan, Z., Eickhout, B., Song, X-H., Buydens, L. M. C., & Hopke, P. K. (2003). Comparison of Positive Matrix Factorization and Multilinear Engine for the source apportionment of particulate pollutants. *Chemometrics and Intelligent Laboratory Systems, 66*(1), 15-28. doi:http://dx.doi.org/10.1016/S0169-7439(02)00160-0

Robinson, A. L., Donahue, N. M., Shrivastava, M. K., Weitkamp, E. A., Sage, A. M., Grieshop, A. P., . . . Pandis, S. N. (2007). Rethinking organic aerosols: Semivolatile emissions and photochemical aging. *Science, 315*(5816), 1259-1262. doi:Doi 10.1126/Science.113306

Rome, K., & Mcintyre, A. (2012). Intelligent use of relative response factors in gas chromatography-flame ionisation detection. *Chromatography Today*, (June), 52–56.

Sabolis, A. W. (2010). *Quantifying Marine Emissions of Biogenic Volatile Organic Compounds Using Laboratory Measurements, Field Measurements and Remote Sensing Data*. Master of Science Thesis, North Carolina State University, Department of Marine, Earth, and Atmospheric Science.

Scarratt, M. G., & Moore, R. M. (1999). Production of Chlorinated Hydrocarbons and Methyl Iodide by the Red Microalga Porphyridium purpureum. *Limnol. Oceanogr., 44*, 703.

Schmidbauer, N., & Oehme, M. (1988). Comparison of solid adsorbent and stainless steel canister sampling for very low ppt-concentrations of aromatic compounds (≥C 6) in ambient air from remote areas. *Fresenius' Zeitschrift Für Analytische Chemie, 331*(1), 14-19.

Shaw, G. E. (1983). Bio-Controlled Thermostasis Involving the Sulfur Cycle. *Climatic Change, 5*(3), 297-303. doi:Doi 10.1007/Bf02423524

Shaw, S. L. (2001). *The production of non-methane hydrocarbons by marine plankton*. PhD Thesis, Massachusetts Institute of Technology. Boston, MA.

Shaw, S. L., Chisholm, S. W., Prinn, R. G. (2003). Isoprene production by Prochlorococcus, a marine cyanobacterium, and other phytoplankton. *Marine Chemistry, 80,* 227– 245.

Shaw, S. L., Gantt, B., & Meskhidze, N. (2010). Production and Emissions of Marine Isoprene and Monoterpenes: A Review. *Advances in Meteorology, 2010*. doi:10.1155/2010/408696

Silva, A., Palma, S., Oliveira, P. B. & Moita, M. T. (2009). *Calcidiscus quadriperforatus* and *Calcidiscus leptoporus* as oceanographic tracers in Lisbon Bay (Portugal). *Estuarine Coastal and Shelf Science* 81: 333-344.

Sinha, V., Williams, J., Meyerhöfer, M., Riebesell, U., Paulino, A. I., & Larsen, A. (2007). Air-sea fluxes of methanol, acetone, acetaldehyde, isoprene and DMS from a Norwegian fjord following a phytoplankton bloom in a mesocosm experiment. *Atmos. Chem. Phys., 7*(3), 739-755. doi:10.5194/acp-7-739-2007

Smythe-Wright, D., Boswell, S. M., Breithaupt, P., Davidson, R. D., Dimmer C. H., Diaz, L. B. E. (2006). Methyl iodide production in the ocean: Implications for climate change. *Global Biogeochemical Cycles, 20*(3).

Song, X-H., Polissar, A.V., & Hopke, P.K. (2001). Sources of fine particle composition in the northeastern US. *Atmospheric Environment, 35,* 5277-5286.

Sunda, W., Kieber, D. J., Kiene, R. P., & Huntsman, S. (2002). An antioxidant function for DMSP and DMS in marine algae. *Nature, 418*, 317-320. TDTS 61 Application Note. (2009). Diffusion-locking technology overview. Markes International.

Sundstrom, J., Collen, J., Abrahamsson, K., & Pedersen, M. (1996). Halocarbon production and in vivo brominating activity of Eucheuma denticulatum. *Phytochemisty 42*(6): 1527–1530.

Teather, K., Hogan, N., Critchley, K., Gibson, M. D., Craig, S. E., & Hill, J. (2013). Examining the Links Between Air Quality, Climate Change and Respiratory Health in Qatar. *Avicenna*. doi:10.5339/avi.2013.9

Thomas, H., Craig, S. E., Greenan, B. J. W., Burt, W., Herndl, G. J., Higginson, S., . . . Urrego-Blanco, J. (2012). Direct observations of diel biological CO2 fixation on the Scotian Shelf, northwestern Atlantic Ocean. *Biogeosciences, 9*(6), 2301--2309. doi:10.5194/bg--9--2301--2012

Tokarczyk, R., & Moore, R. M. (1994). Production of volatile organohalogens by phytoplankton cultures. *Geophys. Res. Lett., 21*, 285–288, doi:10.1029/94GL00009

Trivitayanurak, W., Adams, P. J., Spracklen, D. V., & Carslaw, K. S. (2008). TOMAS implementation in GEOS-Chem: Tropospheric aerosol microphysics simulation with assimilated meteorology: model description and intermodel comparison. *Atmospheric Chemistry and Physics, 8*(12), 3149-3168

Unity 2 Operators' Manual. (2012). Markes International. Retrieved from http://www.ingenieria-analitica.com/unity-2-markes-international.html

USEPA, (1999). *Compendium Method TO-17: Determination of Volatile Organic Compounds in Ambient Air Using Active Sampling Onto Sorbent Tubes*. Retrieved from https://www.epa.gov/ttnamti1/files/ambient/airtox/to-17r.pdf

USEPA, (2009*). Current Methodologies in Preparing Mobile Source Port-Related Emission Inventories: Final Report*. Retrieved from http://www.epa.gov/cleandiesel/documents/ports-emission-inv-april09.pdf

Wai-mei Sin, D., Wong, Y., Sham, W., & Wang, D. (2001). Development of an analytical technique and stability evaluation of 143 C 3 – C 12 volatile organic compounds in Summa ® canisters by gas chromatography–mass spectrometry. *The Analyst, 126*(3), 310-321.

Waugh, D., Inkpen, D. T., Hingston, M., Keast, S., McPherson, J., Worthy, D., & Forbes, G. (2010). Sable island air monitoring program report: 2003-2006. (No. 181). Dartmouth: Environmental Studies Research Funds.

Waugh, D. L. (2006). Particulate Matter Climatology for Atlantic Canada. *Environment Canada Science Report Series 2006-04, Catalogue No. En57-36/2006-4E,* 58.

WHO, (2002). *Acrylonitrile: Concise International Chemical Assessment Document 39*. Retrieved from, http://www.inchem.org/documents/cicads/cicads/cicad39.htm

WHO, (2003). *Hexachlorobutadiene in Drinking-water (Chemical Fact Sheet),* 379-380

Woodhouse, M. T., Carslaw, K. S., Mann, G.W., Vallina, S. M.,Vogt, M., Halloran, P. R., & Boucher, O. (2010). Low sensitivity of cloud condensation nuclei to changes in the sea-air flux of dimethyl-sulphide. *Atmospheric Chemistry and Physics, 10*(16), 7545. doi: 10.5194/acp-10-7545-2010

Woolfenden, E. (1997). Monitoring VOCs in air using sorbent tubes followed by thermal desorption-capillary GC analysis: Summary of data and practical guidelines. *Journal of the Air and Waste Management Association, 47*(1), 20-36.

Yu, H., Kaufman, Y. J., Chin, M., Feingold, G., Remer, L. A., Anderson, T. L., . . . Zhou, M. (2006). A review of measurement-based assessments of the aerosol direct radiative effect and forcing. *Atmospheric Chemistry and Physics, 6*, 613-666.

APPENDIX

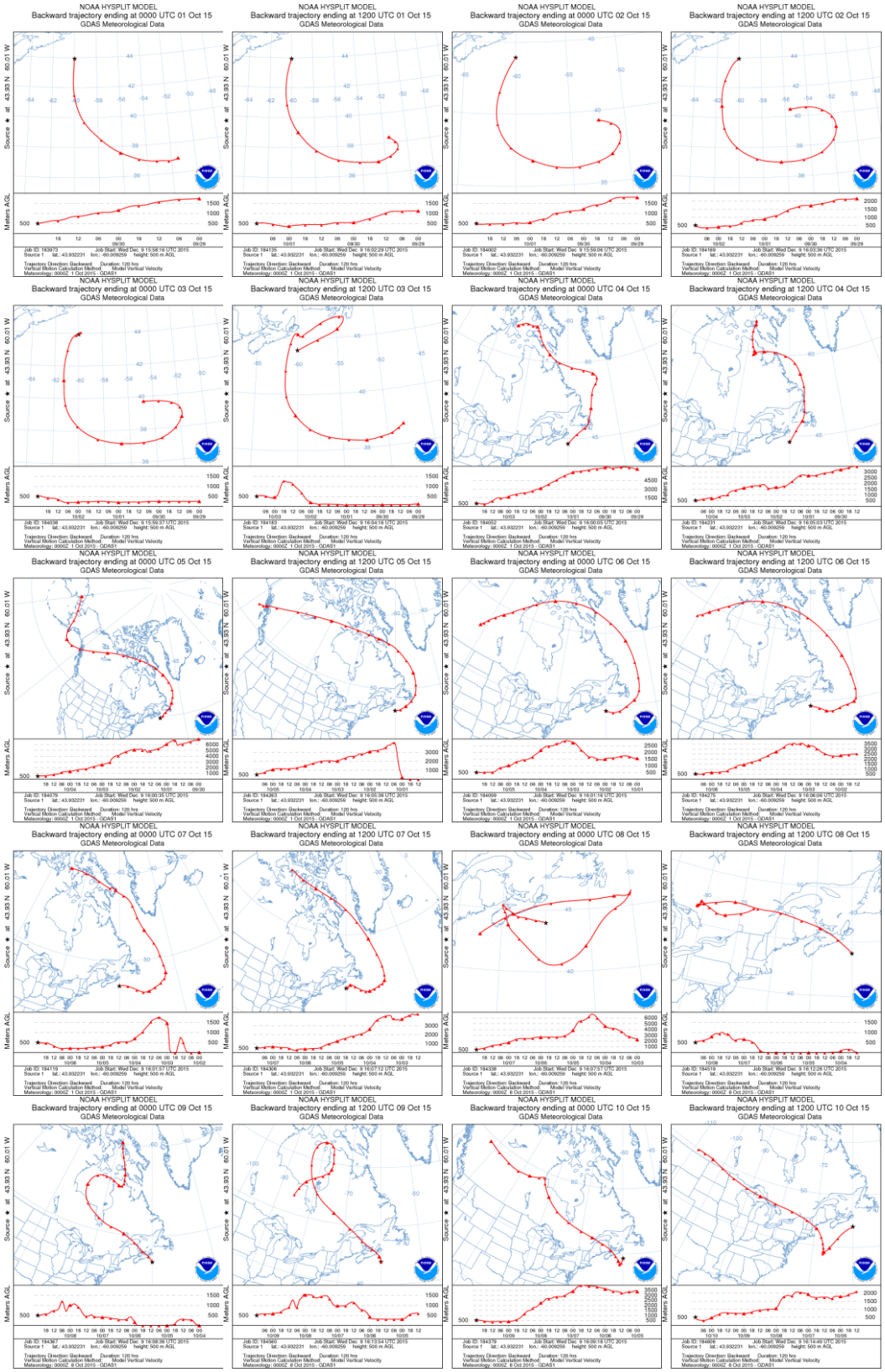
NOAA HYSPLIT MODEL
Backward trajectory ending at 0000 UTC 01 Oct 15
GDAS Meteorological Data
NOAA HYSPLIT MODEL
Backward trajectory ending at 1200 UTC 01 Oct 15
GDAS Meteorological Data
NOAA HYSPLIT MODEL
Backward trajectory ending at 0000 UTC 02 Oct 15
GDAS Meteorological Data
NOAA HYSPLIT MODEL
Backward trajectory ending at 1200 UTC 02 Oct 15
GDAS Meteorological Data
NOAA HYSPLIT MODEL
Backward trajectory ending at 0000 UTC 03 Oct 15
GDAS Meteorological Data
NOAA HYSPLIT MODEL
Backward trajectory ending at 1200 UTC 03 Oct 15
GDAS Meteorological Data
NOAA HYSPLIT MODEL
Backward trajectory ending at 0000 UTC 04 Oct 15
GDAS Meteorological Data
NOAA HYSPLIT MODEL
Backward trajectory ending at 1200 UTC 04 Oct 15
GDAS Meteorological Data
NOAA HYSPLIT MODEL
Backward trajectory ending at 0000 UTC 05 Oct 15
GDAS Meteorological Data
NOAA HYSPLIT MODEL
Backward trajectory ending at 1200 UTC 05 Oct 15
GDAS Meteorological Data
NOAA HYSPLIT MODEL
Backward trajectory ending at 0000 UTC 06 Oct 15
GDAS Meteorological Data
NOAA HYSPLIT MODEL
Backward trajectory ending at 1200 UTC 06 Oct 15
GDAS Meteorological Data
NOAA HYSPLIT MODEL
Backward trajectory ending at 0000 UTC 07 Oct 15
GDAS Meteorological Data
NOAA HYSPLIT MODEL
Backward trajectory ending at 1200 UTC 07 Oct 15
GDAS Meteorological Data
NOAA HYSPLIT MODEL
Backward trajectory ending at 0000 UTC 08 Oct 15
GDAS Meteorological Data
NOAA HYSPLIT MODEL
Backward trajectory ending at 1200 UTC 08 Oct 15
GDAS Meteorological Data
NOAA HYSPLIT MODEL
Backward trajectory ending at 0000 UTC 09 Oct 15
GDAS Meteorological Data
NOAA HYSPLIT MODEL
Backward trajectory ending at 1200 UTC 09 Oct 15
GDAS Meteorological Data
NOAA HYSPLIT MODEL
Backward trajectory ending at 0000 UTC 10 Oct 15
GDAS Meteorological Data
NOAA HYSPLIT MODEL
Backward trajectory ending at 1200 UTC 10 Oct 15
GDAS Meteorological Data

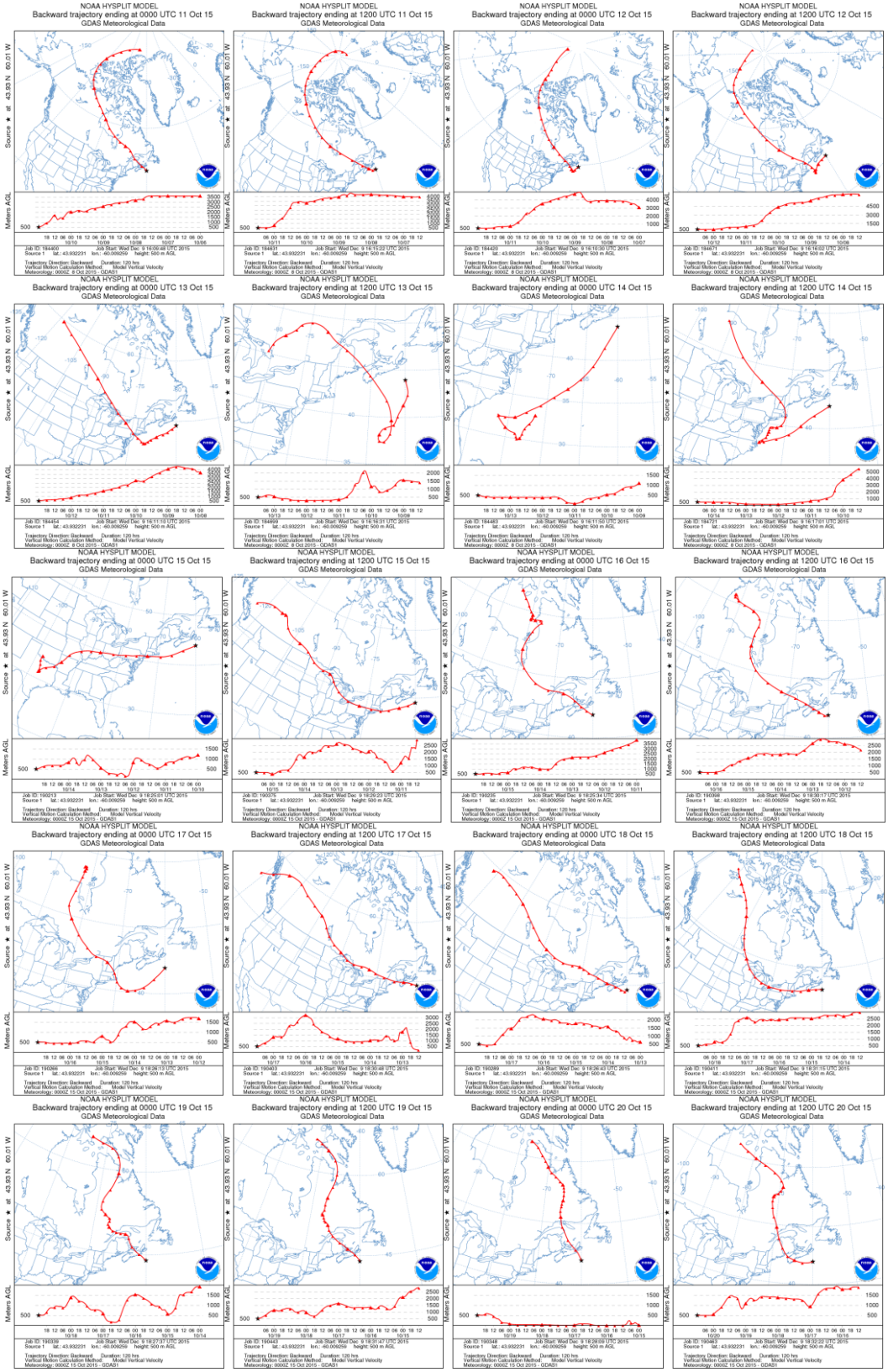
NOAA HYSPLIT MODEL
Backward trajectory ending at 0000 UTC 11 Oct 15
GDAS Meteorological Data
NOAA HYSPLIT MODEL
Backward trajectory ending at 1200 UTC 11 Oct 15
GDAS Meteorological Data
NOAA HYSPLIT MODEL
Backward trajectory ending at 0000 UTC 12 Oct 15
GDAS Meteorological Data
NOAA HYSPLIT MODEL
Backward trajectory ending at 1200 UTC 12 Oct 15
GDAS Meteorological Data
NOAA HYSPLIT MODEL
Backward trajectory ending at 0000 UTC 13 Oct 15
GDAS Meteorological Data
NOAA HYSPLIT MODEL
Backward trajectory ending at 1200 UTC 13 Oct 15
GDAS Meteorological Data
NOAA HYSPLIT MODEL
Backward trajectory ending at 0000 UTC 14 Oct 15
GDAS Meteorological Data
NOAA HYSPLIT MODEL
Backward trajectory ending at 1200 UTC 14 Oct 15
GDAS Meteorological Data
NOAA HYSPLIT MODEL
Backward trajectory ending at 0000 UTC 15 Oct 15
GDAS Meteorological Data
NOAA HYSPLIT MODEL
Backward trajectory ending at 1200 UTC 15 Oct 15
GDAS Meteorological Data
NOAA HYSPLIT MODEL
Backward trajectory ending at 0000 UTC 16 Oct 15
GDAS Meteorological Data
NOAA HYSPLIT MODEL
Backward trajectory ending at 1200 UTC 16 Oct 15
GDAS Meteorological Data
NOAA HYSPLIT MODEL
Backward trajectory ending at 0000 UTC 17 Oct 15
GDAS Meteorological Data
NOAA HYSPLIT MODEL
Backward trajectory ending at 1200 UTC 17 Oct 15
GDAS Meteorological Data
NOAA HYSPLIT MODEL
Backward trajectory ending at 0000 UTC 18 Oct 15
GDAS Meteorological Data
NOAA HYSPLIT MODEL
Backward trajectory ending at 1200 UTC 18 Oct 15
GDAS Meteorological Data
NOAA HYSPLIT MODEL
Backward trajectory ending at 0000 UTC 19 Oct 15
GDAS Meteorological Data
NOAA HYSPLIT MODEL
Backward trajectory ending at 1200 UTC 19 Oct 15
GDAS Meteorological Data
NOAA HYSPLIT MODEL
Backward trajectory ending at 0000 UTC 20 Oct 15
GDAS Meteorological Data
NOAA HYSPLIT MODEL
Backward trajectory ending at 1200 UTC 20 Oct 15
GDAS Meteorological Data

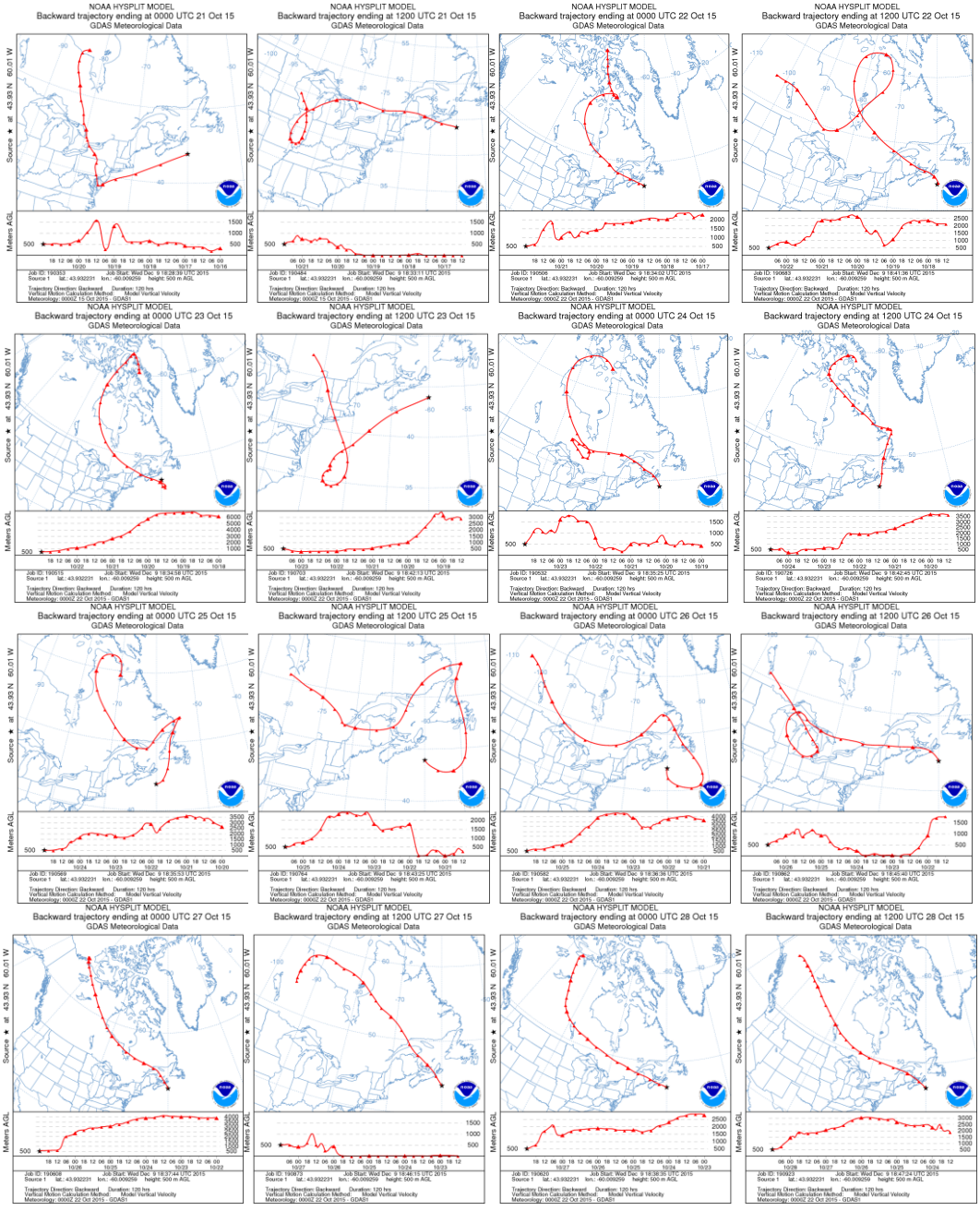
NOAA HYSPLIT MODEL
Backward trajectory ending at 0000 UTC 21 Oct 15
GDAS Meteorological Data
NOAA HYSPLIT MODEL
Backward trajectory ending at 1200 UTC 21 Oct 15
GDAS Meteorological Data
NOAA HYSPLIT MODEL
Backward trajectory ending at 0000 UTC 22 Oct 15
GDAS Meteorological Data
NOAA HYSPLIT MODEL
Backward trajectory ending at 1200 UTC 22 Oct 15
GDAS Meteorological Data
NOAA HYSPLIT MODEL
Backward trajectory ending at 0000 UTC 23 Oct 15
GDAS Meteorological Data
NOAA HYSPLIT MODEL
Backward trajectory ending at 1200 UTC 23 Oct 15
GDAS Meteorological Data
NOAA HYSPLIT MODEL
Backward trajectory ending at 0000 UTC 24 Oct 15
GDAS Meteorological Data
NOAA HYSPLIT MODEL
Backward trajectory ending at 1200 UTC 24 Oct 15
GDAS Meteorological Data
NOAA HYSPLIT MODEL
Backward trajectory ending at 0000 UTC 25 Oct 15
GDAS Meteorological Data
NOAA HYSPLIT MODEL
Backward trajectory ending at 1200 UTC 25 Oct 15
GDAS Meteorological Data
NOAA HYSPLIT MODEL
Backward trajectory ending at 0000 UTC 26 Oct 15
GDAS Meteorological Data
NOAA HYSPLIT MODEL
Backward trajectory ending at 1200 UTC 26 Oct 15
GDAS Meteorological Data
NOAA HYSPLIT MODEL
Backward trajectory ending at 0000 UTC 27 Oct 15
GDAS Meteorological Data
NOAA HYSPLIT MODEL
Backward trajectory ending at 1200 UTC 27 Oct 15
GDAS Meteorological Data
NOAA HYSPLIT MODEL
Backward trajectory ending at 0000 UTC 28 Oct 15
GDAS Meteorological Data
NOAA HYSPLIT MODEL
Backward trajectory ending at 1200 UTC 28 Oct 15
GDAS Meteorological Data

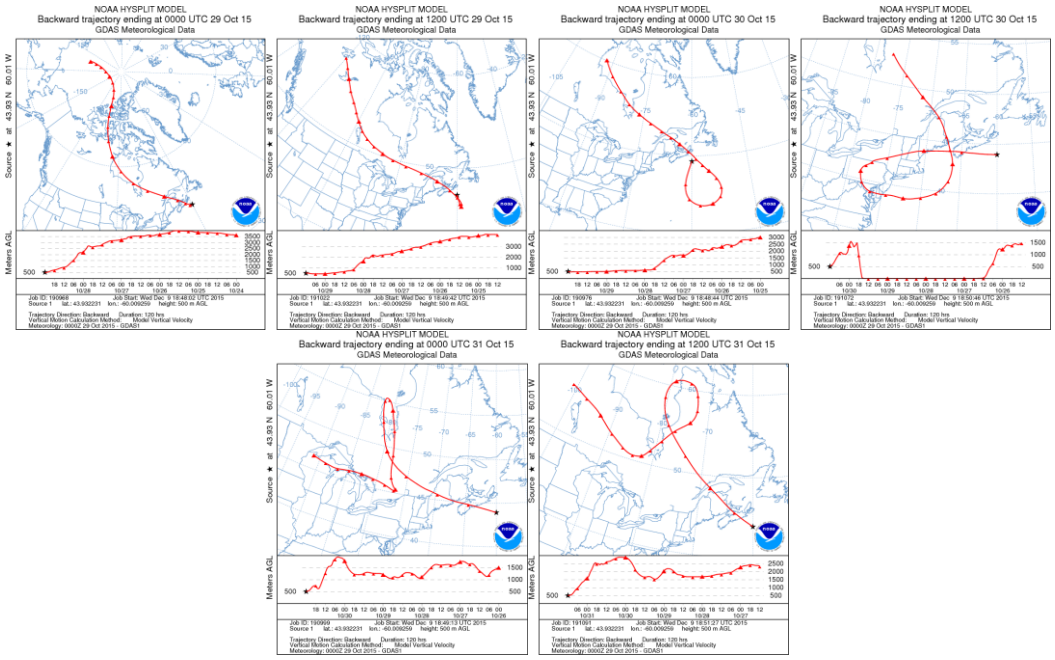

Figure 58. Daily HYSPLIT back trajectories over the sampling period October 1st to October 31st, 2015